dc_265_11

STOCHASTIC AND DETERMINISTIC MODELS FOR THE DEVELOPMENT AND MANUFACTURE OF WOOD-BASED COMPOSITES

by

Elemer M. Lang

Dissertation submitted to the Hungarian Academy of Sciences,
in partial fulfillment of the requirements for the degree of
Doctor of the Hungarian Academy of Sciences

September, 2011
Sopron, Hungary

Preface

This Dissertation describes four somewhat connected research projects that were either directed, guided, performed, or combinations of the above by the author. His tenure at the West Virginia University, Division of Forestry and Natural Resources, Morgantown, WV, U.S.A, covers the period between 1993 and 2008. The selected works from this time frame presented here focus on stochastic and deterministic modeling of the expected mechanical and performance characteristics of solid wood and existing or new, innovative, structural, wood-based composites. Results and the advanced models may be applied to novel product development. Furthermore, the scientific background for processing technologies of several, new, load-bearing products are also discussed.

The body of the Dissertation contains six numbered chapters. Chapter I, the General Introduction provides limited information to readers who are less familiar with the unique characteristics of wood and wood-composites. Chapters II through V are stand-alone documents, containing all the necessary sections including references. Chapter VI contains an overall summary and the conclusions in the form of theses. Each Chapter has an Appendix numbered accordingly. Appendices consist of materials that were deemed redundant in the text, but may help with clarifications and better understanding.

Although the majority of the works presented here employed the English Customary units, this Dissertation applies SI units only. Whenever the use of other system's units was unavoidable, detailed explanations and SI equivalents are provided. All the text, captions and headings are in English, using U.S. spelling and idioms.

Copyrighted materials (figures, diagrams, photographs, etc.) may be incorporated. If the insert was essential, it is marked by the usual citation format and the complete bibliography is listed in the references of the appropriate chapters. Unmarked figures, pictures, diagrams and other illustrations are the author's or his collaborators' works.

*Tremendous credits are due to many individuals who contributed to these works. The list of these people is long. Only a few could be mentioned by name in the Acknowledgements section. Nonetheless, to salute those who provided scientific and physical help, encouragement, friendship and love during the course of this undertaking, instead of using the big ego" **I**"; the plural version "**we**" is practiced in this write-up.*

Sopron – Morgantown, WV

(2010 -2011) *Elemer M. Lang*

Acknowledgements

Many thanks are due to Dr. Geza Ifju, formerly Department Head of Wood Science & Forest Products at Virginia Tech, Blacksburg, VA. He provided the opportunity to compliment my education in a research oriented, challenging environment. Members of my Ph.D. committee: Drs. Joseph R. Loferski, Frederick A. Kamke, J. Daniel Dolan and Frank E. Woeste, should receive special recognition for their valuable contributions to my research resulting in a Ph.D. Dissertation.

Dr. Michael P. Wolcott, who supervised my Post-Doctoral work at West Virginia University, Division of Forestry, Morgantown, WV, deserves tremendous credit for his gifted, scientific mind and for his friendship towards me.

Partners, colleagues at the University of Western Hungary, Sopron included: Drs. Zsolt Kovacs, Jozsef Szalai, Ferenc Divos, and Tamas Fodor. Without their significant contributions, many of our joint projects would not have been possible.

Dr. Laszlo Bejo and Dr. Balazs G. Zombori[1] *- former graduate students - should receive enormous appreciation for their exceptional research work during the course of their studies. Their attitude made my life as a faculty member more bearable. Dr. Levente Denes a Ph.D. student at the UWH, Post-Doctoral Fellow and Visiting Professor at WVU, remarkably contributed to the works presented here.*

Dr. R. Bruce Anderson a scholar, colleague and friend should receive my sincere appreciation for providing guidance in the "jungle" of technical writing in English. Without his help and valuable comments this manuscript would have been just a technical term paper written by an undergraduate sophomore.

Last but not least, I owe immense gratitude to my wife Marietta and to our son Aurel. They believed in the recovery from a deep, dark period of my life and gave me the will, moral and physical support, encouragement and love that I badly needed to undertake this very challenging endeavor.

[1] *Tragically, Balazs G. Zombori was killed in a car accident in 2003. It was a senseless death for a very talented young individual.*

TABLE OF CONTENTS

CHAPTER I

"WE MAY USE WOOD WITH INTELLIGENCE IF WE UNDERSTAND WOOD."

FRANK LLOYD WRIGHT
(1867 – 1959)

I. General Introduction

Throughout human history, wood has been a readily available, natural material that is easy to exploit and work with. Trees provided shelter, comfort, tools, vehicles and weaponry over millennia for individuals and societies. Being a biological origin material wood is porous, anisotropic and inhomogeneous. Furthermore; wood can be characterized by complex organic compounds that form elementary fibers, cell walls, cells and tissues. Because of its hygroscopic nature, depending on the ambient temperature and relative humidity, wood may change its shape and dimensions significantly. Consequently, its processing and utilization for various purposes has always called for appropriate knowledge and expertise.

Even the remaining wooden artifacts from the ancient Egyptian times demonstrate efforts to improve the aesthetic and strength properties. Over thousands of years these quality improvement practices made substantial progresses. All of these can be observed on the Renaissance, Baroque and Rococo masterpieces of furniture and interior wooden structures. The cross-laminated veneers in these hundreds of years old artifacts were to preserve the size, shape and trouble free functional operations.

The logs or the stem of trees, initially by instinct and later deliberately, have been used as load supporting structural elements since the Stone Age. The prime applications of debarked and sawn timber triggered improvements in changing the limited dimensions of the available stock; including elongations and the increase of width and thickness. These innovative processes are going on from the ancient time to present date.

Byproducts of rough woodworking like chips and shavings as a result of ax forming and debarking usually were used as fuel. At the end of the XIXth and at the beginning of the XXth centuries with the advancement of synthetic resin technology rapid improvement occurred in the manufacture of different wood-based composites.

Besides the introduction of plywood and the waste utilizing particle board and fiberboard; however, the first definitely load supporting wood composite, the glued-laminated timber, gained acceptance only in the 1950's (Moody and Hernandez 1997). Another version of structural wood composites, the I-joists, was developed during the II World War in the aircraft industry. The favorable strength to weight ratio made these products very competitive, albeit their civil application was introduced only during 1960's (Nelson 1997).

I.1 The Unique Mechanical Characteristics of Wood

From engineering point of view, the most valuable part of trees comes from the stem after logging. The body of solid wood is primarily composed of hollow, tube-like, elongated cells that are arranged parallel to each other along the longitudinal direction of the trunk of a tree. Additionally, the alternating early wood late wood rings provide the unique layered feature of solid wood. Although solid wood is more or less cylindrically orthotropic in nature; it is frequently treated for simplicity as an orthogonally orthotropic material. *Figure I.1* shows the principal directions of orthotropy on a pine block where *L*, *T* and *R* represent the longitudinal, tangential and radial directions, respectively. Arrows pointing out the macroscopic layered

structure of wood where ***a.*** indicates the early- or springwood and ***b.*** marks the late- or summerwood comprising an annual ring.

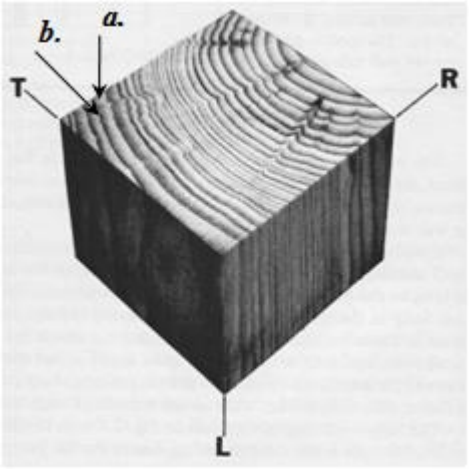

Figure I.1. *Orthotropic axes of a solid wood block, Loblolly pine (Pinus taeda) (Adapted from Hoyle and Woeste 1989).*

Unfortunately, the geometric and orthotropic axes seldom coincide. The deviation of the global and orthotropic coordinate systems may originate from the taper of the logs, and from growing defects, such as spiral and diagonal grain. This attribute of wood is generally called as cross grain. Therefore, the mechanical property determinations of cross grained load bearing wood elements require three dimensional transformations of known strength and stiffness values in the principal anatomical directions. However, experimental and theoretical works have shown that 3-D transformations for solid wood are not always trustworthy. Nevertheless, in the principal anatomical planes (i.e., *LT, LR* and *TR*) the transformations are quite reliable (Bodig and Jayne 1993, Goodman and Bodig 1970). During the research works presented here such transformations were frequently used to predict strength and stiffness values of oblique specimens. The appropriate Chapters or their Appendices contain the detailed descriptions and derivations of these transformations.

An orthotropic material is characterized by six elastic constants and six Poisson's ratios. Exercising the notations related to the coordinate system of the principal anatomical directions: E_L, E_R, E_T are the *moduli of elasticity*, G_{LR}, G_{LT} and G_{RT} are the *shear muduli* or *moduli of rigidity*. Finally, the six Poisson's ratios are: ν_{LR}, ν_{RL}, ν_{LT}, ν_{TL}, ν_{RT} and ν_{TR}. Literature values of these characteristic mechanical properties for wood species involved in these research works are compiled in *Tables A.I.1 – AI.3* in *Appendix I.*

The assumption of rectilinear orthotropy introduces errors in determination of elastic constants of solid wood. *Figure I.2* illustrates the effects of location and size of lumber cut from logs on the relative magnitude of these errors. The minimum error occurs when the lumber is cut from the edges of the log (*1, 6*). Because smaller radius of annual ring curvature is linearized,

the error toward the pit increases (*2, 3*). By decreasing the size of the specimens in the tangential direction toward the pit, the error remains fairly constant (*4, 5 and 6*).

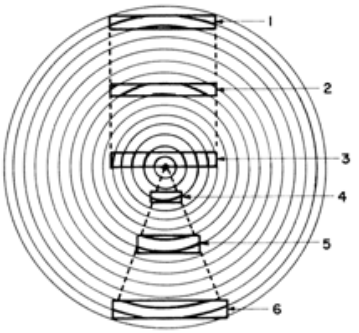

Figure I.2. *Errors in orthotropic models for wood by size and location of lumber in the log. Legend described in text (Bodig and Jayne 1984).*

In assessment of strength and stiffness properties of wood or wood-based composites by short term testing the assumption of elasticity is quite reasonable. However, the long term time-dependent stress-strain behavior of wood indicates elastic, plastic and viscous attributes. The dominancy among these three behavioral characteristics depends on a number of factors including moisture content temperature, magnitude, alignment and duration of load and loading history just mentioning a few. From both technological and engineering points of view creep and relaxation are critical rheological features of wood and wood composites. However, the in depth discussion of these rheological characteristics is beyond the scope of this dissertation.

I.2 Key Physical Properties of Wood

Density and moisture content are the two most crucial physical characteristics of wood and wood based composites. Both have notable effects on mechanical properties such us strength, stiffness and rheological attributes. Because the gravitational acceleration varies by altitude over the sea level and influenced by the latitude on the Earth, one can expect the variation of weight density (ρ) by these two factors. To eliminate the discrepancies a normalized weight density or *specific gravity* (*SG*) is frequently used. By definition the specific gravity is given as follows:

$$SG = \frac{mg / V}{m_w g / V_w} \qquad (I.1)$$

where the unknowns m, m_w and V, V_w stand for the mass and volume of substrate and water, respectively and g represents the gravitational acceleration. After simplification and setting the two volumes equal, we can state that in terms of general physics, the specific gravity is the mass or weight of the substance divided by the mass or weight of equal volume of water. This physical property is dimensionless and independent from any gravitational forces. Furthermore, it is compatible with both measurement systems. Consequently, it is used frequently as a

measure of wood compactness throughout this work along with the SI unit of mass (weight) density.

For hygroscopic materials a slightly different definition applies. Accordingly, the SG is the ratio of the oven-dry mass (m_0) to the mass of water ($V\rho_w$) displaced by the bulk specimen at given moisture content. Expressed by a mathematical formula:

$$SG = \frac{m_o}{V\rho_w} \qquad (I.2)$$

Life without water is nonexistent. Wood as a biological material during its life cycle and beyond always contains large amount of water. Because of the hygroscopic nature of many chemical compounds in wood, moisture is present even after the tissues and cells are already dead. There are two distinct types of water that occurs in wood including chemically bound water to the macromolecules in the cell walls and the free or capillary water that may be present in the cells' cavities (i.e., in the lumen). The bound water is attached to the free hydroxyl groups of polymers mostly to the hemicelluloses and to the cellulose chains in the amorphous region by hydrogen bounds. The capillary or free water may or may not be present in the lumens. Nevertheless, the net moisture of a wood sample can be calculated according to the following equation:

$$MC = 100u = 100\frac{W_{wt} - W_o}{W_o}(\%) \qquad (I.3)$$

Where *MC* is the moisture content by %, *u* is the fractional moisture content, W_{wt} is the original, wet weight of the sample and W_0 denotes the oven-dry weight.

A distinct moisture condition of solid wood - the fiber saturation point (*FSP*) - is defined as the amount of water necessary to saturate the cell walls, but without any free water in the cells' lumens. *FSP* is very species specific, higher extractive contents usually results in lower *FSP*. The absorbed or bound water is especially important because it modifies the physical and mechanical properties of solid wood and wood composites. Free water has no significant effect on these attributes unless it is frozen. The fiber saturation point may vary between 20 to 30 % *MC*. Its determination by various methods gives somewhat ambiguous results. Nonetheless, for species having low extractive content the *FSP* is assumed to be between 25 and 30 % (Bodig and Jayne 1982).

The hygroscopic nature of solid wood and wood based composites means that a wooden object is able to gain or lose moisture from the surrounding environment. Air and liquid water are the most frequent surroundings. The amount of bound water in wood depends on the air temperature (*T*) and relative humidity (*RH*). While submerged in water, after reaching the *FSP*,

the cavities of the lumens in wood fill up with free or capillary water. Small amount of free water may accumulate as condensate in the lumen in case of abrupt drop of air temperature that had high *RH*. If a block of wood is kept long enough in constant environmental conditions (i.e., constant *T* and *RH* or submerged in water) the block will reach a steady state moisture content termed as equilibrium moisture content (*EMC*). The relationship among densities (ρ), specific gravity (*SG*) and moisture content (*MC*) is manifold. The interested reader may get more in-depth information from the literature (Faipari Kézikönyv I. 2000; Siau 1984 and 1995).

Below *FSP* any loss or gain in moisture is always accompanied by dimensional changes that can be calculated by the general formula:

$$S_{T,R,V} = \frac{d_{MC} - d_0}{d_0} 100 \ [\%], \qquad (I.4)$$

Where $S_{T,R,V}$ represents shrinkage or swelling. Indexes denote the principal anatomical directions in which the changes were measured. Subscript $_V$ indicates volumetric values. Variables d_{MC} and d_0 are the wet and oven-dry dimensions, respectively. Although, the shrinkage and swelling may be linearly related to the moisture content below *FSP*, the expansion and contraction have different rates of changes in dimensions per *1 % MC* changes. These features are termed as coefficients of moisture expansion/contraction with the unit *m/m/%*. Furthermore, both the total shrinkage and swelling have different values in the different anatomical directions. For woods grown in the temperate region the average total shrinkage or swelling ratios from *0% MC* to *FSP* are as follows: $S_V:S_T:S_R:S_L$ = *1:0.63:0.34:0.03*,where S_L = 0.03 the longitudinal shrinkage is practically negligible (Faipari Kézikönyv I, 2000). However, cross-grain wood can shrink significantly. The anisotropy of shrinkage may result in deformation of lumber after drying. *Figure I.3* shows some of these distorted shapes as a function of the location in the trunk.

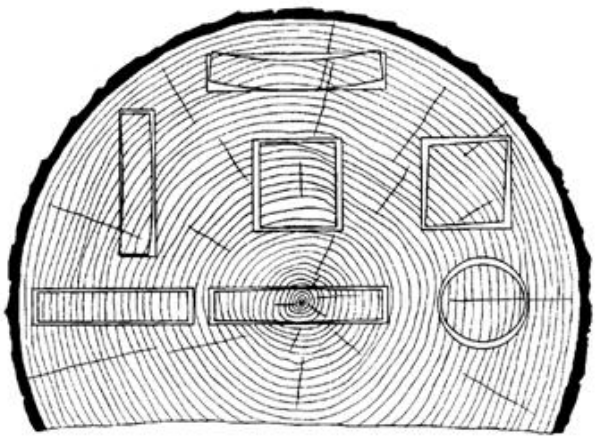

Figure I.3. *Deformed shapes of various cross sections of lumber, after drying, cut from different location of the log (U.S. Forest Products Laboratory, Wood Handbook 1999).*

In *Appendix I, Table A.I.4* contains the average green specific gravity and total shrinkage values of selected hardwoods.

I.3 Environmental Modifiers

It is well known that the ambient relative humidity and temperature controls the adsorbed water in wood and wood-composites. Hence, the effect of temperature and moisture content as environmental modifiers on the mechanical properties is briefly discussed next. The influence of temperature on the stress-strain relations and creep behavior of wood is schematically represented in *Figure I.4*.

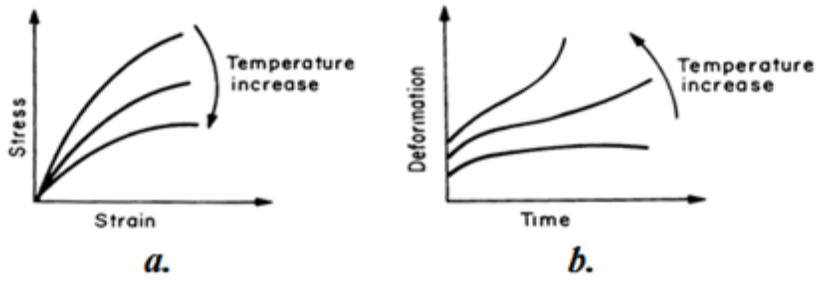

***Figure I.4**. Schematic representation of the effect of temperature on the stress-strain (**a**.) and creep behavior (**b**.) of wood and wood-composites (Adapted from Bodig and Jayne 1984.)*

Experimental data indicate linear decline of modulus of elasticity and strength values by increasing temperature (Bodig and Jayne1984). Increasing temperature accelerates the creep at every stage and increases the deformation at failure.

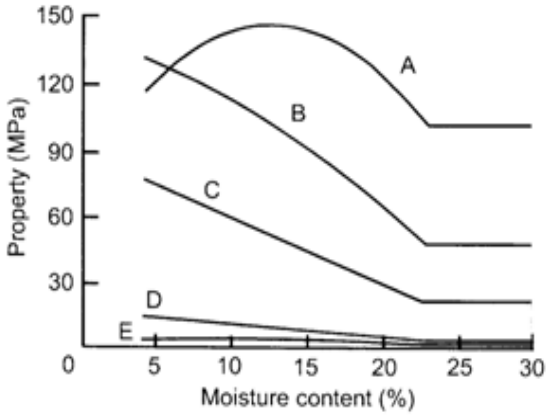

***Figure I.5.** The effect of moisture content on the strength properties of wood. A tension parallel to the grain, B bending strength, C compression parallel to the grain, D compression perpendicular to the grain and E tension perpendicular to the grain (Wood Handbook 1999).*

At constant temperature, the most properties increase with decrease of moisture content changes below the fiber saturation point (*FSP*). *Figure I.5* demonstrates these average adjustments for a number of species at normal (~ 21℃) temperature. The relationship that describes these changes between 12 % MC and FSP can be approximated by a negative

exponential function. However, care should be exercise adjusting properties below 12 % MC. While the majority of species demonstrate increase of mechanical properties with drying, some species may be erratic in response for a certain property/*MC* combinations.

The combined effect of temperature and moisture content on the mechanical properties of wood and wood composites is depicted in *Figure I.6* at two moisture content levels. At room temperature hardly any differences can be observed, however, significant increase or decrease in mechanical properties take place below and above 20 ℃, respectively.

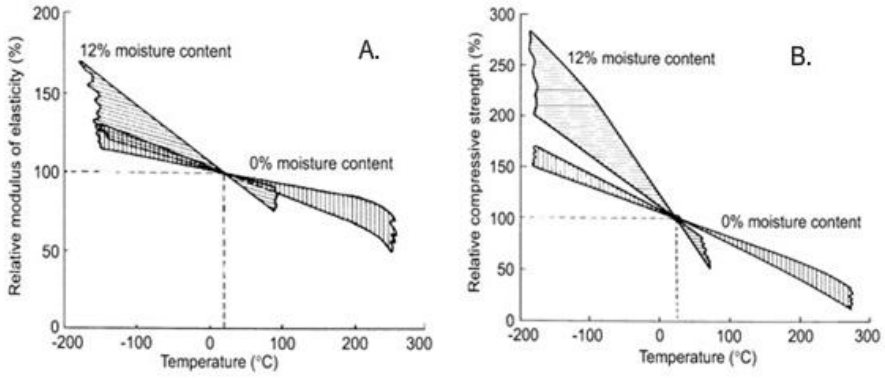

Figure I.6*. The effect of temperature at two moisture content levels relative to the values at 21°C.* ***A*** *modulus of elasticity;* ***B*** *compression strength parallel to the grain. (Wood Handbook 2000)*

The plots are composites of several test results performed on different wood species. The width of the bands illustrates the variability between and within reported trends. The significant effects of the environmental modifiers indicate that all research dealing with wood and wood-based composites should be conducted in controlled environment. Reports must include the specifications of ambient temperature and relative humidity. Special treatment such as hot water bath or any treatment by chemicals including surface finishing, staining or resin coating requires the specification of the agents. The application volumes and methods need to be identified as well. The proper description of ambient and treatment conditions ensure the comparison of research data and repeatability of experiments.

I.4 About Modeling

The general purpose of a model or theory is to establish a framework - based on scientific observations - which can explain or predict phenomena. Major features of models include supporting data, logical sequence of events, expected outcomes and validation possibilities. The later include a simulation that is the implementation of a model. Usually a steady state simulation provides knowledge about the system's behavior at a particular time. On the other hand, a dynamic simulation supplies information over a period of time. One might say that the simulation brings a model to life. Thus, the model shows how a particular object or phenomenon will behave. Changing the parameters in a model optimization of performance

characteristics and/or processing may be achieved. Furthermore, the two major types of models include deterministic and probability or stochastic models. The first is a mathematical model in which outcomes are precisely determined through well established relationships among states and events, excluding any random variation in input parameters. In comparison, stochastic models use probability distributions for generating input variables. Consequently, the outcome of a stochastic model is never the same. Scientific models or concepts should remain open to revisions. As additional research develops new data and different approaches can refine a model.

Wood, being a biological material, has substantial variation in physical and mechanical properties. Therefore, a combination of deterministic and stochastic models or one of these alone have been used in some of the research projects discussed in this Dissertation.

I.5 Products and Technologies

Three of the research works discussed in later Chapters dealt with prefabricated, structural, composites and newly developed products. The purpose of this short section is to provide elementary information about existing structural composites and their manufacturing technologies. Detailed provisions and the discussion of technologies regarding the innovations are provided in the appropriate Chapters of this work.

Four existing products were involved in the works presented here. These structural wood-based composites have well defined material properties and developed manufacturing technologies (Lang 2006). *Figure I.7* illustrates these products followed by brief descriptions and technological specifications.

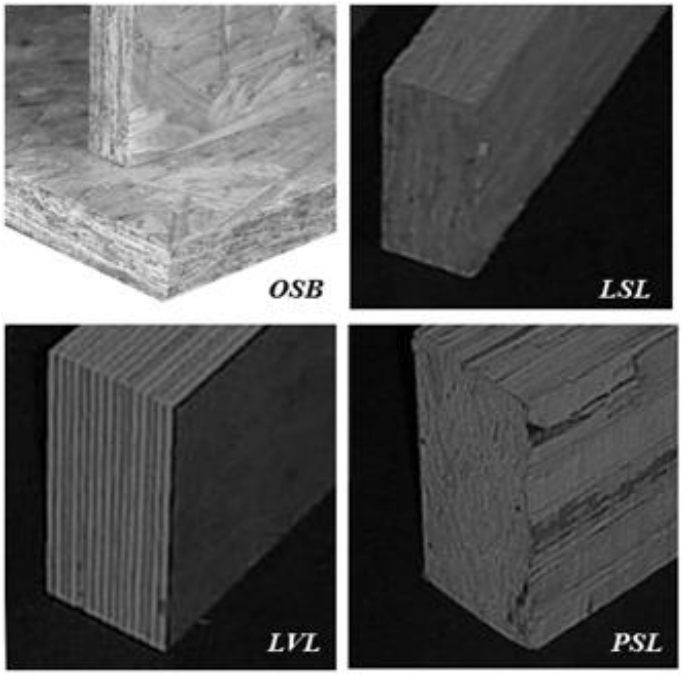

***Figure I.7**. Structural wood-based composites. **OSB** – oriented strand board; **LSL** – laminated strand lumber; **LVL** – laminated veneer lumber; **PSL** - parallel strand lumber.*

OSB - A type of layered particle panel product composed of strand-type flakes which are purposely aligned in directions (usually perpendicular) which makes a panel stronger, stiffer and with improved dimensional properties in the alignment directions. Usual constructions have an odd number of layers; 3 to 5. Outside layers are called faces, inside layers are called the core. Common thickness ranges from 6 to 20 mm with panel size of 1.33 x 2.66 m. Material components include wood strands (flakes), ring or disk flaked having approximate dimensions of 1 mm in thickness and ~ 12 x 150 mm width and length. Preferred species are: softwoods: Southern pine; hardwoods: Aspen, yellow-poplar and other various medium density hardwoods. Adhesives types: phenol-formaldehyde, isocyanate (pMDI) for exterior grades.

LSL - Laminated Strand Lumber is an engineered load bearing composite product, manufactured from highly consolidated wood strands. Strands are produced from logs or bolts by disk flakers. Strands are 300 mm long or less and are highly oriented parallel to the longitudinal axis of the panel. Strand widths are oriented parallel with the panel width. Material components consist of strands ~1 mm in thickness, having random width (12 – 75 mm). Preferred species are: aspen, yellow-poplar, mixed-softwood and hardwoods. The product has comparatively low resin content <10%, which is usually isocyanate cross-linked PVA.

LVL - is a beam element produced from laminates of structural veneer (~ 3mm in thickness).Veneer is laminated vertically for most application. Overlap, scarf and butt joints are used to end-joint the laminates. All laminates are oriented parallel to the longitudinal axis of the beam. Material components comprise structural (peeled) veneer sheets (1.33 x 2.66 m). Preferred species group: Hem-Fir, Southern pine, yellow-poplar. Typically phenol-formaldehyde resin is used for lamination and isocynate x-linked PVA for regluing.

PSL - is a beam/column element produced from consolidated veneer strands. The process is similar to poltrusion. Resin is cured by radio frequency microwaves. Strands are cut from structural veneer (~3 mm thick). Veneer is chopped into ~ 25 mm wide strands and are 2.66 m or less in length. Strands have some orientation within the cross section, however, are highly oriented to the longitudinal axis of the beam. Material components: structural veneer strands. Preferred species: Hem-Fir, Southern pine, yellow-poplar. Resin is a phenol-formaldehyde type applied by roller or curtain coating (~ 15%).

The furnish materials for the newly developed wood composite were mostly decorative veneer residues and some peeled structural veneers. *Figure I.8* shows the schematic of slicing and peeling operations.

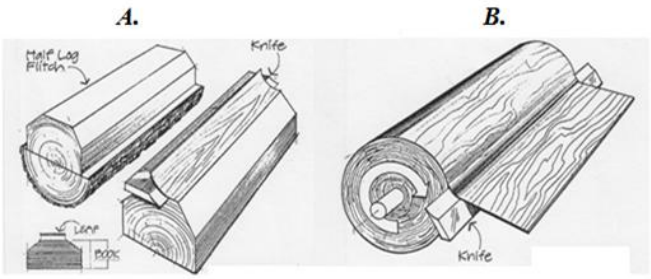

Figure I.8. *Methods of veneer manufacturing: A. - plain slicing; B. – rotary cut or peeling (unknown source).*

After plasticization and pre-shaping of logs, the plain slicing operation produces veneer leafs by a horizontal cutting action of the long knife (*A*). Note, that the resulting thin wooden plates have changing orthotropic properties because of the transition between *L-T* and *L-R* anatomical planes as the knife approaching the center of the log. Rotary cut or peeling operation produces a long veneer ribbon along an Archimedean spiral. This is then cut to the standard size of 1.33 x 2.66 m sheets. The process results in an almost perfect orthotropic plate (*L-T*) where the thickness is in the *R* direction. However, properties can change significantly sheet by sheet because of the location of veneer cut relative to the center of the log (i.e., sapwood, heart wood or Juvenal wood).

Finally, I-joists with newly developed, corrugated web panels are mentioned. The flanges of these structural elements were manufactured from LVL, PSL or solid pine wood. The discussion of these joists may be less detailed because of intellectual property rights.

The reader should bear in mind that solid wood itself, even in strand or veneer forms, is a complex composite material in molecular, micro and macroscopic levels. Therefore, the mechanical and physical characterization, development and design of wood-based composites require reasonable compromises that incorporate the natural variability of the wood constituents.

I.6 Closure of Chapter I

The field of wood and wood-based composite science is very broad. Many books and publications are available on separate aspects of wood science and technology (Ashkenazi 1976, Panshin and de Zeeuw. 1980, Tsoumis 1991, Szalai 1994, etc.). Here, the mechanical and physical characteristics of solid wood were briefly outlined that may help the better understanding of wood as a natural origin raw material for thousands of uses. The author feels that this basic knowledge is imperative to comprehend the overall behavior of wood in ever changing environmental conditions. For some readers there are obvious details, for others the entire Chapter might be unfamiliar. Nevertheless, this Introduction tried to summarize the essential features of solid wood with the hope that it is deep enough to provide valuable facts and information and short enough to avoid redundancies and tediousness.

References I

1. Ashkenazi, E. K. 1976. Anisotropy of Wood and Wood-Base Materials. First edition. (in Russian) Izdatelstvo Lesnaja Promuslennosty. Moscow, USSR.
2. Bodig, J. and J. R. Goodman. 1973. Prediction of Elastic Parameters of Wood. Wood Science, (4):249-264.
3. Bodig, J. and B. A. Jayne, 1982. Mechanics of Wood and Wood Composites. Van Nostrand Reinhold Co., N.Y. 712 pp.
4. Faipari Tudományos Alapítvány, 2000. Molnár, S. szerk. Faipari Kézikönyv I. FTA, Sopron, 428 pp.
5. Forest Products Laboratory. 1999. Wood Handbook: Wood as an Engineering Material. Washington DC: U.S. Department of Agriculture. 384 pp.
6. Goodman, J. R. and J. Bodig. 1970. Orthotropic Elastic Properties of Wood. J. Struc. Div. ASCE 96(ST11):2301-2319.
7. Hoyle, J.and F., Woeste.1989. Wood Technology in the Design of Structures**.** 5th Edition. Iowa State University Press, Ames, IW, 394 pp.
8. Láng, E. M. 2006. WDSC 465 Wood-based Composites. Digital lecture notes. West Virginia University, Division of Forestry and Natural Resources. Morgantown, WV. Slides: 535.
9. Molnár S. 1999. Faanyagismerettan. Mezőgazdasági Szaktudás Kiadó, Budapest. pp. 467.
10. Panshin, A. J, and C. de Zeeuw. 1980. Textbook of Wood Technology. Vol. I, 4th Edition. McGraw Hill, New York, NY. 722 pp.
11. Siau, J. F. 1995. Wood: Influence of Moisture on Physical Properties. Department of Wood Science and Forest Products, VPI&SU, Blacksburg, VA, 227 pp.
12. Siau, J. F. 1984. Transport Processes in Wood. Springer Verlag, Berlin, Heidelberg, New York. 245 pp.
13. Szalai, J. 1994. A Faanyag és Faalapú Anyagok Anizotróp Rugalmasság- és Szilárdságtana I. rész: A Mechanikai Tulajdonságok Anizotrópiája. Private Edition, 398 pp.
14. Tsoumis, G. 1991. Science and Technology of Wood. Van Nostrand Reinhold, New York, NY, 494 pp.

List of Figures I

Nomenclature I

Upper case letters:

E	*modulus of elasticity*
EMC	*equilibrium moisture content*
FSP	*fiber saturation point*
G	*modulus of rigidity*
L,R,T	*anatomical directions*
LSL	*laminated strand lumber*
MC	*moisture content*
OSB	*oriented strand board*
PSL	*parallel strand lumber*
RH	*relative humidity*
S	*shrinkage, swelling*
SG	*specific gravity*
T	*volume*
V	*temperature*
W	*weight*

Lower case letters:

d	*dimensions*
g	*gravitational acceleration*
m	*mass*
u	*Fractional moisture content*

Greek letters:

ρ	*density*
ν	*Poisson's ratio*

Subscripts:

0	*oven dry, initial*
L,R,T	*anatomical direction indexes*
MC	*at the given moisture content*
w	*water*
wt	*wet*

CHAPTER II

JOHN VON NEUMANN

(1903 – 1957)

"ANYONE WHO ATTEMPTS TO GENERATE RANDOM NUMBERS BY DETERMINISTIC MEANS IS, OF COURSE, LIVING IN A STATE OF SIN."

II. Modeling the Consolidation of Wood-strand Mats

II.1 Introduction

From the late 1980's, oriented strand-board (OSB) became a dominant structural panel material for the construction industry. Gradually replacing plywood by the early 90's, OSB manufacturers were seeking research supports to improve the performance properties and manufacturing technologies of their products. Research institutes and universities with wood science programs had no difficulty obtaining research grants from the industry and from Federal and State Government agencies. However, at the turnover of the millennia this golden age of OSB research started to deteriorate. The global economic crisis penetrated into the wood composite industry. The decreasing number of new commercial and residential constructions resulted in declining demand for structural panels. Currently, most of the OSB manufacturing plants in North America are running at half capacity. Nevertheless, during the past two decades significant volume of research was devoted to explore the different aspects of OSB manufacturing. This Chapter describes one of the early attempts to model the consolidation of strand type composites.

During the hot–pressing of OSB, a loosely formed combination of adhesive and wood material is consolidated into a contiguous composite panel. For laminated wood composites such as plywood, laminated veneer lumber (LVL) and glued laminated beams, the material structure after consolidation is primarily dictated by the geometry of the constituting wood elements. However, for materials produced with discontinuous constituents like fibers, particles and strands, the final material structure is governed by not only the wood elements itself, but the forming method and the pressing operation as well.

With non-veneer composites, void space is incorporated into the wood mat (*Figure II.1*) as a consequence of the forming operation. The goal of pressing is to remove the void space that separates the individual wood elements, thereby providing contact between strands and promoting adhesion. Heat is used in this operation to both soften the wood components and accelerate the cure of the adhesive.

Figure II.1. *A typical OSB mat after formation.*

During the 1960's, at the beginning of the introduction of OSB the vertical density distribution of strand mats was investigated (Suchsland, 1962). Later, Suchsland and Xu (1989) researched the horizontal density distributions. Results were related to the internal bond strength and thickness swell properties of the OSB panels. Focusing on the wood component, the non-linear transverse compression behavior was studied by Wolcott at al. (1989a). Wolcott's model for structural collapse of wood strands was based on the theories of cellular materials. The influence of heat, moisture on polymer viscoelasticity was studied by Wolcott at al. (1990). Experimental data for various mat density gradients agreed well with analytical results.

Dai and Steiner (1993) were the first to address the relationship between mat forming and the static stress-strain behavior during consolidation. Their model was based on the infinite summation of overlapping strands. The model worked well in the higher stress region. Later, they realized the importance of spatial characteristics of the mat and the forming process and gave rationale to further model developments (Steiner and Dai 1994). Furthermore, parallel to this work presented here, Dai and Steiner (1194a, 1994b) published two papers on simulation modeling of randomly formed mat structures. During the last 15 years since our model was developed several researches targeted the oriented strand board manufacturing processes from different directions. Unfortunately by the time of 2005, due to the moribund global economy, research on OSB declined significantly.

II.2 Objectives

In order to better understand the wood composite manufacture, a fundamental model was developed to describe the mechanical behavior of wood-strand mats during the pressing operation. Although the consolidation involves heat and mass transfer phenomena that have significant effect on the stress-strain relation during hot pressing, investigation of these physical events were beyond the scope of this study. To achieve the ultimate goals of the project, two major tasks with specific objectives were targeted as follows.

1. Development of a conceptual model for mat structure characterization.

   1.1 To experimentally measure the relevant parameters in randomly formed wood strand mats.

   1.2 To develop and statistically validate a simulation procedure to reconstruct the mat structure.

   1.3 To experimentally validate the model.

2. Development of a mathematical model based on solid mechanics to approximate the stress response of randomly formed wood-strand mats under compression.

   2.1 Experimentally validate the model by comparing the behavior of realistic mats to the model predictions.

   2.2 To determine the model sensitivity to the changes of variables describing the mat structure.

To achieve the objectives we divided the research into two different segments. The first part dealt with reconstruction of virtual mat structures via stochastic modeling (Monte Carlo simulation). After validation of the reconstruction model, a stress response concept was formulated to describe the stress-strain behavior of the mats under cold pressing.

II.3 Background and Concept of the Mat Characterization

To characterize a randomly formed, wood-strand mat several characteristics such as strand size and geometry, their position and orientation can be used. Although some of these parameters are either fully or partially controlled in manufacture, they all remain stochastic parameters to a certain degree with statistical variability. For this reason, any modeling effort must incorporate methodologies using statistical principles that allow a mat structure to be recreated with computer simulation.

Suchsland (1962) studied the density distribution of flake boards – the precursor of OSB – and he modeled the mat as a system of columns that contain horizontally stacked flakes. It was hypothesized that the numbers of flakes in the imaginary columns follow a binominal probability distribution. Dai and Steiner (1994a, b) stated that the formation of random strand mats may be adequately modeled by the Poisson distribution of strand centers and strand coverage.

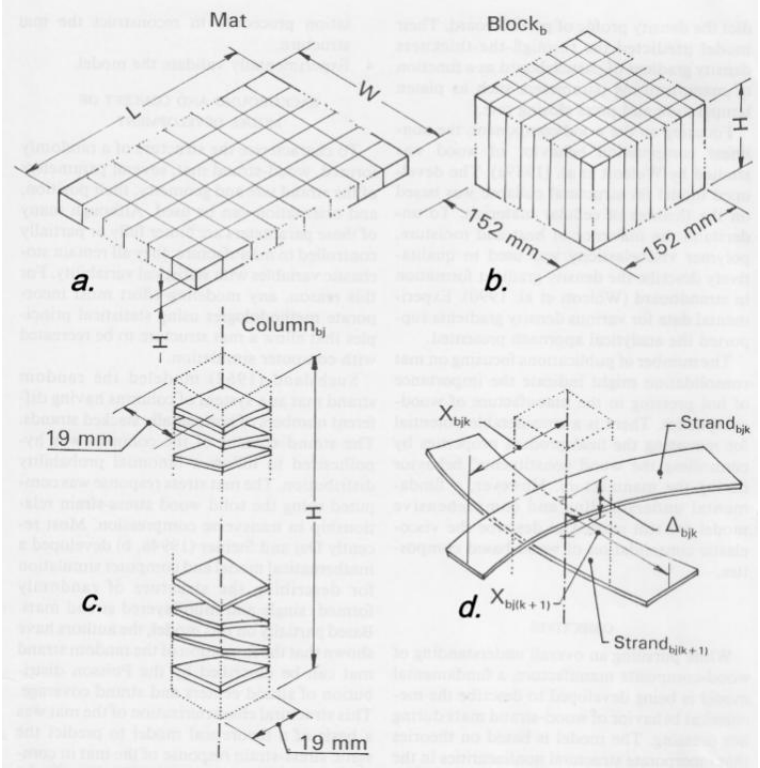

Figure II.2. *A schematic of the conceptual model to characterize the mat structure.* ***a****.- an arbitrarily sized mat divided into blocks;* ***b.****- experimental block divided into 64 columns;* ***c.****- the theoretical structure of a column;* ***d.****- the random position of the strands and the interpretation of the spatial variables.*

We used somewhat different method to characterize and digitally preserve mat structures for further incorporation to a deterministic model which predicts the static stress-strain behavior under cold pressing. *Figure II.2* shows the concepts of our mat characterization model.

Accordingly, an arbitrarily sized mat was divided into square sample blocks (152 x 152 mm). Each block was further divided into effective columns. The column width was 19 mm square (the average size of the strand width). This resulted in 64 columns within a block.

The following variables characterized the mat structure (*Figure II.3*):

1. The number of overlapping strands in a column (N_{bj}).
2. The distance between the adjacent strands measured at the hub of the column or as further referred to as void height (Δ_{bjk}).
3. The location of the column centroid relative to the strand length (X_{bjk}).
4. The average height of the sample block/mat (H).

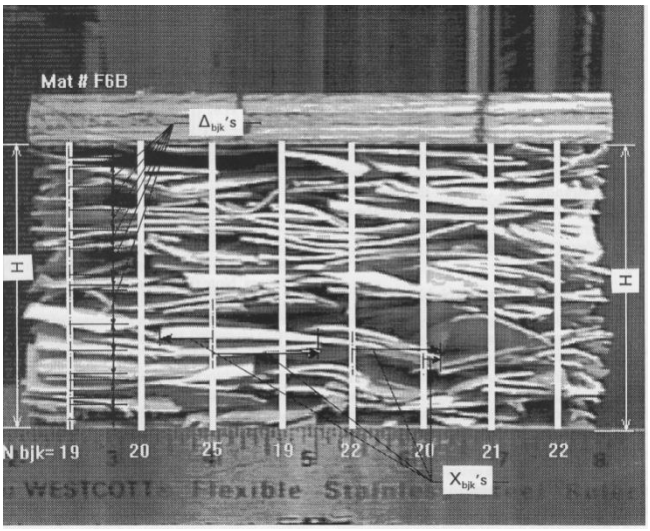

Figure II.3. *Digitized images of one side of a sample block showing the spatial mat characteristics.*

The subscripts b = 1,…,20; j = 1,…,32 and k = 1,…,N_{bj} denote the block, column and strand numbers, respectively. Accordingly, measurements of 640 columns from 20 sample blocks were used for database development. Note that although each block was divided into 64 columns, only 32 column hubs along the perimeter of the block could be measured without disturbing the initial mat structure. The average mat height (H) was considered as control variable because the overlapping strands with constant thickness (h = 0.8 mm), and the void height between the adjacent strands within a column control the initial height of the mat according to the following:

$$H = \Sigma\Delta_{bjk} + hN_{bj} \qquad (II.1)$$

The next section presents the development of the simulation procedure to generate arrays of the mat structural characteristics (N_{bj}, Δ_{bjk} and X_{bjk}). In general the simulation should maintain the marginal distributions and preserve any correlation structures of the multiple random variates. Statistical methods used to validate the simulation procedure are also presented.

II.4 Simulation Routine Development

II.4.1 Materials and methods for data base assessment

Twenty sample mats (blocks) were manufactured from uniformly sized (0.8 x 19 x 70 mm) strands. Mats were prepared by hand forming in a 305 x 305 mm box with removable bottom. The central section, having a base of 152 x 152 mm, was cut out with a large paper shear. This technique eliminated the edge effect and the sample blocks were considered as a section of a randomly formed mat. The mat was formed to a target density of 600 kg/m^3 based on 13 mm final panel thickness. From each side of the blocks, a scaled video image was acquired and analyzed with a computerized data acquisition system (*Figure II.3*). On the images eight column centroids were marked 19 mm apart. For each column the number of overlapping strands were manually counted and recorded. The acquisition system recorded the average height (H) of each mat image. In addition one hundred concomitant void height (Δ_{bjk}) and location (X_{bjk}) values were assessed.

Table II.1. *Descriptive statistics of sample mats' variables.*

Statistics	λ_b	N_{bj}	X_{jk} *(mm)*	Δ_{jk} *(mm)*	***H*** *(mm)*
Mean (μ)	24.42	24.17	12.69	3.22	73.91
Std. Dev.(σ)	1.82	3.89	7.86	2.37	3.56
Size (n)	20	640	100	100	20
Min.	21.62	10	2.65	0.71	67.06
Max.	28.38	42	38.72	14.56	80.52
Skewness	0.28	0.12	1.65	2.48	-0.25

λ_b - average overlapping flake numbers in 32 columns of a sample mat.

Table II.1 contains the descriptive statistics of the acquired parameters. Note, that the Δ_{bjk} and X_{bjk} measurements could be performed at strands whose lengths were aligned parallel with the image plane. Based on the average H values the bulk density of each sample block was calculated. The average overlapping strand numbers (λ_b) were approximated by computing the mean of the 32 counts at the column hubs along the perimeter of a sample block. The role of λ_b

is discussed later. The assessed data were analyzed for correlation structure and for the marginal distribution of the population.

II.4.2 The correlation structure and the probability distributions of the original data sets

The overlapping strand numbers (N_{bj}) were tested for lag-1 and lag-2 type serial correlations. The void height (Δ_{bjk}) and location (X_{bjk}) parameters were not consecutive measurements; therefore, no serial correlation tests were performed on these data sets. For void height, the serial correlation analyses were done for each block having an equal sample size of observation. Of the twenty sample blocks six showed only slight lag-1 type correlation, while only one lag-2 type correlation was detected. This result seemingly contradicts the fact that Dai and Steiner (1984b) observed spatial correlation between adjacent overlapping strand numbers in randomly formed aspen strand mats. However, the distance between the adjoining counts in their study was approximately 1/10 of their strand width (i.e., 9.31 mm). Such a high resolution must have serial correlation because a particular strand can be present in ten adjacent imaginary columns. In this work the overlapping strands were counted 19 mm (a strand width) apart from each other, showing no significant correlations.

In the next step, the correlation between void height (Δ_{bjk}) and location (X_{bjk}) data was investigated. The correlation coefficient $\rho_{\Delta X}$ = -0.0316 indicated no correlation between these variables. *Appendix II* contains some more information about the association between these variables. Finally, theoretical probability distribution functions were fitted to the data to determine the marginal distributions of the spatial variables. The parameters of the probability distributions were estimated by the least-squares method. Visual appraisal and formal goodness-of-fit test, such as Chi-square (χ^2) and Kolmogorov-Smirnov (KS) tests, helped to assess the estimated probability density functions. *Table II.2* contains the results of these tests.

Table II.2. *Summary of the Goodness-of-Fit test results. All tests were performed at 95 % confidence level, α=0.05.*

Mat properties	***Fitted distribution***	***Parameters***		***D.O.F.*** [c]	***Test Statistics & Critical Values*** [d]			
		μ	σ^2		χ^2	$c_{1-\alpha}$	KS	$c'_{1-\alpha}$ [e]
N_{bj}	Poisson(λ)	24.17	15.13	17	414.16	27.587	-	-
λ_b	N(μ,σ^2)	24.42	3.32	9	4.00	16.919	0.320	0.895
Δ_{jk}	LN(μ,σ^2)	0.98[a]	0.52[b]	17	12.40	27.587	0.545	0.895
X_{jk}	LN(μ,σ^2)	2.36[a]	0.25[b]	17	21.60	27.587	0.812	0.895

a. - mean of natural logarithms
b. - variance of natural logarithms
c. - degree of freedom
d. - test statistics and critical values were computed according to the relevant literature
e. - critical value of KS test when the parameters are unknown

For both location (X_{bjk}) and void height (Δ_{bjk}), the formal tests failed to reject the hypothesized lognormal (LN (μ, σ^2)) probability distributions (*Figure II.4* and *Table II.2*).

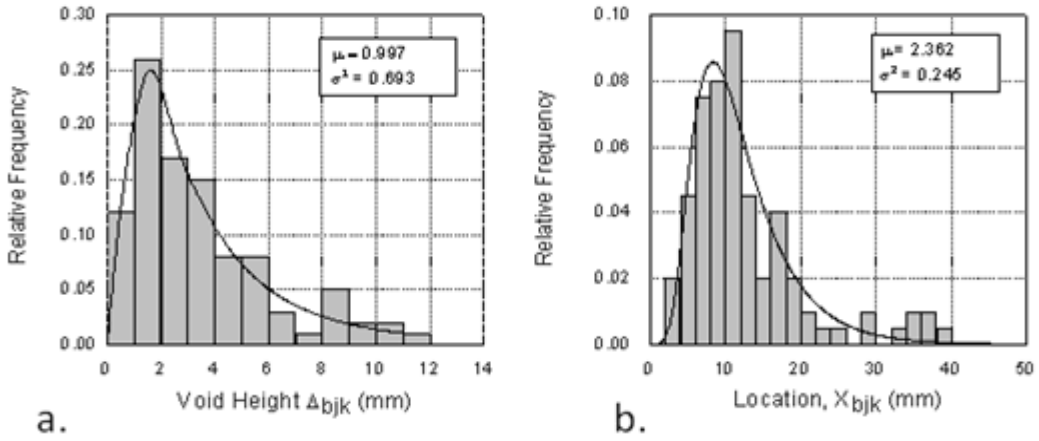

Figure II.4. *Frequency histogram of 100 observed void height (**a**.) and location (**b.**) data. The two-parameter lognormal density functions, with the parameters of natural logarithms listed, are overlaid.*

Based on the work of Dai and Steiner (1993, 1994a, b), it was theorized that the strand deposition in randomly formed OSB strand mats follows the Poisson process. However, formal tests rejected the null hypothesis that N_{bj} data came from Poisson (λ) distribution where λ is both the mean (μ) and the variance (σ^2). Note, that the 640 observations of N_{bj} values had a higher mean than variance (*Table II.2* and *Figure II.5a*).

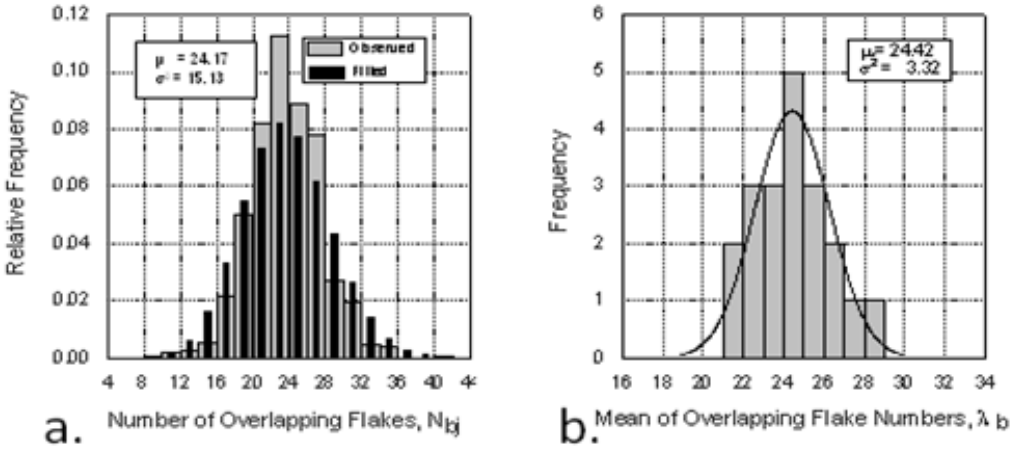

Figure II.5. *Frequency histograms of **(a.)** - 640 observed N_{bj} data and **(b.)** - 20 observed average overlapping strand numbers (λ_b) in 64 columns. The fitted Poisson (λ) and the normal probability density functions, with parameters listed, are overlaid.*

Truncated normal and several discrete probability distributions were fitted to N_{bj} data without success. This failure to specify the stochastic nature of the overlapping strand numbers might be attributed to the low resolution of the count and/or to the fact that the sample blocks were independently formed instead of being sections of a continuous mat.

To overcome the problem a new variable, the mean overlapping strand number (λ_b) was introduced to the simulation procedure. Because λ_b is an average of 32 N_j observations, it tends to be normally distributed according to the Central Limit Theorem. The parameters of this normal distribution are as follows:

$$\mu_{\lambda_b} = \mu_{N_{bj}} \quad \text{and} \quad \sigma_{\lambda_b} = \frac{\sigma_{N_{bj}}}{\sqrt{n}} \qquad \textit{(II.2)}$$

where n is the sample size. *Figure II.5.b* demonstrates the distribution of observed λ_b values. Because the Poisson λ was still the best estimate of N_{bj} data two key assumptions were made. First, the means of the overlapping strand numbers of the experimental blocks can be generated from a normal probability distribution. Second, using these mean values as different λs for each block to generate Poisson (λ_b) variates, the simulation would better approximate the parameters of the overall N_{bj} observation than generating from direct Poisson (λ) using only one mean and variance.

II. 4.3 The simulation routine

Based on the above discussed principles and assumptions, a simulation procedure was developed. The algorithm includes the following main steps.

1. The mean values of overlapping strands of 64 columns in a sample block were generated from normal probability distribution ($\lambda_b \in N(\mu, \sigma^2)$). The polar method (Law and Kelton, 1991) was used to produce normally distributed variates.
2. In the next step, using the λ_b values, 64 N_{bj} data were generated from the Poisson (λ_b) distributions for each sample block. The algorithm utilizes the relationship between Poisson (λ) and expo($1/\lambda$) distributions. The routine computes and stores the sum of the N_{bj} data by b = 1,…,20.
3. For the simulated blocks, according to the results of ΣN_{bj} values, the other two mat characteristics, such as location (L_{bjk}) and void height (Δ_{bjk}) were generated from the previously identified LN(μ, σ^2) probability distributions.

The details and justifications of generating random variates from N(μ, σ^2), Poisson (λ_b) and LN(μ, σ^2) probability distributions are given by Law and Kelton (1991) and in *Appendix II*. The routine for generating discrete and continuous random variates included a subroutine for

producing standard uniform U(0,1) random numbers. This FORTRAN subroutine was published by Etter (1987). Tests, recommended by the ASTM D 5124-91 standard, were performed to confirm the feasibility of this random number generator.

II.5 Result and Discussion of the Virtual Mat Formation

The applicability of the Central Limit Theorem to generate N_{bj} data is demonstrated on *Figure II.6a and b*. First, 20 λ_b values were produced (*Fig. II.6.b*) using the parameters of the observed data set (*Table. 3*). The resultant λ_bs helped to acquire 1280 N_{bj} data. This two-step

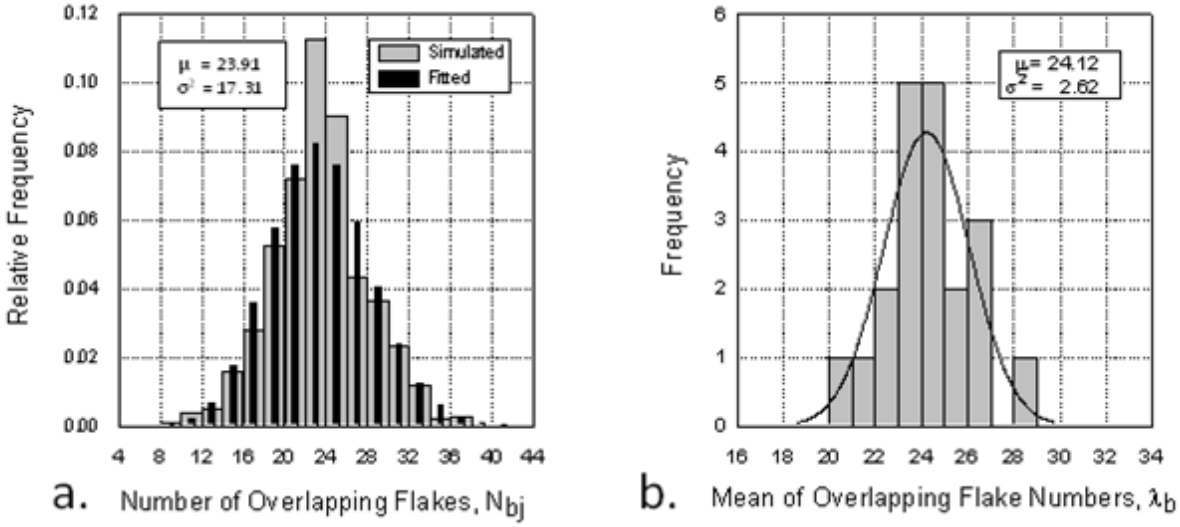

Figure II.6. *Frequency histograms of 1280 simulated overlapping strand numbers (**a.**) and 20 simulated average overlapping stand numbers (**b.**). The original Poisson (λ) and normal mass/density functions, with the parameters of simulated data listed, are overlaid.*

simulation practice produced equivalent distribution of N_{bj} data compared to that observed on 20 experimental blocks. The means and variances of the simulated and real data are very comparable (*Figure II.5a*, and *Figure II.6a*).

The other two mat characteristics generated from LN(μ, σ^2) distributions were visually evaluated. The simulation adequately preserved the marginal distributions and resulted in non-correlated structures similar to that observed (*Appendix II, Figure A.II.1*).

Table II.3. *Descriptive statistics for five replications of mat characteisticss' simulation.*

Repli-cation	λ_b			N_j				Δ_{jk} **(mm)**			X_{jk} **(mm)**			***H (mm)***		
	μ	σ	n	μ	σ	n	ΣN_j	μ	σ	n	μ	σ	n	μ	σ	n
1	24.12	1.62	20	23.91	4.29	64	1174	3.31	2.39	1174	12.78	8.44	1174	73.40	6.10	64
2	24.95	2.30	20	24.35	5.09	64	1274	3.46	2.49	1274	12.96	8.70	1274	74.20	6.30	64
3	24.98	2.07	20	25.31	4.46	64	1649	3.27	2.21	1649	13.08	8.51	1649	75.00	6.20	64
4	23.52	1.85	20	23.09	4.93	64	1425	3.31	2.40	1425	12.79	8.32	1425	73.90	5.90	64
5	24.31	1.53	20	24.79	5.16	64	1210	3.27	2.31	1210	12.58	7.64	1210	74.30	6.20	64
Average	24.38	1.87	--	24.29	4.79	--	--	3.32	2.36	--	12.84	8.32	--	74.20	6.10	--
Original	24.42	1.82	20	24.17	3.89	640	--	3.22	2.37	1000	12.69	7.86	1000	73.90	3.50	20

λ_b - *average number of overlapping flakes in 64 columns in a sample mat;*
N_j - *number of overlapping flakes in a column;*
Δ_{jk} - *distance between adjacent flakes in the j^{th} column at k^{th} flakes (max. deflection);*
X_{jk} - *location of the column centroid relative to the k^{th} flake's length;*
H - *height of a column;*
μ - *mean value;*
σ - *standard deviation;*
n - *sample size.*

The entire simulation procedure was repeated five times to generate the mat characteristics λ_b, N_{bj}, Δ_{bjk} and X_{bjk}. *Table II.3* contains the results and their averages, with the summary statistics of the measured data set. Additionally, from the N_{bj} and the assigned Δ_{bjk} data, the average height of 64 columns in a sample block was computed for each replication using *Eq. II.1* (*Table II.3*). Note, that the means of 64 column heights are similar to the measured values. However, the standard deviations are almost double that of the experimental data. This phenomenon is a result of the initial data acquisition practice and the model structure combined. The simulation assigns one Δ value to each strand. However, the number of cavities in a column vary between $N_{bj} \pm 1$, depending upon the shapes of the first and last strands (i.e., convex or concave). Sensitivity analysis of the static stress-strain model revealed that the variability of void height (Δ_{bjk}) had no significant effect on the stress prediction.

The developed Monte Carlo simulation procedure appears to adequately reproduce the marginal distributions of mat spatial characteristics, preserving the non-correlated structure of the data. Further elaboration of the usefulness of this stochastic model is given in the Conclusion section of this Chapter.

II.6 Theoretical Background and the Stress-strain Model Development

The consolidation of randomly formed wood strand mats may be characterized by a press diagram. The compression force applied to the mat is usually plotted against time as shown in *Figure II.7a*. This curve can be divided into three different regions: 1.- press closing, 2.- stress relaxation and 3.- venting or press opening (Wolcott at al. 1990). During press closing, stress develops nonlinearly with the displacement because of the structural and material nonlinearity of the mat. This region can be converted into stress-strain diagram as shown on *Figure II.7b*. Note that the stress is on logarithmic scale to demonstrate the stress behavior during the initial phase of the consolidation.

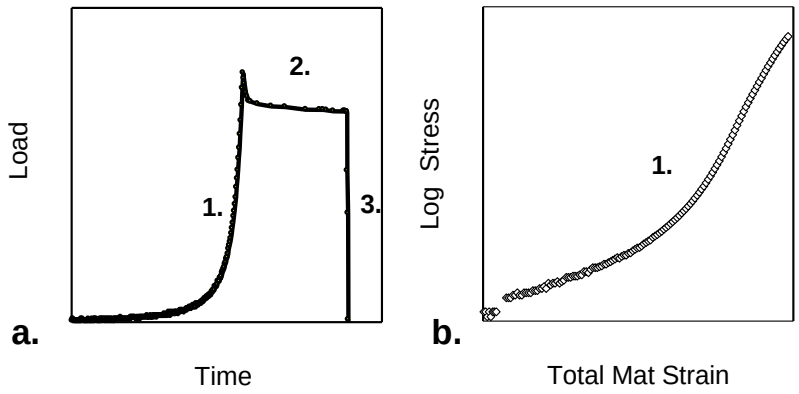

Figure II.7. *Typical load-time diagrams of randomly formed mat in cold pressing (**a.**) a full pressing cycle: 1. – press closing, 2. – stress relaxation, 3. – venting. Stress strain relationship of the of the press closing regime (**b.**)*

By examining these diagrams, the following observations can be made:

1. The stress e development is minimal at the beginning of the consolidation.
2. As the displacement continues, the stress increase becomes continuous and smooth because the individual strands deform in bending.
3. Rapid stress development can be observed for mat strains greater than 60%, where the consolidation is dominated by the compression of stacked, solid wood strands.

Studying the changes in real mat structure during consolidation leads to similar conclusions. *Figure II.8a* shows the initial structure of a randomly formed wood strand mat. At mat strain of approximately 30%, the void heights decrease and most of the strands flatten (*Figure II.8b*). When the total mat strain is about 60%, the void heights approach a minimum value (*Figure II.8c*).

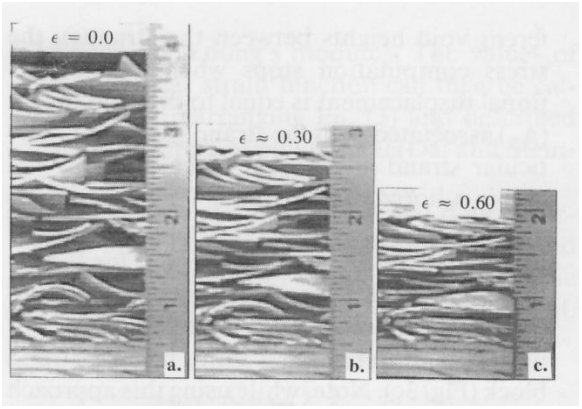

Figure II.8. *Structural changes in a randomly formed wood strand mat during consolidation.*

a. *- initial bulk structure;* ***b.*** *- at mat strain* ***e****≈0.3;* ***c.*** *- at strain* ***e*** *≈0.3*

Based on the above discussion and results of earlier research projects (Suchsland 1962; Harless et al. 1987; Suchslanad and Xu 1989; Dai and Steiner 1993, 1994a, b) it was assumed that the static compression response of a strand mat can be separated into two components. In the early stage of the consolidation, the cumulative stress development results from the bending resistance of the individual wood strands. As consolidation continues, overlapping strands form solid columns of varying height that deform in transverse compression. To facilitate the numerical solution for the stress development in virtually reconstructed mat blocks - described earlier - the following theories were used.

II.6.1 Stresses due to strand bending

Figure II.9 provides a graphical demonstration of the concepts for stress computation where detail *a.* just a reiteration of the previously defined spatial characteristics of the mat. To maintain the simplicity and mathematical tractability of the model, several assumptions were made. Each strand was considered as a small simply supported beam under linearly distributed load (ω_{ijk}) and index $_i$ denotes the total mat strain (*Figure II.9.b*). Beam deflections were computed at the column hubs, and the location variable (X_{jk}) identified the position of the strand

relative to the central axis of the column. The possible maximum deflection of a strand beam was the assigned Δ_{jk} to the k^{th} strand in the j^{th} column.

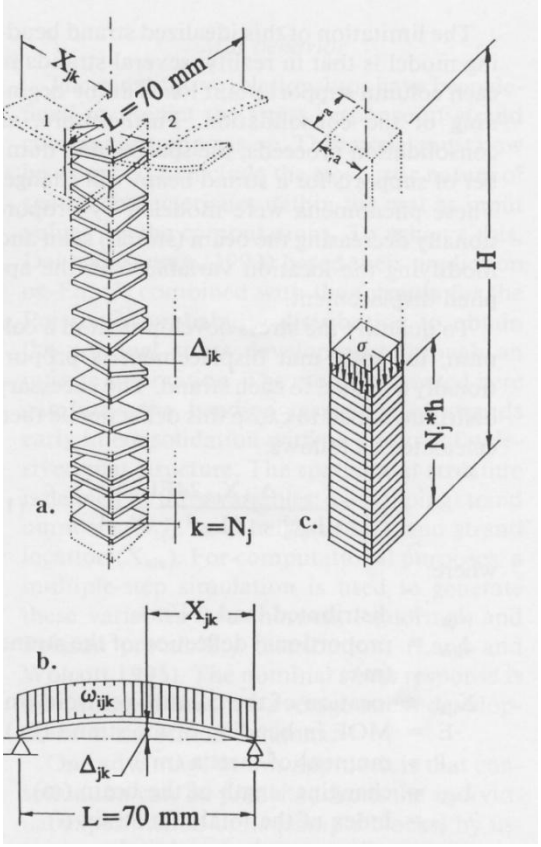

Figure II.9. *The theoretical units of the static stress-strain model.* ***a.*** *- idealized initial structure of a column;* ***b.*** *– the "beam" model;* ***c.*** *– the solid strand stacking.*

An inverted form of a beam deflection equation was used to determine the distributed load to deflect the strand beams that eventually form a solid column. The limitation of this idealized strand bending model is that in reality, several strands in each column support point loads at the beginning of the consolidation. Furthermore, as consolidation proceeds, the spacing and the number of supports for a strand beam will change. These phenomena were modeled by proportionally decreasing the beam (strand) span and gradually modifying the location variable as well.

To quantify the stress development due to strand bending in a column, the total mat displacement was proportionally assigned to each strand. The necessary load, to cause this deflection, can be calculated as follows:

$$\omega_{ijk} = \frac{\Delta_{ijk} X_{ijk} 24EI}{L_{ijk}^3 - 2L_{ijk}^2 + X_{ijk}^3} \qquad (II.3)$$

Where:

ω_{ijk} - distributed load (N/m)

Δ_{ijk} - proportional deflection of a strand (m)

X_{ijk} - location of the column centriod (m)

E - modulus of elasticity in bending (Pa)

I - moment of inertia (m^4)

L_{ijk} - changing length of the beam (m)

$_i$ - index of the total mat strain (ε)

$_{jk}$ - column and strand indexes, respectively

The obtained distributed load values than can be converted into stresses by the following summation:

$$\sigma_{ij} = \sum_{k=1}^{N_j} \frac{\omega_{ijk}}{a} \qquad (II.4)$$

Where:

σ_{ij} - stress in column j at strain i (Pa)

N_j - number of overlapping strands in column j

a - width of the column/strand (m)

The total mat displacement is distributed to the strand until the entire void height is eliminated or the target thickness has been achieved. Because each strand has a different maximum deflection value (i.e., different void height between the strands), the stress computation stops when the proportional displacement is equal to the void height (Δ_{jk}) associated with the strand. Then, this particular strand is assumed to be perfectly flat in a horizontal position. The corresponding stress value is preserved and the proportional displacements are increased for the remaining strands. The procedure continues until all void spaces are eliminated and the column is compressed to a solid layered stack of strands (*Figure II.9c*).

II.6.2 Stress development in solid strand columns

Initially, the mat strain in compression induces bending but not compression stresses in the strands. When the voids in a column have been eliminated, columns begin to undergo compression strain as consolidation continues toward the target mat thickness.

The compression behavior of wood strands can be modeled using theories of cellular materials. The characteristic stress-strain curve of wood in transverse compression has been discussed in details by several authors (Maiti at al., 1984; Wolcott at al., 1989b; Dai and Steiner 1993). Hookes's Law modified with a nonlinear strain function ($\Phi(\varepsilon)$) can be used to establish a constitutive relation (Rush 1969; Wolcott 1989a; Gibson and Ashby 1988). This modified Hooke's Law takes the following form:

$$\sigma = E\varepsilon\Phi(\varepsilon) \qquad (II.5)$$

Where:
σ - compressive stress
ε - strain
E - Young's modulus of the cellular material
$\Phi(\varepsilon)$ - nonlinear strain function

The nonlinear strain function can be determined experimentally by compressing strand columns. The linear regime is analyzed to ascertain the Young's modulus. The values of the nonlinear strain function can then be calculated by rearranging *Equation II.5* and described using an empirical polynomial (Dai and Steiner 1993).

In the absence of experimental data, structural theories developed for honeycomb and closed cell foams may be applied to determine $\Phi(\varepsilon)$ with the equation provided below (Asby and Gison 1988; Woloctt et al. 1989b):

$$\Phi(\varepsilon) = \frac{C_3/C_2}{\varepsilon}\left[\frac{1-\rho_r^{1/3}}{1-(\rho_r(\varepsilon))^{1/3}}\right]^3 \qquad (II.6)$$

Where:
ε - compressive strain
ρ_r - relative density of the wood
$\rho_r(\varepsilon)$ - changes of relative density
C_3 - yield strain (ε_y)
C_2 - linear elastic constant
$\Phi(\varepsilon)$ - nonlinear strain function in transverse compression

In this equation the relative density is defined as the ratio between the solid wood density and cell-wall density. The linear elastic constant is a function of the strand thickness. The changes of relative density ρ_r (ε) can be computed from the relationship between the plastic strain and the expansion ratio as follows:

$$\rho_r(\varepsilon) = \rho_r\left[1 - \varepsilon_y + (2/3)\mu\varepsilon_p - \mu\left(\varepsilon_p\right)^2\right]^{-1} \qquad (II.7)$$

Where the unknowns:
ε_p - plastic strain
μ - expansion ratio

The expansion ratio is defined as the ratio of lateral strain to compressive strain in the nonlinear stress-strain region (Wolcott et al. 1989a). In both approaches, the value of $\Phi(\varepsilon)$ is equal to unity for strains less than ε_y. *Equation II.6* becomes singular as the relative density (ρ_r) approaches 1 (i.e., total densification of the cellular material). However, total densification seldom occurs during manufacture of wood-based composites.

II.6.3 The overall model for mat behavior under consolidation

The constitutive relationship for predicting the stress response – discussed above – should be applied to the virtual mat structure in order to predict the compression behaviors of randomly formed wood strand mats. In general, the model combines the bending resistance of the strands at the early stage of the consolidation. As the press closure advances, voids are eliminated for a gradually increasing area in the initial bulk structure of the mat. The stress development in the void-less area is due to the transverse compression of solidly stacked strands. One of the advantages of this model structure is that consolidation can be predicted from individual experimental units (blocks) by using actual measured parameters as inputs for the simulations. The predicted stress-strain response then can be compared to the actual behavior of the same experimental unit.

In the initial stage of the model (steps 1-3), the mat structure is reconstructed on a probabilistic basis. Steps 4-8 are the stress calculations for a mat section (block). Step 9 improves the resolution and usually 5 repetitions were found to be adequate. The following list summarizes the model structure:

1. Generate the mean overlapping strand numbers (λ_b) in a mat block: $\lambda_b \in N(\mu, \sigma^2)$.
2. Generate the number of overlapping strands (N_{bj}) for the 64 columns in block b: N_{bj} **v** Poisson (λ_b).
3. Generate and assign location (L_{bjk}) and void height (Δ_{bjk}) for each strand in each column: $L_{bjk} \in LN(\mu, \sigma^2)$ and $\Delta_{bjk} \in LN(\mu, \sigma^2)$.

The stress is then calculated for a mat as follows:

4. Assign an incremental total mat displacement.
5. Compute the proportional deflection in a column. Calculate the cumulative stress in the column according to *Equations II.3 and II.4*.
6. If $\Sigma\Delta_{ijk} \leq$ the total mat displacement (Δu_H), compute the stress by *Equation II.5*.
7. Repeat steps 4 – 7 until the target mat thickness is reached.
8. Repeat steps 1 – 8 for each of ***n*** block comprising the mat and calculate the average stress response.

The stress prediction requires inputs for the Young's modulus of strand in bending and in transverse compression. The bending modulus (E_b) was obtained from the literature (USDA Forest Service 1982). We evaluated the compression modulus (E_c,) experimentally and that procedure is discussed next.

II.7 Experimental Validation of the Static Stress-strain Model

II.7.1 Materials

For validation of the stress response model, we used the same 20 experimental sample blocks that were prepared for database development to assess the spatial mat characteristics. The description of the employed materials and mat formation technique is given by *Section I.4.1*. The target density of the panels (600 kg/m^3) after consolidation to 13 mm final thickness required 0.702 kg furnish for the given sized forming box. This resulted in an average of 74 mm thickness for the loosely formed mats, having approximately 100 kg/m^{3}bulk densities.

II.7.2 Methods

For determination of the compression modulus (E_c), twelve 19 mm square strands with 0.8 mm thickness were stacked to form a solid column. A walk in environmental chamber set for 60 % relative humidity (*RH*) and 21 °C temperature ensured approximately 12% equilibrium moisture content (*EMC*) for the strands columns and for the experimental blocks as well. Compression tests were carried out using an MTS universal servo-hydraulic testing machine. The machine had a max. 60 ± 0.01 kN load cell capacity. The machine load cell was calibrated daily and a computerized data acquisition system collected load and displacement data in real time.

II.8 Results and Discussion and the Overall Model Performance

II.8.1 Material property tests

From compression tests of the nine solid strand columns, the mean of E_c was estimated to be 4.2 MP, while the mean of yield strain (ε_y) was found to be 0.14. These values are comparable to those reported by Wolcott et al. (1989a) with yellow-poplar strands. The empirical, nonlinear strain function was approximated by fitting a tenth order polynomial to experimental data above the yield strain. *Table II.4* contains the coefficients resulted from the regression analysis. Graphical representation of the test results are in *Appendix II (Figure A.II.3*).

Table II.4. *The approximated regression coefficients for the empirical strain function $\Phi(\varepsilon)$.*

Coefficients	***Numerical Values***	***Coefficients***	***Numerical Values***
β_0	*0.71*	β_6	*-5269.08*
β_1	*5.19*	β_7	*6578.05*
β_2	*-53.13*	β_8	*-5307.15*
β_3	*295.24*	β_9	*2459.07*
β_4	*-1114.44*	β_{10}	*-528.69*
β_5	*2917.08*	-----	-----

The theoretical, nonlinear strain function defined by *Equation II.6* is graphically compared to the empirical result in *Figure II.10*. Good agreement can be observed between the two strain functions.

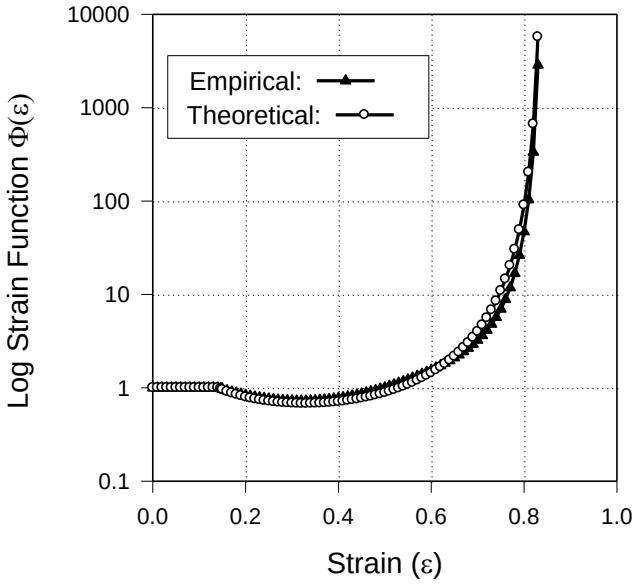

Figure II.10. *Comparison of strain functions obtained by polynomial fitting and by theory of cellular solids (Equation II.6).*

II. 8.2 Experimental and model predicted behavior of the mat blocks

For validation, the average overlapping strand numbers (λ_b) were used as input to simulate mat structures for five sample blocks. This parameter provided a link between the experimental and predicted stress-strain data for each block. Thus, the average stress-strain behavior of 64 columns in a sample block was modeled. The five experimental and predicted stress-strain relationships are compared in *Figure II.11*.

In general, good agreement was found. For the mat blocks tested, approximately 60-65 % compaction was required to initiate rapid stress development. The model tends to over-predict the stresses in the densification regions, although this error does not appear to be major.

To enhance the model prediction, another five sample block were prepared and tested. The mean of the overlapping flake numbers in 160 columns along the perimeters of the five sample blocks was used to generate λ_b values for each block.

Figure II.12a shows comparison of the average predicted and experimental stress-strain response of five sample blocks. Significant improvement was observed in the prediction quality compared to the individual blocks.

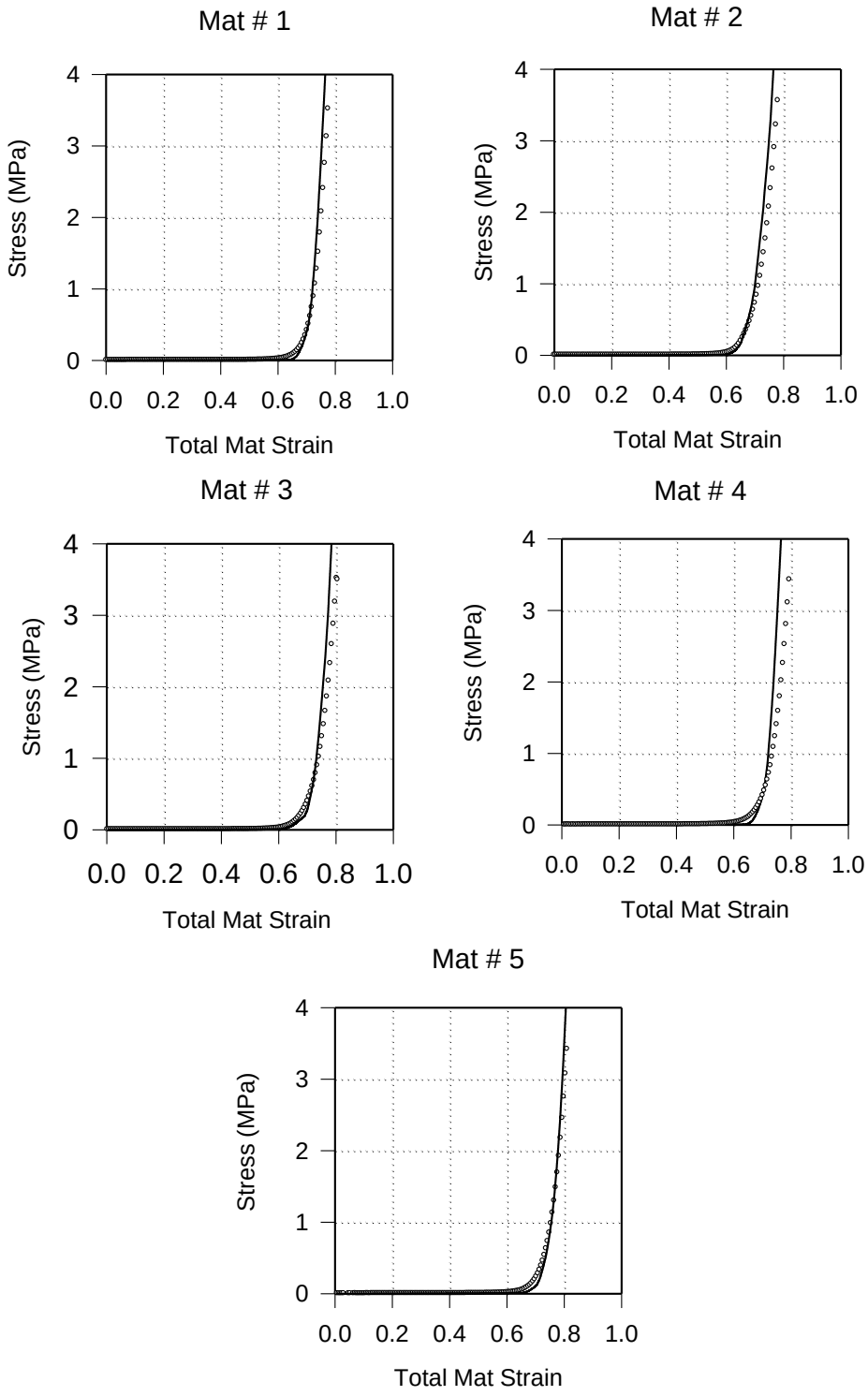

Figure II.11. *Results of the model validation. Symbols and lines represent the experimental and predicted data, respectively.*

In this case the model prediction was based on the average stress response of 320 theoretical units (columns). Although the model still slightly over-predicts the stress response; this inaccuracy is not as severe as for the individual blocks. The slope of the predicted and experimental curves shows excellent agreement. Enhancing the resolution (i.e., simulating more than five sample blocks) did not improve the model prediction, but the computation time increased significantly.

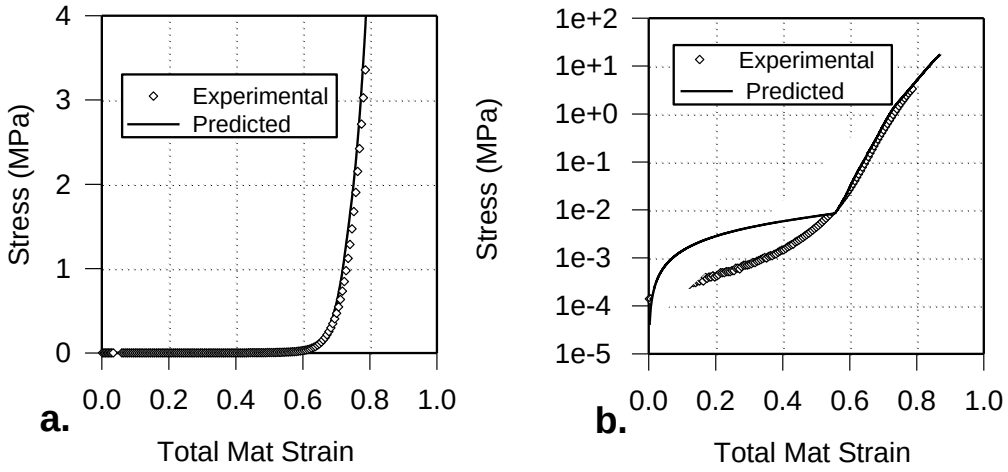

Figure II.12. *Final results of the of the model validation. The average experimental stress response of five sample blocks compared to the model prediction. a. – normal and b. – logarithmic scale for stress.*

To amplify the response of the low stress region, the average and experimental curves are depicted on logarithmic stress scale (*Figure II.12b*). While no significant deviation could be observed on the normal scale below 0.01 MPa, the cumulative strand bending does not properly predict the stress response below this stress value. Dai and Steiner (1993) reported fairly accurate predictions over 1.5 MPa mat stresses. By including the contribution of strand bending to dissipate voids, the model presented here predicts stress response accurately for the range of .01 – 4.0 MPa. The low stress region of the consolidation is extremely important when pressing low-density panel products.

Predicting the consolidation of randomly formed strand type composites is not limited to the overall mat stress-strain relationship. The five sample block, used for model validation, represent a 320 x 320 mm total mat area measured from the hubs of edge columns. Using the simulated N_{bj} (b=1,…5 and j=1,…64) data the average bulk and target densities for the panel were 102 and 601 kg/m^3, respectively (*Figure II.13a, b*). These values showed excellent agreement with the observed densities of 100 and 600 kg/m^3 indicating that the simulation procedure reconstituted the mat structures with preserved density characteristics. The coefficients of variation (COV) for the in-plane target densities are slightly higher for the panel

(17.72%) than for the bulk (17.58%). The densification or cellular collapse of wood strands in some of the over-stacked columns explains the differences.

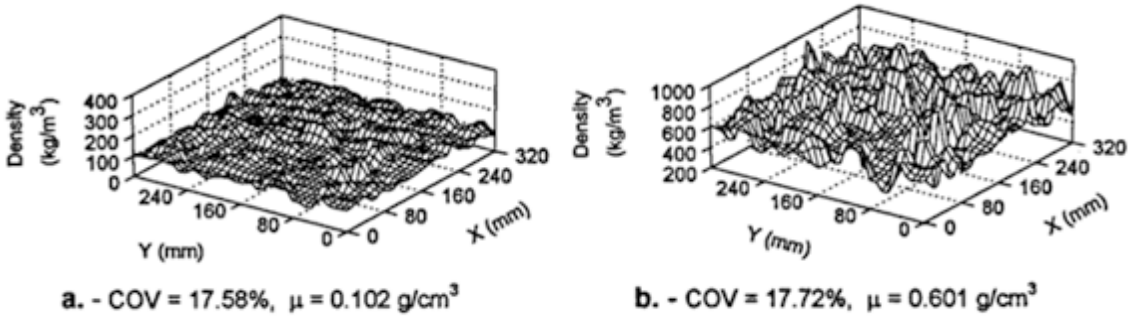

Figure II.13. *Horizontal density distribution of simulated mat area of 320 x 320 mm.* ***a.*** *– bulk density;* ***b.*** *– target density of the 13 mm thick panel.*

The residual void volume may be calculated thorough the simulation by detecting the columns that do not fully consolidate. In 19 of the 320 columns, the sum of the strand thicknesses is less than the panel target thickness. These 19 columns represent 6% of the total mat area where the adhesion might be inadequate.

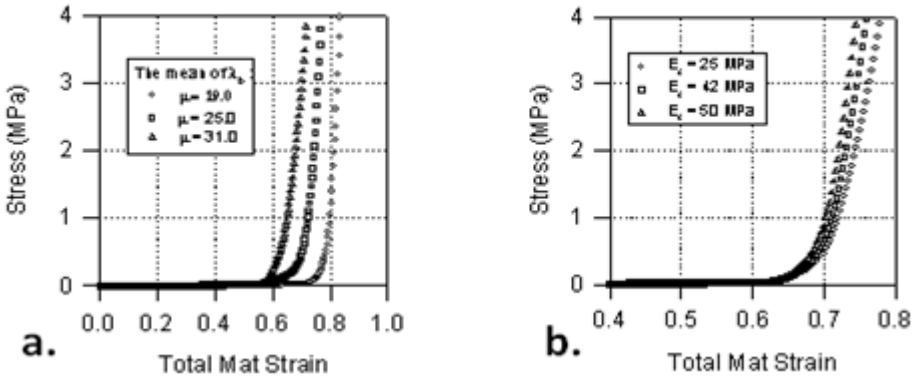

Figure II.14. *Results of the sensitivity analyses;* ***a.*** *– the effect of void height (l_b), and* ***b***. *– the compression modulus of elasticity (E_c) on the model prediction.*

Sensitivity analyses were carried out to reveal if a particular input variable has a significant effect on the overall model prediction. When holding all the parameters constant, the variability in the mean overlapping strand numbers (λ_b) had the strongest effect on the stress prediction (*Figure II.14a*). This result was expected because more strand in the columns initiate rapid stress development at lesser mat strain. In turn, the E_c for the wood strands influences the slope of the rapid stress development region. In *Figure II.14b*, the 25 MPa for transverse compression modulus represents aspen (*Populus tremoloides*) strands reported by Dai and Steiner (1993). The 42 MPa value was experimentally determined on yellow-poplar

(*Liriodendron tulipifera*) strands and the 50 MPa value may depict the behavior of higher density strands (i.e., SG > 0.5). No statistically significant effect of the location (X_{bjk}) and void height (Δ_{bjk}) input parameters could be observed on the model performance. However, it should be noted that the strand's shape, length, width and orientation may be strongly correlated to the location and void height characteristics of the mat. Thus, they may have strong influence on the early stage of consolidation.

II.9 Summary and Conclusions

A stochastic – deterministic model for predicting stress-strain response of randomly formed oriented strand board mats was developed. In this model the mat structure was considered as a finite number of imaginary columns with varying numbers of overlapping strands and size of void spaces. The stress approximation was based on a simple beam theory and the compression behavior of cellular materials. The non-linearity resulting from the macro structure was anticipated and modeled on a stochastic basis. The effects of heat and moisture content on the consolidation process were out of scope of this research. However, the knowledge about general behavior of wood under different temperature and moisture content conditions indicates that the ambient parameters have definite effect on the consolidation process. This demonstrated on *Figure A.II.3,* in *Appendix II*. These preliminary experimental results regarding the effect of temperature and MC were obtained by testing identical sample blocks that were described in this chapter.

The explained model can predict the stress response of randomly formed wood strand mats to compression strain with good accuracy over 0.01 MPa. The results of the analytical and experimental works indicated the following conclusions.

1. The developed Mont Carlo simulation procedure appears to adequately reproduce the structure of randomly formed, uniform sized strand mats.
2. The stochastic part of this model can be easily extended to incorporate additional variables such as length, width and orientation of the strands.
3. The average values of the overlapping strand numbers control the rapid stress development relative to the total mat strain in compression.
4. The transverse modulus of elastic in compression (E_c) and the nonlinear strain function ($\Phi(\varepsilon)$) control the slope of the stress-strain curve in the rapid stress development phase of the consolidation.
5. The in-plane variability of the overlapping strands governs the horizontal density distribution, residual void volume and the inadequate bonding area in the panel.
6. Because the strand deposition depends mainly on the mat forming technique, the panel structure and indirectly its mechanical properties may be improved by modifying the forming process or equipment.

The model was validated with random strand mats constituted from uniformly sized yellow-poplar strands. The simulation-routines are based on probability distributions and do not

generally apply to all mat structures. However, theories for the structural reconstruction and consolidation processes have universal value. The model is easily adaptable to realistic mat structures. The representation of the virtual mat structure and the mechanical approach to compute its stress response under pressure is comparatively simple. Thus, the model provides a good basis for further enhancement. The expansion should include the time, temperature and moisture interaction during hot pressing and stress relaxation under constant strain.

II.10 Closure of Chapter II

This research was completed in 1995 and resulted in three peer reviewed scientific publications (Lang and Wolcott 1995, 1996a, 1996b) and three presentations at scientific symposia. The work discussed here, received significant international attention and was cited approximately 45 times in highly regarded scientific journals.

Over the last fifteen years several researchers applied, improved, sometimes criticized or modified our model. Lenth and Kamke (1996a, b) used extensively the approach we developed to characterize the mat structure and the consolidation process. Qudjehane et al. (1998a, 1998b) in their continuum model, to explore the interaction between manufacturing parameters and consolidation of wood composite mats, incorporated the void elimination and the compression of solid strand column concept.

The first significant improvement based on our perception was presented by Zombori (2001) and Zombori at al. (2001). He introduced additional mat characteristics such as strand length, width, density and orientation into the Monte Carlo simulation process. Furthermore, Zombori addressed the layered structure of the mat; however his primary objective was to model the transient effects (heat and mass transfer) during the consolidation. Nevertheless, his virtual mat model demonstrated similar horizontal density distributions as we observed with single layer mat structures. (*Figure A.II.4*).

Finally, experiences and insights of orthotropic material properties of wood and wood-based composites lead to several related research projects. Some of these investigations are discussed in the following Chapters of this Dissertation.

References II

1. Dai-CP Yu-CM. 2004. Heat and Mass Transfer in Wood Composite Panels during Hot Pressing. Part 1I - A Physical Mathematical Model. Wood and Fiber Science, 2001, Vol. 36, Iss. 4, pp 585-597.
2. Etter, D. M. 1987. Structured Fortran for engineers and scientists, 2nd ed. The American Society for Testing and Materials. 1996. Annual Book of ASTM Standards. Section 4 Construction. Volume 0.4.10, Wood. ASTM, West Conshohocken, Pa. 645 pp.
3. American Society for Testing and Materials. 1991. Standard practice for testing and use of random number generator in lumber and wood products simulation. ASTM Philadelphia, Pa.
4. Dai Cand and P.R. Steiner. 1994a. Spatial structure of wood composites in relation to processing and performance characteristics. Part 2. Modelling and simulation of of randomly formed strand layer network. Wood Science and Technology, 28(2):135-146.
5. Dai Cand and P.R. Steiner. 1994b. Spatial structure of wood composites in relation to processing and performance characteristics. Part 3. Modelling the formation of multi-layered random strand mat. Wood Science and Technology, 28(3):229-239.
6. Dai Cand and P.R. Steiner. 1993. Compression behavior of randomly formed wood strand mat. Wood Science and Technology, 25(4):349-358.
7. Benjamin/Cummings Publishing Co.,, Inc., Menlo Park, CA, 519 pp.
8. Gibson, L. and M.F. Ashby. 1997. Cellular solids. 2nd edition. Cambridge University Press, Cambridge, UK, pp. 510.
9. Harless, T.E.G., F.G. Wagner, P.H. Short, R.D. Seale, P.H. Mitchell and D.S. Ladd. 1987.
10. Lang, E. M. and M. P. Wolcott. 1996a. A Model for Viscoelastic Consolidation of Wood Strand Mats. Part I: Structural characterization of the mat Via Monte Carlo simulation. Wood and Fiber Science. 28(1):100-109.
11. Lang, E. M. and M. P. Wolcott. 1996b. A Model for Viscoelastic Consolidation of Wood Strand Mats. Part II: Static stress-strain behavior of the mat. Wood and Fiber Science. 28(3):369-379.
12. Lang, E. M. and Wolcott, M.P. 1995. Modeling the Consolidation of Wood Strand Mat, AMD-Vol.209/MD-Vol. 60, Mechanics of Cellulosic Materials ASME 1995, pp.153-165.
13. Law, A.M. and W.D. Kelton. 19991. Simulation modeling and analysis. McGraw-Hill, Inc. New York, NY., 759 pp.
14. Lenth-CA Kamke-FA. 1996. Investigations of Flakeboard Mat Consolidation .2. Modeling Mat Consolidation Using Theories of Cellular Materials. Wood and Fiber Science, 2001, Vol. 28, Iss. 3, pp 309-319.
15. Lenth-CA Kamke-FA.1996. Investigations of Flakeboard Mat Consolidation .1. Characterizing the Cellular Structure. Wood and Fiber Science 2001, 1996, Vol. 28, Iss. 2, pp 153-167.
16. Maiti, S.K., L.J. Gibson and M.F. Asby. 1984. Deformation and energy absorption diagrams for cellular solids. Acta Metall. 32(11):1963-1975.

17. Rush, K.C. 1969. Load-compression behavior of flexible foams. Journal of Applied Polymer Science, 13:2297-2311.

18. Steiner, P.R. and C. Dai. 1994. Spatial structure of wood composites in relation to processing and performance characteristics. Part 1. Rationale for model development. Wood Science and Technology, 28(1):100-109.

19. Suchsland, O. 1959. An analysis of the particle board process. Michigan Quart. Bull. 45(1):350-372.

20. Suchsland, O. 1962. The density distribution in strand boards. Michigan Quart. Bull. 45(1):104-121.

21. von Haas, G Fruhwald, A. 2000. Compression Behavior of Fibre, Particle and Strand Mats. HOLZ ALS ROH-UND WERKSTOF, Vol. 58, Iss.5, pp. 317-323.

22. Wolcott, M.P. 1990. Modeling viscoelastic cellular materials for the pressing of wood composite. Ph.D. dissertation, Virginia Polytechnic Institute and State University, Blacksburg, VA 170 pp.

23. Wolcott, M.P., F.A. Kamke, and D.A. Dillard. 1990. Fundamentals of strand board manufacture: Viscoelastic behavior of the wood component. Wood and Fiber Science, 22(4):345-361.

24. Wolcott, M.P., B. Kasal, F.A. Kamke and D.A. Dillard. 1989a. Modeling wood as a polymeric foam: An application to wood-based composite manufacture. Proc. Third joint ASCE-ASME Mechanics Conference, University of California, LaJolla, CA, Pp. 53-60.

25. Wolcott, M.P., B. Kasal, F.A. Kamke and D.A. Dillard. 1989b. Testing small wood specimens in transverse compression. Wood and Fiber Science, 21(3):320-329).

26. USDA Forest Service. 1987. Wood Handbook: Wood as an Engineering Material. USDA Forest Service, Forest products Laboratory, Madison, WI. 466 pp.

27. Zombori, BG.2001. Modeling the transient Effects During the Hot-Pressing of Wood-Based Composites. Ph.D. Dissertation. Virginia Polytechnic Institute and State University, Blacksburg, Va. pp.212.

28. Zombori-BG Kamke-FA Watson-LT. 2001. Simulation of the Mat Formation Process Wood and Fiber Science 2001, Vol. 33, Iss. 4, pp 564-579.

List of Figures II

List of Tables II

Nomenclature II

Upper case letters:

C_2	*yield strain (ε_y)*
C_3	*linear elastic constant*
COV	*coefficient of variation*
E	*modulus of elasticity*
E_c	*E, in compression*
H	*column height*
I	*moment of inertia*
L	*length of a strand beam*
LVL	*laminated strand lumber*
MC	*moisture content*
N	*overlapping strand numbers*
OSB	*oriented strand board*

Lower case letters:

a	*strand width*
h	*strand thickness*
n	*sample size*
u	*displacement*

Greek letters:

α	*probability type-I error*
β	*regression coefficients*
Δ	*void height, differential*
ε	*strain*
$\Phi(\varepsilon)$	*nonlinear strain function*
λ	*mean overlapping strands*
μ	*mean value, expansion ratio*
ρ	*density*
σ	*stress, standard deviation*
ω	*linearly distributed load*

Subscripts:

b	*block index*
c	*in compression*
H	*total mat height*
i	*strain index*
j	*column index*
k	*strand index*
p	*plastic*
r	*relative*

CHAPTER III

BENEDICT (BARUCH)
DE SPINOZA
(1632 - 1677)

"NOTHING IN NATURE IS RANDOM. … A THING APPEARS RANDOM ONLY THROUGH THE INCOMPLETENESS OF OUR KNOWLEDGE."

III. The Orthotropic Mechanical Properties of Wood and Veneer: Assessments and Models

III.1 Introduction

Immanuel Nobel (1801 - 1872) invented the rotary lathe that eventually resulted in the industrial-scale plywood manufacture. Since then, worldwide resource utilization trends and the year by year decreasing quality and quantity of the available resources have forced the industry to use smaller wood elements such as veneers, strands, flakes and fibers. Also, the increasing demand for structural, wood-based composites - up to the end of the second millennia - triggered more intensive utilization of fast growing species previously neglected because of unfavorable physical and mechanical properties.

Wood-based composite materials have largely been developed through empirical studies. In these products, the constituting wood elements have broad spectrums in species, size and anatomical orientation relative to their own dimensions. The inherent orthotropic, physical and mechanical properties which govern the performance of these structural composites are dependent on the physical and mechanical properties of the constituents. The location and the strength axis' direction of the furnish components influence the strength and stiffness performance of the final composite products. Furthermore, the manufacturing processes used to consolidate individual wood elements into a contiguous composite also intrinsically affect the final performance of the product. For instance, the furnish preparation may or may not adversely influence the physical and mechanical properties of the wood elements. Conversely, the consolidation process – usually hot pressing – can improve strength and stiffness, unless the compression stress is too high for the given temperature at which point cellular collapse occurs.

To achieve the ultimate goal: fully engineered structural composites, a thorough understanding of the origin and nature of orthotropic elasticity and strength of the raw materials is necessary. The described material properties then can be related to the properties of composites with incorporation of the effect of manufacturing parameters. The gained information will provide a basis for further product development.

During the past couple of decades researchers have realized the need for fundamental understanding of composite manufacture. Our ability to establish universal guidelines for wood-based composite design is limited by the lack of knowledge regarding raw material properties and the vast array of interacting processing variables. One can easily realize that the unpredictable laws of nature govern many of these material properties and interactions. These facts prevent researchers from developing completely deterministic design procedures. As a result, combined stochastic/deterministic models have been developed over the years for predicting one or more properties of composite products. The lack of reliable data for orthotropic properties of wood as a furnish material for composites, and the necessary introduction of new material resources initiated this research with objectives as follows.

III.2 Objectives

In quest for fully engineered design of wood-based, structural composites this research was aimed at identifying the anisotropic characteristics of raw materials, exploring the effect of manufacturing parameters on the constituents' properties and relating these results to the performance of composite products. The first phase - discussed in this Chapter - includes the development of an adequate database for validations of different models that can describe the orthotropic strength and elasticity of underutilized Appalachian hardwoods and species grown in Hungary.

Specific objectives were as follows:

1. Develop a statistically reliable database for selected species and for critical mechanical properties by extensive testing.
2. Apply non-traditional experimental techniques if standard ASTM procedures are not viable.
3. Analyze the obtained data by standard statistical methods.
4. Review and evaluate existing models for prediction of orthotropic properties of solid wood and veneer furnish materials.
5. Develop theoretically-backed property prediction models for specific composite applications.
6. Statistically evaluate the different model performances.

Exploration of the direction dependent mechanical properties included three Appalachian hardwood species: quaking aspen (*Populus tremuloides*), red oak (*Quercus rubra*) and yellow-poplar (*Liriodendron tulipifera*); and two European hardwood species: true poplar (*Populus x. Euramericana cv. Pannonia*) and Turkey oak (*Quercus cerris*).

Tests were carried out to evaluate planar shear strength; uniaxial compression and compression modulus of elasticity for all the species mentioned above. In veneer form, the in-plane dynamic MOE and tension strength were investigated using red oak and yellow-poplar structural veneers. Additionally, black cherry (*Prunus serotina*) and read oak decorative veneer bundles allowed the approximation of dynamic MOE in three dimensions. The next section contains the review of relevant literature in the order as stated above according to the progress of this research.

III.3 Literature Review

Orthotropy of the mechanical properties has been an area of interest for a long time. Uniaxial stresses, like compression and tension have been the first to get attention, both because of their ease of assessing and importance in practical applications. Much research effort was concentrated in this area, but most of these works focused on the effect of grain or ring angle, separately. Only a few researchers addressed the three-dimensional orthotropy of solid wood in relation to the mechanical properties (i.e., strength and stiffness).

III.3.1 Literature on Shear

True shear strength is one of the most difficult characteristics to measure. Creation of the pure shear stress state is a real challenge. Furthermore, the always present normal stresses combined with the inherent anisotropy of wood make the strength determination uncertain. Several publications have dealt with the improvement of shear strength assessment. One of the most comprehensive studies on this topic was provided by Yilinen (1963). The author investigated and critically reviewed several standardized shear testing methods. He concluded that the majority of block shear tests usually underestimate the true shear strength of solid wood.

The standard ASTM block shear test has received much criticism for not providing pure shear load on the specimens. A number of investigators dealt with this problem and some also proposed alternative solutions. Norris (1957) recommended the panel shear test, and Liu (1984) suggested the adaptation of a device proposed by Arcan et al. (1978) for wood. The drawback of these tests is that they involve complicated specimen preparation and testing procedures. Lang (1997) proposed a new device for shear strength assessment of solid wood. The advantages of the described testing apparatus are the smaller specimen size, alleviation of normal stresses and acceptable agreement with shear strength values obtained by the ASTM method. Lang and Kovacs (2001) investigated the size effect of the sheared planes using standard ASTM specimens. They concluded that the size of the sheared plane parallel to the grain has no significant effect of the shear strength of the specimen.

The majority of previous research projects have focused on the shear strength of solid wood parallel to the grain. Limited publications are available that address the anisotropy of wood in shear strength assessment. The first formula that described the strength anisotropy of wood is the well-known Hankinson's formula (Hankinson, 1921). It was developed empirically from compression tests. This equation describes the effect of grain-orientation changes on the measured properties. Many researchers examined the validity of this formula finding that it fits experimental data well (Goodman and Bodig, 1972; Bodig and Jayne, 1982). However, the equation was deemed to provide adequate predictions only for compression and tension strength as well as moduli of elasticity. Kollman and Cote (1968) proposed some changes to the formula. They stated that using an experimentally determined power will provide better approximation of the direction dependent strength and elastic properties.

The first attempt to describe the orthotropy of shear strength was made by Norris (1950). He applied the general Henky - von Mises theory to orthotropic materials. Although in his study the predicted shear strength values agreed reasonably well with experimental data for structural plywood, the approach has received criticism from others (Wu, 1974; Cowin, 1979). Over the decades, with the advancement of man-made composites, ample research has been devoted to explore the strength and elasticity of anisotropic materials. Many of these results and theories developed can be applied to wood with care.

Ashkenazi (1976) used the tensor theory for describing the anisotropy of wood and wood-based composites. In an earlier work he measured the shear strength of pine at various grain angles (Ashkenazi, 1959). Her results were unusual in that shear strength showed maximum values at approx. 15° grain orientation, rather than in the longitudinal direction.

Cowin (1979) stated that a quadratic form of the Hankinson's formula describes Ashkenazi's data reasonably well. The proposed model, however, cannot describe the shear strength maximum at 15° grain orientation. Liu and Floeter (1984) measured the shear strength of spruce at 0°, 30°, 60° and 90° grain angles with the special device described by Arcan et al. (1978) designed to provide uniform plane stress. Their results agreed well with the theory of Cowin (1979).

Some other researchers incorporated the effect of ring orientation in their works. The experiment of Bendsten and Proter (1978) included ring-angle, but only as a blocking factor, its effect was not of interest. Okkonen and River (1989) examined, among other factors, the effect of radial and tangential ring orientation on the shear strength in the longitudinal direction. They concluded that Douglas-fir had higher strength when the orientation of the sheared plane was radial, while oak and maple were stronger in the tangential direction. Riyanto and Gupta (1996) tried to establish a relationship between ring angle and shear strength parallel to the grain. Using a completely randomized design, they found that ring angle had very little effect on the shear strength of Douglas-fir and Dahurian Larch. Rather, the specific gravity, the percentage of latewood, and the number of rings per unit length were much more deterministic factors. Szalai (1994) provided an integrated approach that tackles both ring and grain angle orientation. A general equation, derived from tensor analysis, can determine the shear strength at any given ring and grain angle combination.

III.3.2 Research on compression properties

The most well known model to describe the effect of sloping grain on compression properties is the Hankinson's formula. Radcliffe (1965) investigated the accuracy of the equation, comparing its predictions to theoretical values of MOE that were derived from the relationships of orthtotropic elasticity. He showed that Hankinson's solution is quite accurate in the LR plane, while in the LT plane around 25° grain inclinations it may underestimate the compression MOE by 30%. Other researchers also verified the validity of this model (Goodman and Bodig 1972; Bodig and Jayne 1982). Kollmann and Cote (1968) suggested some modifications to the original formula. Cowin (1979) gave a good overview of these developments, and concluded that the valid formula should be the one Hankinson originally proposed. Some published research works claimed that another version, the so-called Osgood formula, approximates better the effect of sloping grain than the Hankinson's equation (Kim 1986; Binzi and Samson 1995). The Osgood formula, that is also empirical, is given as follows:

$$n = \frac{pq}{q+(p-q)\sin^2\phi\left(\sin^2\phi+a\cos^2\phi\right)} \qquad \textit{(III.1)}$$

Where n, p and q are the compression properties at grain angles of φ, $0°$ and $90°$, respectively. Constant a is a species-specific coefficient that should be determined experimentally. However, no extensive validation of this model was reported in the literature (Kim 1986).

Transverse compression has received much attention, too. Bodig (1965), Kunesh (1968) and Bendsten et al. (1978) provided more in-depth analysis of the question. Ethelington et al. (1996) incorporated variation of ring orientation in their work, and concluded that it had significant effect on the compression strength perpendicular to the grain.

The exact determination of the strength perpendicular to the grain is practically impossible because of the incompressibility of the wood substance. The ASTM D 143 – 83 standard requires that the test shall be discontinued after 2.54 mm (0.1 inch) crosshead-displacement. This procedure was developed to evaluate the reaction force supporting capacity of solid wood joists. Consequently, there is no standard testing method that regulates the exploration of orthotropy in compression. However, there are several theories for predicting the failure envelope of solid wood and/or wood-based composites. Usually these approaches are based on six-dimensional, tensor analyses like the Tsai-Wu strength criterion (Tsai and Wu 1971) that was developed two decades ago for homogeneous, orthotropic materials such as glass or carbon fiber and epoxy composites. The fiber direction in these synthetic composites is better controlled and the materials are transversely isotropic (i.e., identical strength and elastic properties in any directions perpendicular to the fiber). Thus, such analyses can be successfully used in exploring the strength orthtotropy of relatively homogeneous materials as demonstrated through an analysis of paperboard by Suhling et al. (1985).

III.3.3 Publications regarding tension properties and NDT of wood

Very limited research has been done on the tensile orthotropy of wood. Gerhards (1988) examined the effect of sloping grain on the tensile strength of Douglas-fir. At small angle deviations (less than 20°) he found that the modified Hankinson's formula as reported by Kolman and Cote (1968 provided acceptable fit. In another work that included the full grain orientation range (Woodward and Minor 1988), the authors found that the same theory worked well, but resulted in a worse prediction than by the hyperbolic formula. Pugel (1990) developed an angle-to-grain tensile setup for thin specimens. Tensile test results of Douglas-fir and Southern pine, measured by this new technique, showed reasonable agreement with the predictions of the original Hankinson's formula. These studies dealt with the tensile strength only, and did not address the effect of sloping grain on the modulus of elasticity.

Nondestructive testing is a simple and inexpensive alternative to static tests. Its advantages are obvious: the specimen is not destroyed during the measurement, which is usually fast and less labor-intensive. Furthermore, nondestructive evaluation is often much simpler than

the static test. Vibration methods are particularly suitable for quantitative, as well as qualitative evaluation of materials. The relationship of vibration properties to the elastic characteristics of materials was recognized as early as 1747 by Riccati. Researchers started to apply this relationship for wood in the early 1950's (Pellerin 1965).

Vibration methods include two subtypes: transverse and longitudinal (stress-wave) vibration. According to theory, measured transverse vibration frequency and wave propagation velocity are related to the bending and uniaxial MOE, respectively. Many studies verified these relationships experimentally, typically with excellent results. Researchers also endeavored to find empirical correlation between vibration and strength properties. Many considered the damping characteristics of wood to be promising, but experiments were not invariably successful. Pu and Tang (1997) gave a comprehensive overview of the research conducted in this area.

The application of static tension tests to veneers is especially limited due to their small thickness. The mechanical properties of veneer can be very different from those of the wood it originated from, and assessment of veneer properties is sometimes desirable. This is an area where nondestructive testing (specifically, stress-wave timing) is very helpful. There are two areas where vibration testing of veneers can be particularly useful: 1.) relating the mechanical properties of logs to those of the veneer peeled from them (Ross et al. 1999; Rippy et al. 2000), and 2.) veneer classification prior to Laminated Veneer Lumber manufacture, to engineer or improve the consistency of the product's end properties (Koch and Woodson 1968; Jung 1982; Kimmel and Janiowak 1995; Shuppe et al. 1997). The latter gained practical application, too, and a commercial tool is now widely used for classifying veneer sheets according to their stress-wave characteristics (Sharp 1985.)

Other studies about veneer testing by stress-waves include that of Jung (1979), who presented a comprehensive study in stress-wave application on veneers. He examined the potential of this technique to detect knots and slope of grain; and investigated the effect of specimen size and different testing devices. Hunt et al. (1989) correlated the tensile and stress-wave MOE of veneer with acceptable results. Most recently, Wang et al. (2001) investigated the potential of two stress-wave techniques to detect lathe checks and knots in veneer. Stress wave propagation parameters were sensitive to the presence of defects when measured perpendicular to grain.

Few studies dealt with the effect of sloping grain on nondestructive testing parameters. Kaiserlik and Pellerin (1977) attempted to predict tensile strength of woods containing sloping grain. Divos et al. (2000) used ultrasonic propagation velocity and attenuation parameters to predict grain deviations. They showed that both ultrasonic velocity and the magnitude of the first received amplitude are good indicators of grain deviation. Attenuation is better to detect small grain angles, while propagation velocity – which is a function of the direction-dependent MOE – is a better estimator for the entire grain orientation range. Jung (1979) examined (among other factors) the effect of sloping grain on the stress-wave characteristics of veneers. He found that at

small angles there is little change in stress-wave velocity, but at slightly larger angles it decreases rapidly. There appears to be no study in the literature that uses vibration methods to describe the relationship between MOE and grain angle of wood or veneers.

III.4 Orthotropy of Shear Strength

III.4.1 Background

The orthotropic nature of solid wood is usually depicted in a three-dimensional Cartesian coordinate system as shown on *Figure III.1,* as it has already been mentioned in *Chapter I* (*Fig. I.1*). The principal directions of the material coordinate system are noted as L, R and T, longitudinal, radial and tangential directions, respectively. If an aligned global coordinate system (x_i; i=1,2,3) is systematically rotated around R and L axes, the angles between the axes of L, R, T and x_i'(i=1,2,3) systems denote the grain and ring orientation of solid wood relative to the global coordinate system as marked on Figure 1. Note, that the x_1' x_3' plane is always parallel to the grain. If shear forces are acting in the above mentioned plane and the direction of the applied forces is x_1', the orthotropy of shear strength can be investigated as a function of grain and ring angle.

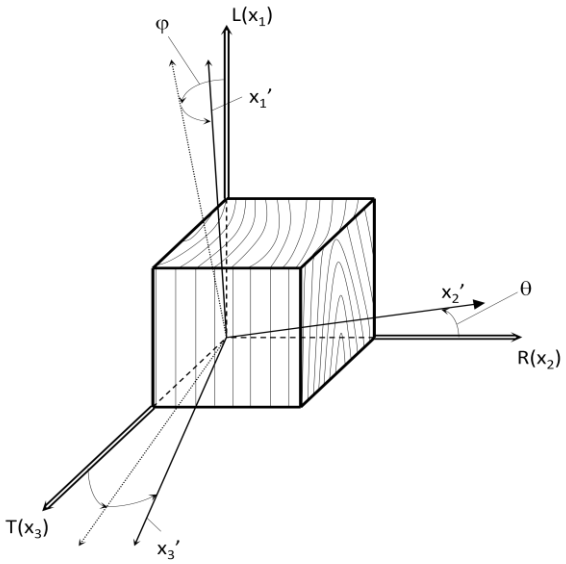

Figure III.1. *Orthotropy of solid wood in principal and global coordinate systems. The interpretation of grain angle (φ) and ring angle* (*θ*).

Using the described rotation, block shear specimens can be machined and tested. Such specimens are shown on *Figure III.2* representing the shear strength (τ) measurements in the principal material directions. The first subscript of τ marks the direction normal of the sheared plane while the second denotes the direction of shear forces. Specimens on *Figures 2a* and *2c* represent the standard shear applications parallel to the grain, while shear strength measured on specimens *b* and *d* are sometimes referred to as rolling shear of solid wood.

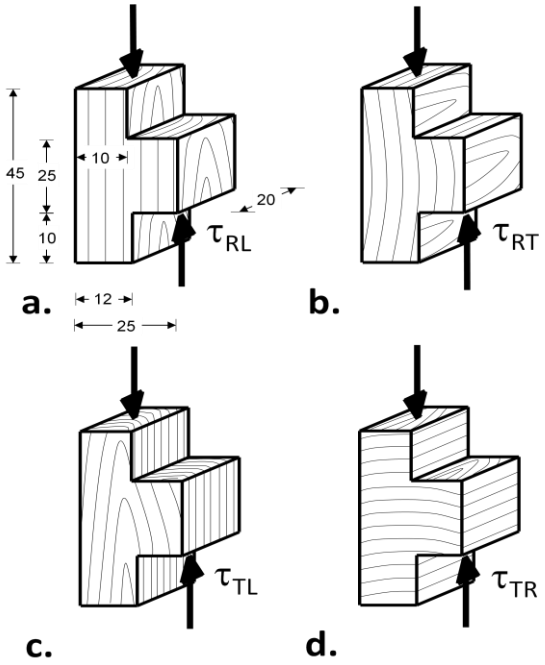

Figure III.2. *Shear in the principal anatomical planes and notation of the corresponding shear stresses. Specimen dimensions in millimeters.* ***a., c.*** *– shear parallel to the grain;* ***b., d.*** *– rolling shear.*

Because of the inherent duality of shear stresses, the failure of the specimens may not manifest in the theoretically sheared plane. Furthermore, the unavoidable normal stresses may induce and propagate cracks along the weakest interface within the volume of the specimen. Such out-of-sheared-plane failure may occur with certain grain and ring angle combinations at the earlywood – latewood boundary or along the ray tissues. Consequently, the experimentally determined values can be considered as apparent shear strength only.

In the following sections theoretical and empirical models are critically evaluated that may be suitable to assess the direction dependent shear strength of solid wood. Experimental materials and methods are outlined along with standard statistical procedures to assess the accuracy of the different approaches.

III.4.2 Models Predicting the Orthotropy of Shear Strength

THE ORTHOTROPIC TENSOR THEORY

In a comprehensive work Szalai (1994) used the orthotropic tensor theory to describe the direction dependent strength and elasticity of wood. Based on Ashkenazi's (1976) strength criteria he applied a four-dimensional tensor approach to predict the shear strength of wood in any oblique plane and direction of shear forces. Substituting the tensor components with the appropriate strength values and eliminating the zero components, resulting from the constraint that shear is applied only in the planes parallel to the grain; the equation takes the following form:

$$\frac{1}{\tau_{\varphi,\theta}} = \frac{4}{\tau_{90^\circ}^{45^\circ}}\cos^2\theta\sin^2\theta\sin^2\varphi + \frac{1}{\tau_{RT}}\cos^2 2\theta\sin^2\varphi + \\ + \frac{1}{\tau_{TL}}\sin^2\theta\cos^2\varphi + \frac{1}{\tau_{RL}}\cos^2\theta\cos^2\varphi \qquad (III.2)$$

where:

φ – grain angle

θ – ring angle

$\tau_{\varphi,\theta}$ – shear strength at grain angle φ and ring θ angle.

τ_{ij} – shear strength in the main anatomical planes, (i = *R,T*; j = *T,L*) where i is the direction normal of the sheared plane and j is the direction of the applied load.

$\tau_{90^\circ}^{45^\circ}$ – shear strength at 90° grain and 45° ring angle (φ = 90°, θ = 45°)

Note that this solution requires four experimentally predetermined strength values: three obtained in the principal anatomical planes such as τ_{RL}, τ_{RT} *and* τ_{TL} shown on *Figure III.2a, b* and *c*, respectively and a strength value at 90° grain and 45° ring angle ($\tau_{90^\circ}^{45^\circ}$). The advantages of this model are that it has a firm theoretical basis, uses only four experimentally determined data points for prediction, and is very straightforward.

QUADRATIC MODEL

Cowin (1979) demonstrated that the shear strength of wood may follow the Hankinson-type strength criterion in a quadratic form. Liu and Floeter (1984) used a tensor polynomial theory, developed by Tsai and Wu (1971), to re-derive the formula for predicting shear strength in a principal material plane of solid wood. The equation in general form is given as follows:

$$\tau_{\varphi}^{\,2} = \frac{\tau_{0^\circ}^{\,2}\tau_{90^\circ}^{\,2}}{\tau_{0^\circ}^{\,2}\sin^2\varphi + \tau_{90^\circ}^{\,2}\cos^2\varphi} \qquad (III.3)$$

where:

τ_{φ} – estimated shear strength at grain angle φ

τ_{0° – shear strength at grain angle j = 0°

τ_{90° – shear strength at grain angle j = 90°

Like Szalai's approach, this formula has a well-defined theoretical basis. However, it does not include the effect of ring orientation and has been verified experimentally in the LT plane only using Sitka spruce specimens.

MODIFIED HANKINSON'S FORMULA

Kollman and Cote (1968) modified the original Hankinson's formula replacing the power 2, to which the trigonometric terms are raised, by an arbitrary power *n*.

The authors claimed that this equation provides better fit than the original Hankinson's formula for predicting tensile strength and modulus of elasticity.

$$\tau_{\varphi} = \frac{\tau_{0^\circ}\tau_{90^\circ}}{\tau_{0^\circ}\sin^n\varphi + \tau_{90^\circ}\cos^n\varphi} \qquad (III.4)$$

Although this model is purely empirical, it has a capability to describe peak shear stresses at inclined grain, by using a higher power (i.e., $n > 2$). Beside the lack of theoretical basis, this model is probably very species specific and requires a significant database for accurate determination of the value of *n*. Like the quadratic formula, it can handle only fixed ring orientation in its present form.

COMBINED MODELS

So far, the orthotropic tensor theory was the only model that could handle both grain and ring angle changes. Researchers addressed the effect of ring orientation on the shear strength parallel to the grain and usually found it negligible. The apparent low degree of orthotropy of shear strength between the LT and LR main anatomical planes (i.e., $\tau_{RL} \approx \tau_{TL}$) did not trigger extensive model development to describe the phenomenon. The only available model was published by Szalai (1994). It includes two equations derived from tensor analysis as follows:

$$\tau_{0^\circ;\theta} = \frac{1}{\left(\cos^2\theta/\tau_{RL} + \sin^2\theta/\tau_{TL}\right)} \qquad (III.5)$$

$$\tau_{90^\circ;\theta} = \frac{1}{\cos^4\theta/\tau_{RT} + \sin^4\theta/\tau_{TR} + \left(1/\tau_{90^\circ}^{45^\circ} - 1/4\tau_{RT} - 1/4\tau_{TR}\right)\sin^2 2\theta} \qquad (III.6)$$

where:

$\tau_{0^\circ;\theta}$ – shear strength at θ ring angle, $\varphi = 0°$;
$\tau_{90^\circ;\theta}$ – shear strength at θ ring angle, $\varphi = 90°$;

and the other symbols are as given at Equation *III.2*

Equation III.5 approximates the shear strength of traditional, parallel to the grain specimens as a function of ring orientation. It requires two experimentally predetermined strength values. The rolling shear strength variations are given by *Eq. III.6* where three predetermined strength values are needed. Note that τ_{RT} and τ_{TR} represent the maximum stresses (*i.e., shear strength*) values. Due to the duality, the stresses in these two directions are identical. However, it is not necessarily true for the strength values of wood because of the unpredictable

failure mode as discussed earlier. Although these equations have not been experimentally verified, theoretically they should describe the effect of ring orientation on the shear strength of orthotropic materials.

One can realize that these equations can provide predetermined strength data for the quadratic model and for the modified Hankinson's formula for predicting the effect of grain orientation. Consequently, combining *Equations III.5* and *III.6* with *Equations III.3* or *III.4* we can obtain additional two models for estimating the orthotropy of shear strength as a function of grain and ring orientation. This combination for the quadratic model is given in a short-hand form as follows:

$$\tau_{\varphi,\theta}{}^{2} = \frac{\tau_{0°;\theta}{}^{2}\,\tau_{90°;\theta}{}^{2}}{\tau_{0°;\theta}{}^{2}\sin^{2}\varphi + \tau_{90°;\theta}{}^{2}\cos^{2}\varphi} \qquad (III.7)$$

Furthermore, using the modified Hankinson's formula we obtain:

$$\tau_{\varphi,\theta} = \frac{\tau_{0°;\theta}\,\tau_{90°;\theta}}{\tau_{0°;\theta}\sin^{n}\varphi + \tau_{90°;\theta}\cos^{n}\varphi} \qquad (III.8)$$

Figure III.3 gives a graphical explanation of these combined models. Note that both of these approximations require five experimentally predetermined strength values and *Equations III.6 or III.7* should be solved *m* times where *m* is the resolution (*i.e., m = (1 + 90/ring angle increment*)). During this research these two models along with the orthotropic tensor theory (*Equation III.2*) were fitted to experimental data and statistically analyzed.

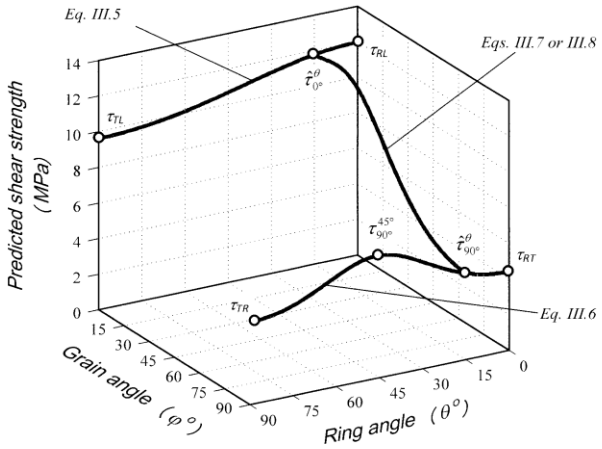

Figure III.3. *The principle and interpretation of the combined model.*

III.4.3 Materials and methods for shear strength assessment

Experimental determination of shear strength values included three Appalachian hardwood species: quaking aspen (*Populus tremuloides*), red oak (*Quercus rubra*) and yellow-poplar (*Liriodendron tulipifera*); and two European hardwood species: true poplar (*Populus x. Euramericana cv. Pannonia*) and turkey oak (*Quercus cerris*). *Figure 2a* shows the specimen shape and target dimensions which differed from that specified by the ASTM D 143-94 standard.

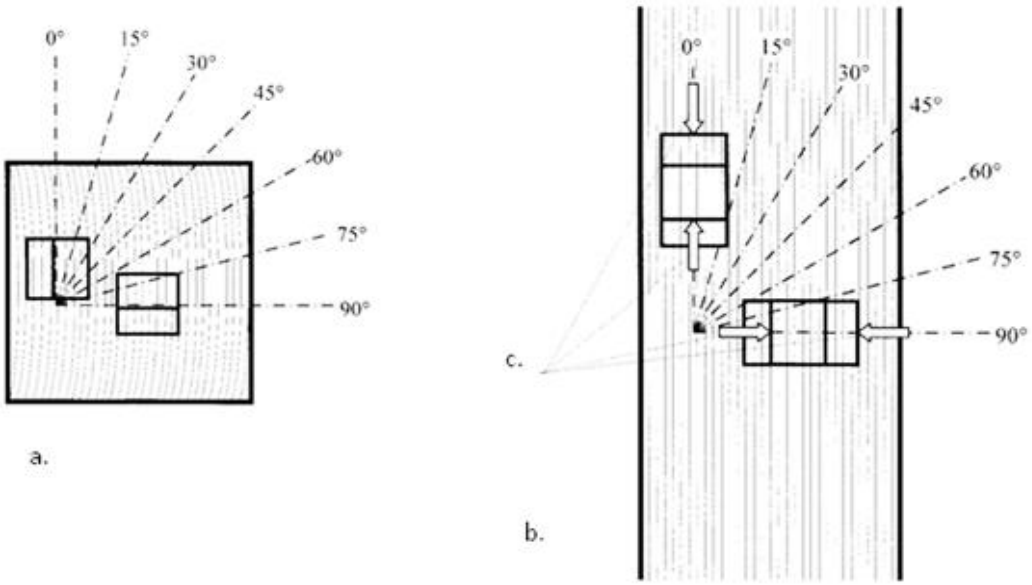

Figure III.4. *Schematic of the specimen manufacturing practice from straight-grained blanks.* ***a.*** *- top view;* ***b.*** *- side view and* ***c.*** *- direction of the applied shear forces.*

The double-notched shear blocks were prepared from blanks having varying ring and grain angle between 0° and 90° with 15° increments. *Figure III.4* demonstrates this specimen preparation practice. Test series included sets for all combinations of the above angles, for all the examined species. The sample size for each set varied between six and fifteen.

Prior to testing, specimens were conditioned to approximately 12% moisture content in a controlled environment (i.e., 21°C and 65% RH). Representative samples of specimens (n=10) were prepared for moisture content and specific gravity determination. The evaluation of these physical properties followed the specifications of the relevant ASTM standards such as ASTM D 4442-94 and ASTM D 2395-93. *Table III.1* contains the summary statistics of these measured properties. Shear forces were applied through a special device providing a single plane of shear within the specimens. The area of the sheared section was approximately 500 mm^2 according to the target dimensions shown on *Figure III.2a.* The advantages of this alternative shear strength assessment and the description of the device were discussed by Lang (1997). *Figure III.5* shows the principle and schematic of the shear testing apparatus along with the experimental setup. The justification of this alternative testing method lies in the smaller specimen dimensions for which

the grain and ring orientations are better controlled. Furthermore, it requires significantly less volume of raw material and waste is minimized when machining more than 1800 specimens.

Table III.1. *Summary statistics of the measured physical properties*

Species	***n***	***Moisture Content [%]***		***Specific Gravity***	
		Mean	*COV [%]*	*Mean*	*COV [%]*
Aspen	*10*	*11.4*	*8.11*	*0.39*	*3.57*
Red Oak	*10*	*11.1*	*2.71*	*0.63*	*5.25*
Yellow-poplar	*10*	*11.3*	*4.50*	*0.39*	*3.41*
True poplar	*10*	*10.9*	*11.01*	*0.37*	*9.51*
Turkey oak	*10*	*11.5*	*7.83*	*0.70*	*5.84*

n – sample size

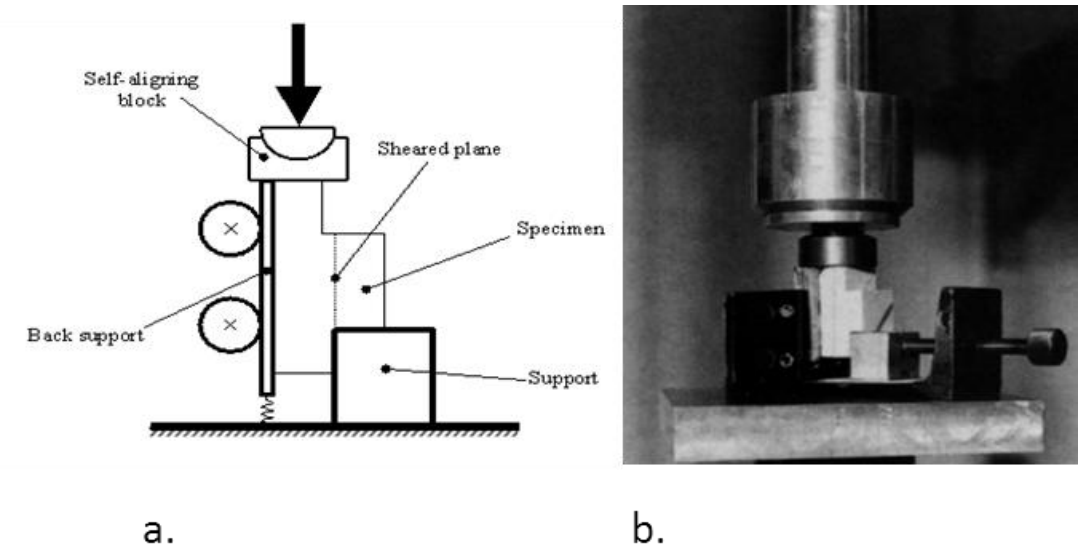

Figure III.5. *Schematic of the testing apparatus* ***(a.)*** *and the experimental setup* ***(b.)****.*

An MTS universal servo-hydraulic testing equipment mounted with 10kN ± 1 N load cell helped to assess the shear strength of the specimens. The machine operated under displacement control with a rate of speed of 0.6 mm/min required by the ASTM D 143 - 94 standard.

II.4.4 Results and discussion of the shear strength exploration

In *Appendix III, Table A.III.1* compiles the basic statistics of all the experimentally obtained shear strength data by species. The mean values - listed in this table - were used to create anisotropy diagrams in three dimensional, Cartesian coordinate systems as shown on *Figures III.6* to *III.8.* The intermediate grid data points were generated by inverse distance interpolation using commercial software: SigmaPlot® (SPSS Inc., 1997) for better viewing.

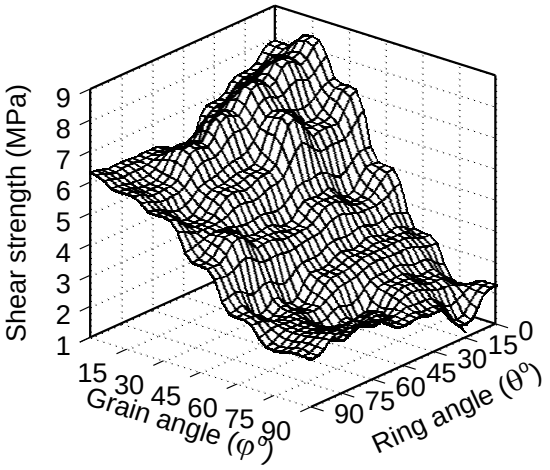

a. - **Aspen** - Experimental values

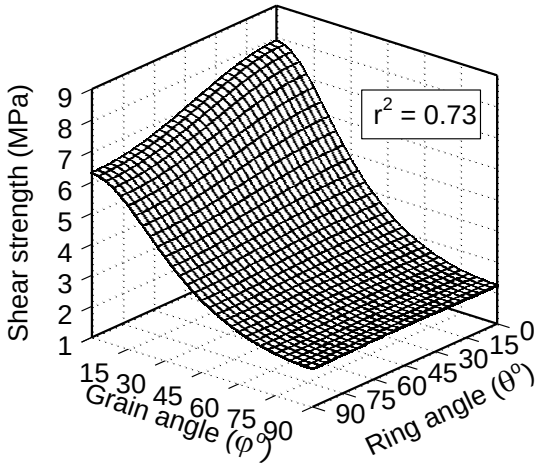

b. - Orthotropic tensor theory

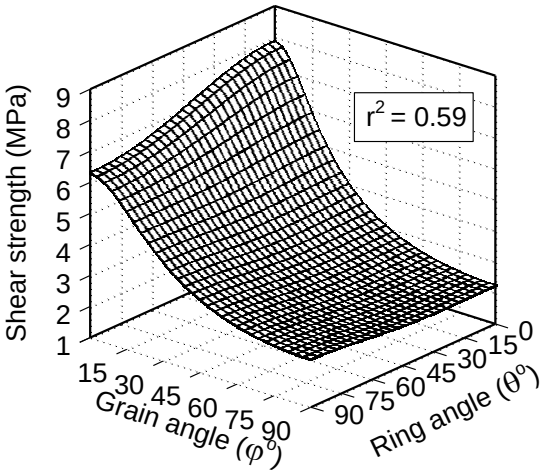

c. - Combined: quadratic formula

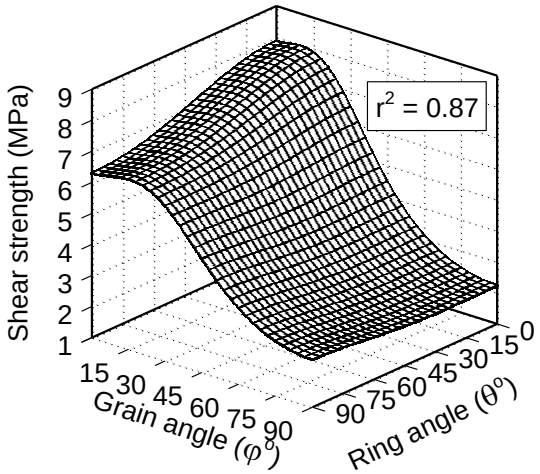

d. - Combined: modified Hankinson's formula

Figure III.6. *Comparison of the experimental and three model predicted shear strength data. Species: aspen (Populous tremuloides). The coefficients of determination (r^2) values are listed.*

In general, shear strength decreased significantly with the increase of grain angle for all species involved in the study. At zero degree grain angle (traditional shear, parallel to the grain), the shear strength decreased slightly as ring angle increased from 0 to 90 degrees. However, this tendency could not be observed at fixed 90° grain angle (i.e., rolling shear). Either a slight increase or local maximum was experienced. It does appear that shear strength at this grain orientation might be species specific as demonstrated by the similarities in strength variations of the two oak species (*Figures III.6a; III.7a&b* and *III.8a&b*).

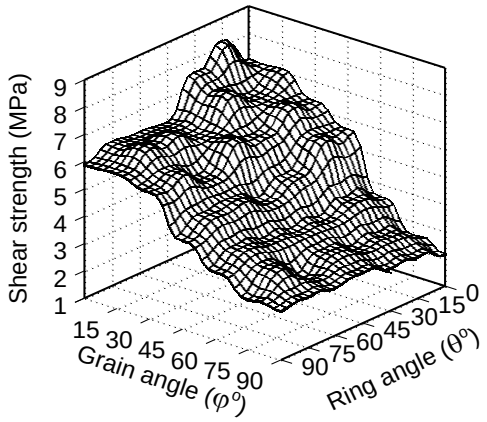

a. - True poplar - Experimental values

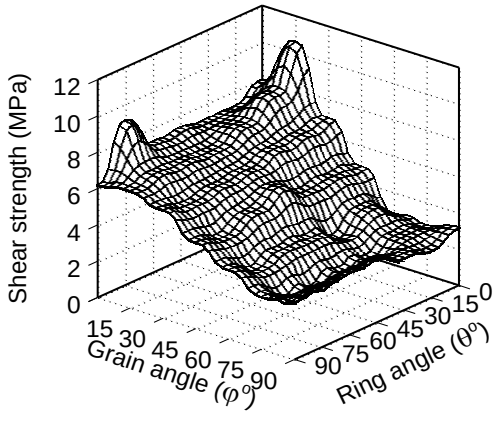

b. - **Yellow-poplar** - Experimental values

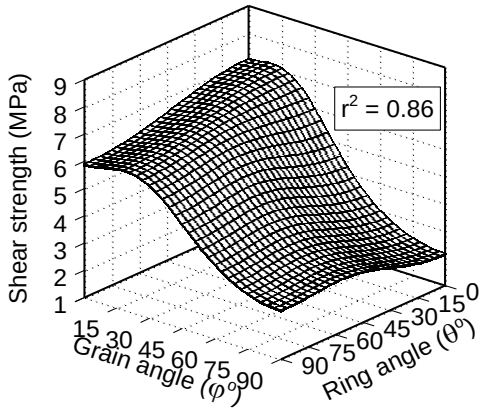

c. - Combined: modified Hankinson's formula

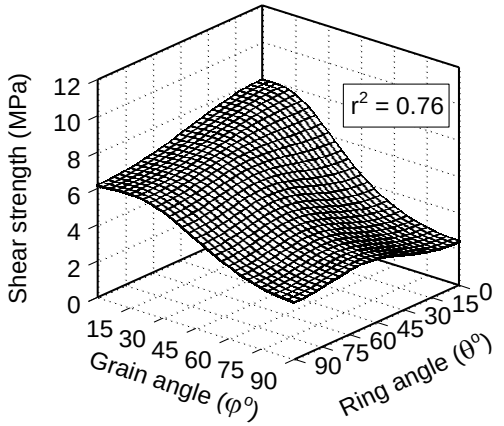

d. - Combined: modified Hankinson's formula

Figure III.7. *Comparison of experimental and model predicted shear strength data by orthotropy diagrams. Species: poplar (Populous x. Euroamericana)* ***a.*** *&* ***c.****; yellow-poplar (Liriodendron tulipifera)* ***b.*** *&* ***d.*** *The coefficients of determination (r^2) values are listed.*

Maximum shear strength values (*MSS*) were not consistently measured at 0° grain orientation. In fact, out of 35 species/ring angle combinations, 23 times the maximum shear strength was observed at 15° grain angle. At 0° ring angle for all the species - except turkey oak - the MSS was measured at 15° grain orientation. No further specific trend or pattern could be detected as demonstrated in *Table A.III.1* by the bold and italic set MSS values. Other researchers reported the same phenomenon (Ashkenazi, 1959; Szalai, 1994). This characteristic may be explained by studying the stress distribution function along the length of the sheared plane. Yilinen (1963) concluded that this function depends on the length to width ratio of the sheared plane and other factors including force application method, etc. It might be suspected that the stress distribution at 15 degree grain orientation becomes more uniform along the length of the sheared plane, while possible stress peaks near the entrance notch at 0 degree grain angle accelerate the failure. This problem needs further investigation.

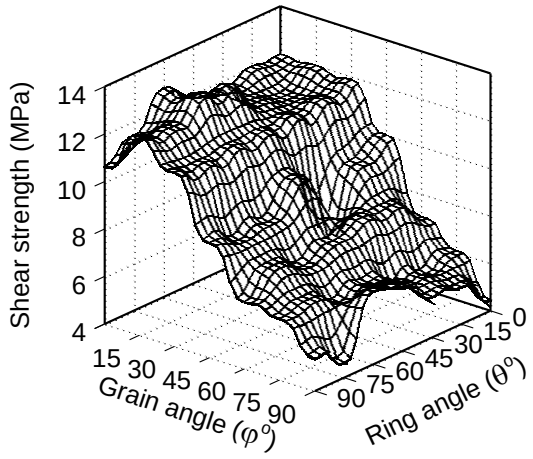

a. - **Red oak** - Experimental values

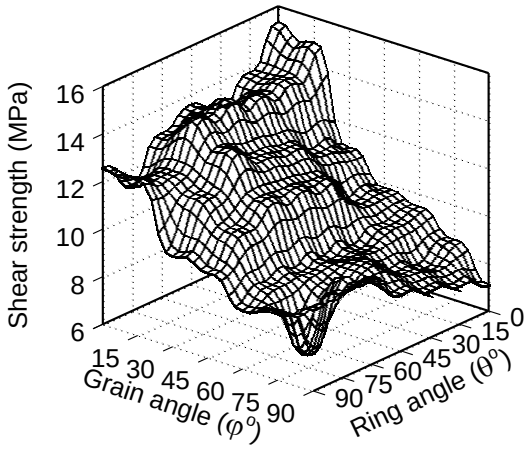

b. - **Turkey oak** - Experimental values

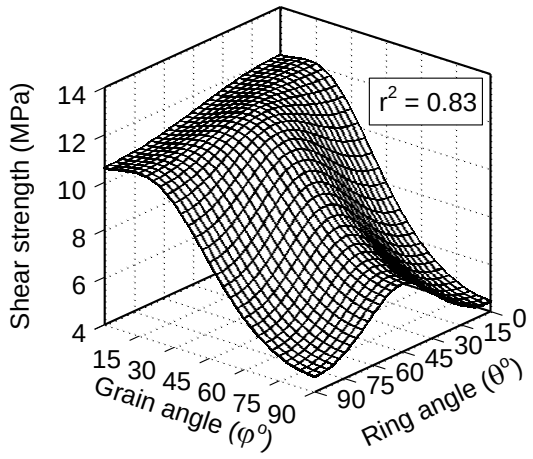

c. - Combined: modified Hankinson's formula

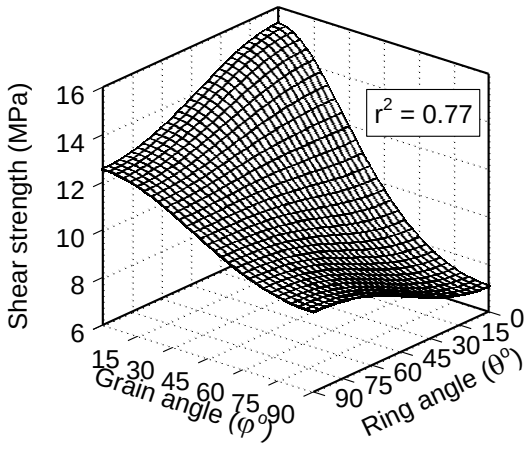

d. - Combined: modified Hankinson's formula

Figure III.8. *Comparison of experimental and model predicted shear strength data by orthotropy diagrams. Species: Red oak (Quercos rubra)* ***a.*** *&* ***c.****; Turkey oak (Quercus cerris)* ***b.*** *&* ***d.*** *The coefficients of determination (r^2) values are listed.*

The failure mode experienced during this study was not always pure shear. Over 45° grain angle, ring-porous wood (oak) inclined to fail along the earlywood/latewood interface or along the ray-parenchyma. The same tendency was encountered regarding the other species as the grain angle approached 90°. Liu and Floeter (1984) observed similar failure modes when testing Sitka-spruce specimens in pure shear in the LT plane. They concluded that the shear strength depends only on the initiation of failure and not on the direction of fracture propagation. Consequently, we deemed the obtained data as apparent shear strength. All of the measured shear strength values were kept, even if the specimen failed in a plane that was out of the theoretically sheared plane.

III.4.4 Prediction of shear strength - inferences based on statistical evaluations

Standard statistical evaluation of the data included two-way ANOVA procedure at 95 % confidence level (α = 0.05). The two factors were the grain and ring orientations, both with seven levels concurring with the 15° angle increments. For all species, the procedure revealed statistically significant differences among the levels of both factors. Furthermore, significant interaction was detected between the two factors. These results justify the applicability of prediction models that account for the effect of both ring and grain angle on the shear strength. *Table III.2* contains a typical ANOVA outcome.

Table III.2. *– ANOVA results – aspen shear strength.*

Source	*df*	*Sum of squares*	*Mean square*	*P value*
Model	48	1727	36.0	<0.0001
Grain angle	6	1530	255.0	<0.0001
Ring angle	6	40	6.7	<0.0001
Grain x Ring	36	125	3.5	<0.0001
Error	364	111	0.3	
Total	412	1383		

Note, that four out of five data sets by species had lack of normality and demonstrated unequal variances. The violation of these statistical assumptions originated from the limited sample size. Based on the standard deviations of the measurements, robust statistical analyses would have required approximately two hundred specimens for each factor and level combination. Thus, complete randomization could not be achieved. More extensive testing and the fulfillment of completely randomized design were beyond the limitations of this research.

In the next step, the selected models, including the orthotropic tensor theory and the two combination models, based on the quadratic formula and the modified Hankinson's equation, were evaluated for the accuracy of their estimation. The necessary input data (τ_{RL}; τ_{TL}; τ_{RT}; τ_{TR}; $\tau_{90^\circ}^{45^\circ}$) were the average measured strength values. The power (n) for the modified Hankinson's equation was determined by curve fitting, using the entire experimental database. Each species had its n value that is listed in *Table III.3.* The model generated strength values were plotted as orthotropy diagrams for visual evaluation. *Figure III.6* shows the comparison between experimental and the three model predicted results for aspen.

Due to the deficiency of complete randomization, conservative statistical fitting procedures resulted in lack of fit for all of the cases. Furthermore, the shear stresses for several species and angle combinations could not be assessed for different reasons. This resulted in unequal sample sizes. Thus, we selected the r^2 analysis to evaluate and rank the performance of the fitted models. The coefficient of determination (r^2) is a measure of how well the model describes the data. Larger values, close to 1, indicate that the model describes the relationship between independent and dependent variables well. A*ppendix III* contains the discussion and justification of the r^2 analysis.

Table III.3. *Coefficients of determination (r^2) provided by the various prediction models.*

Species	***Orthotropic tensor theory***	***Combination models***		
		Quadratic formula	***Modified Hankinson's formula***	
	r^2	r^2	***n***	r^2
Aspen	0.73	0.59	2.72	0.87
Red oak	0.61	0.57	2.62	0.83
Yellow-poplar	0.68	0.62	2.47	0.76
True poplar	0.63	0.55	2.70	0.86
Turkey oak	074	0.76	2.05	0.77

n – power in the Hankinson's formula.

Table III.3 compiles the results of the coefficients of determination analyses by species and model types. For all species, the combination model based on the modified Hankinson's equation resulted in the closest agreement with experimental data. *Figures III.6* to *III.8* show the comparison of experimental data and best model predictions by orthotropy diagrams with the listed r^2 values. The good performance of this model was expected because the power determination was based on the entire experimental data set. Furthermore, only this model can mathematically estimate the peak stresses at small grain angle deviations.

Calculated r^2 values indicate that *Equation III.2*, derived from a 4-dimensional tensor analysis, can predict the orthotropy of shear strength reasonably well. The consistency of this model regarding the quality of the predictions and its strong theoretical background encourage the use, although the model can not predict the peak stresses other than at 0° grain orientation.

Conversely, the combined model, using the quadratic formula, did not provide good fit for four out of five species. Although the calculated r^2 values were over 0.55 that are acceptable for biological materials, compared to the other models the accuracy of the predictions was significantly lower. Results implied that the derived equation may not be valid in all the oblique directions other than the principal anatomical planes because of the unique composite structure of solid wood.

Test results of turkey oak (*Quercus cerris*) revealed high degree of orthotropy as a function of ring angle especially around 0° grain orientation (*Figure III.8b*). The r^2 values were about the same for all three models regarding this species and the power of the modified Hankinson's formula approached 2 as originally proposed. However, compared to the other hardwoods, the r^2 of the Hankinson's model was notably inferior. On the contrary, the prediction performance of the orthotropic tensor theory and the quadratic formula improved significantly for turkey oak. Results of these analyses indicated that the shear strength of solid wood can be reasonably predicted in any oblique direction. One might say that the orthotropic tensor theory and the developed combination model, based on the modified Hankinson formula, provided adequate estimates about the nature of shear strength for wood.

III.5 Orthotropy of Strength and Modulus of Elasticity in Compression

III.5.1 Background and deliberations

Although wood is usually modeled as an orthotropic material, in reality it is cylindrically orthotropic. The compression strength determination of cross-grained wood blocks always depends on the size, shape, manufacturing precision (*parallelism*) and support conditions of the specimen. Furthermore, the inherent natural variability of wood coupled with the ambiguous definition of failure stresses generates several difficulties in application of advanced failure theories.

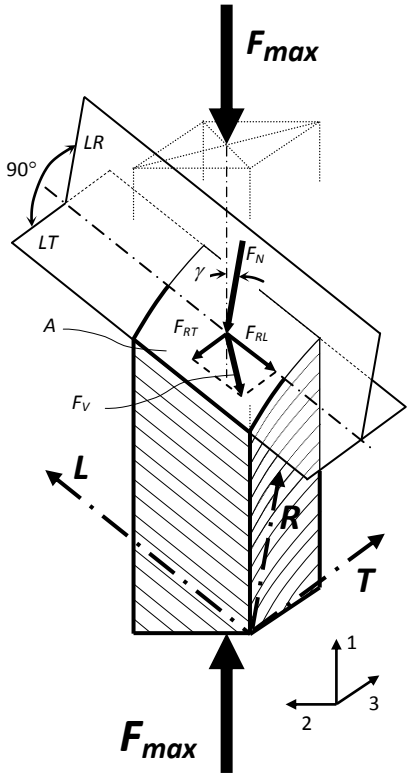

Figure III.9. *Internal force condition of an oblique specimen under compression.*

Consider an ideal, cross-grained specimen for compression strength assessment in a global coordinate system as shown on *Figure III.9* where the anatomical directions (*L*, *R* and *T*) are marked, as well. In an arbitrarily selected *LT* principal anatomical plane of the specimen, the compression force (F_{max}) can be broken into a normal (F_N) and an in-plane (F_V) component. The area (A) of this inclined sectional surface can be approximated using trigonometric identities. F_V can be considered as a resultant of F_{RL} and F_{RT} that induce parallel to the grain shear stress at 0° ring angle and rolling shear, respectively. If the ratio of F_V to the sectional area of the specimen (F_V/A) in the *LT* plane exceeds the shear strength ($\tau_{\vartheta\Theta}$) the specimen will fail in shear under compression. The subscripts, ϑ and Θ are the angles between F_V and the direction of the fibers, and between the sheared and *LT* planes, respectively. For this particular case, $\Theta = 0$. Because several species demonstrated relatively low degree of shear orthotropy concerning the ring

orientation, one can realize that shear failure is possible in any plane between *LT* and *LR*, if the induced shear stresses are large enough. In fact, off axis compression specimens were used to evaluate the shear strength of Finnish pine by Ylinen (1963) in the *LT* and *LR* planes. The relationship between shear and normal stresses for grain inclination range of $12° < \varphi < 32°$ was given as follows:

$$\tau_{max} = \frac{1}{2}\sigma_{max}\, sin2\varphi \qquad (III.9)$$

One should note that this shear failure stress is biased by a compression stress (σ_q) normal to the plane of failure:

$$\sigma_q = \sigma_{max}\, sin^2\varphi \qquad (III.10)$$

Where $\sigma_{max} = \sigma_1$ is the ultimate compression stress (strength) in the global coordinate system and φ is the grain angle.

Experimental results of Ylinen (1963) showed that there is a consistent shear strength difference at the studied grain angles between the *LR* and *LT* planes. This indicates some interactions between grain and ring orientations. The ambiguous failure modes, coupled with the inherent natural variability of wood, allow the exploration of apparent strength only for particularly defined specimens. The size, the slenderness ratio of the specimen, and the end conditions, along with the existence or lack of lateral supports may affect the measured compression strength values. Furthermore, the determination of E in compression may be also biased by some of these conditions and the induced shear strain may affect the measured normal strain.

The complexity of the failure phenomenon and the above-discussed problems make the predictions difficult and sometimes unreliable. However, some approaches that incorporate both the ring and grain angle variations can predict the orthotropic compression strength and stiffness with reasonable accuracy. Such methods, that were verified and used during this research, are briefly discussed next.

III.5.2 Modeling the orthotropy of strength and modulus of elasticity in compression

Selection criteria for models that can predict both E_c and compression strength (σ_c) were simplicity, minimum input requirements, and validity at any grain (φ) and ring angle (θ) combination. While the simplicity is not a vital problem because of the advances in computer science, models that needed all nine independent elastic constants as inputs were not considered. Therefore, two procedures, a theoretical and an empirical, were selected.

STRENGTH /STIFFNESS TENSOR THEORY

Szalai (1994) provided an approach for calculating the normal strength of orthotropic materials in any direction. The equation can be derived from the Ashkenazi's strength tensor (Ashkenazi,1978) by transforming the first element of the tensor. After eliminating the zero components, the equation takes the following form:

$$\begin{aligned}\frac{1}{\hat{\sigma}_{\varphi\theta}} = {} & \frac{1}{\sigma_L}\cos^4\varphi + \frac{1}{\sigma_R}\sin^4\varphi\sin^4\theta + \frac{1}{\sigma_T}\sin^4\varphi\cos^4\theta \\ & + \left(\frac{4}{\sigma_{RT}^{L45^\circ}} - \frac{1}{\sigma_R} - \frac{1}{\sigma_T}\right)\sin^4\varphi\sin^2\theta\cos^2\theta \\ & + \left(\frac{4}{\sigma_{LT}^{R45^\circ}} - \frac{1}{\sigma_L} - \frac{1}{\sigma_T}\right)\cos^2\varphi\sin^2\varphi\cos^2\theta \\ & + \left(\frac{4}{\sigma_{LR}^{T45^\circ}} - \frac{1}{\sigma_L} - \frac{1}{\sigma_R}\right)\cos^2\varphi\sin^2\varphi\sin^2\theta\end{aligned} \qquad (III.11)$$

where: $\hat{\sigma}_{\varphi\theta}$ – predicted compression strength at grain angle φ and ring angle θ;

σ_i – compression strength in the principal anatomical directions ($i = L,R,T$);

$\sigma_{RT}^{L45^\circ}$ – compression strength at $\varphi = 90°$; $\theta = 45°$;

$\sigma_{LT}^{R45^\circ}$ – compression strength at $\varphi = 45°$; $\theta = 0°$;

$\sigma_{LR}^{T45^\circ}$ – compression strength at $\varphi = 45°$; $\theta = 90°$.

The six strength values listed in *Equation III.11* should be determined experimentally. Note that by replacing the strength with the appropriate $E_{\varphi\theta}$ values, the evaluation of the elastic orthotropy can be performed. *Appendix III* contains the derivation of this tensorial approach from the compliance matrix and from the Ashkenazi's strength tensor for E values determination and strength evaluation, respectively.

THREE-DIMENSIONAL HANKINSON 'S FORMULA

Bodig and Jayne (1982) based their approach partly on the Hankinson formula, and on the observed compression strength pattern in the *RT* plane. According to the authors, the strength variation pattern in this plane consists of a linear and a sinusoidal component:

$$\sigma_{90^\circ;\theta} = \left[\sigma_T + \frac{\theta}{\pi/2}\left(\sigma_R - \sigma_T\right)\right] + \left[K\left(-\sin 2\theta\right)\frac{\sigma_R + \sigma_T}{2}\right] \qquad (III.12)$$

where: $\sigma_{90^\circ;\theta}$ – the predicted compression strength at 90° grain angle and ring angle θ;

K– empirical constant (0.2 for hardwoods).

Other notations are as in *Equation III.11*.

After calculating this value for a certain ring angle, strength or MOE properties belonging to any grain angle at the given ring angle level can be obtained by substituting this value and σ_L into the Hankinson formula:

$$\hat{\sigma}_{\varphi\theta} = \frac{\sigma_L \sigma_{90°;\theta}}{\sigma_L \sin^2 \varphi + \sigma_{90°;\theta} \cos^2 \varphi} \qquad (III.13)$$

This empirical approach lacks the firm theoretical basis of the orthotropic tensor theory. However, this method requires only three experimentally determined data points in the principal anatomical directions, and the calculation is no more difficult than in the case of previous formula. *Equations III.11* and *III.12* were first validated and then were used to predict the orthotropic compression properties of the examined species as follows.

III.5.3 Materials and methods for modeling the properties in compression

Standard ASTM specimens (ASTM D 143 – 83, secondary method) were prepared from quaking aspen (*Populus tremuloides*), red oak *(Quercus rubra*) and yellow-poplar (*Liriodendron tulipifera*) species. Trees were harvested from the West Virginia University (WVU) forest and sawn into lumber. Specimens from the European species including turkey oak (*Quercus cerris*) and true poplar (*Populus x. Euramericana cv. Pannonia*) were manufactured at the University of West Hungary using locally available commercial lumber. The final dimensions (25 x 25 x 100 mm) were set after conditioning the blank materials to approximately 12% moisture content (MC) in a controlled environment (i.e., 21°C and 65% RH).

Ring and grain angles of the specimens varied between 0° and 90° with 15° increments. Ring angle is not defined at 0° grain orientation and its effect was disregarded at 15° grain angle. The experimental design, therefore, contained only one set of 10 specimens at both 0° and 15° for each species. *Figure III.10* shows the specimen manufacturing practice and the interpretation of grain (φ) and ring (θ) angles. Moisture content and specific gravity (*SG*) determination were done using representative samples of specimens (*n=10*). The evaluation of these physical properties followed the specifications of standards ASTM D 4442-84 and ASTM D 2395-83.

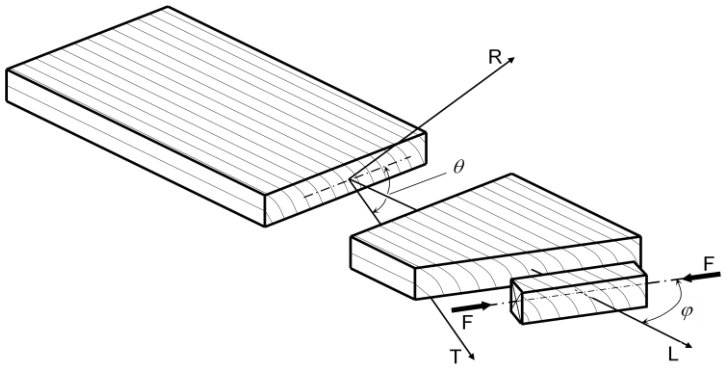

Figure III.10. *Specimen manufacturing practice and the interpretation of φ and θ.*

During the validation of the models for both strength and stiffness, the North American species were used. Approximately 160 specimens of each species provided 4 to 10 replications

for each variable (φ/θ) combination. Testing apparatus included an MTS servo-hydraulic universal machine, equipped with a 10 kN ±1N load cell. Cross-head movement was under displacement control. Compression load application occurred through a self-aligning block placed on top of the specimen. A computerized data acquisition system collected the load and displacement data in real time. Screw-mounted knife-edge pieces held in place the clip-on extensiometers that provided displacement data throughout the test over a gauge length of 41 mm. Two gauges measured the deformations at the opposite, longitudinal side surfaces of the specimens. The obtained pairs of displacement values were averaged and the corresponding load-displacement data were converted into stress-strain diagrams for further analyses. *Figure III.11* demonstrates the experimental assembly. Other parameters of the procedure, including the speed of testing, agreed with the specifications of ASTM D 143 – 83 standard. Load application continued until failure or until the densification plateau of horizontally grained ($\varphi \approx 90°$) specimens was explicitly reached. The failure type of each specimen was visually assessed and recorded.

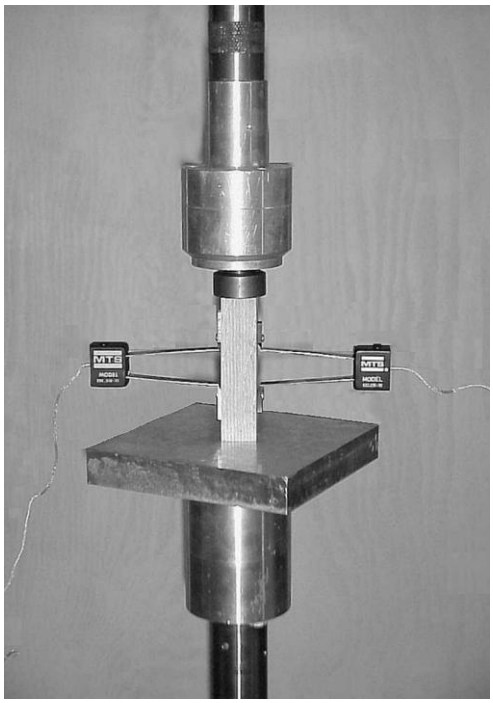

Figure III.11. *Compression force application and the two sided strain measurement.*

Compression E values of the European species were tested at the laboratory of WHU using the above-described techniques. Before testing, the specimens were reconditioned and the parallelism of the surfaces was checked. Only the combinations, required for model inputs, were evaluated by testing 15 replications per factor/level group.

The speed of testing was 0.5 mm/min for the Hungarian species (Turkey oak and true poplar), because of machine constraints. This is slightly higher than that of ASTM requirement. Other parameters including specimen size and conditioning were the same as described above.

The applied statistical methods included the calculation of descriptive statistics and analyses of variances (ANOVA) procedures. We established the validity of the models by curve fitting. Concerns over justification of the usage of these statistical procedures and the detailed description of the r^2 calculation in three dimensional curve fitting is given by *Appendix III* as noted in *Section III.4.4.*

III.5.4 Elaboration on results of the compression property tests and modeling

In *Appendix III, Tables A.III.2 - 4* contain the summary statistics of the measured properties. *Table A.III.5* provides test results for the Hungarian species (Turkey oak and true poplar). These values represent all the experimental data. No outliers were discarded.

In general, the properties of similar species are comparable, except for turkey oak that had somewhat lower E_c values around 0 degree grain orientation compared to the values of red oak. The high degree of orthotropy was evident for all species for both strength and stiffness as a response to grain angle changes. However, the effect of ring orientation was not so clear. It does appear that the changing ring orientation at grain angles < 45° causes strength and stiffness to decrease. At more sloping grain angles, the increasing ring angle tends to improve the compression properties slightly. For all species and for both properties, two-way ANOVA procedures revealed the statistically significant effect of both ring and grain angle at 95% confidence level. Furthermore, the interactions between these factors were also significant. *Table III.4* contains a typical outcome of the ANOVA procedures.

Table III.4. *ANOVA results – aspen compression strength (σ_c).*

Source	*df*	*Sum of squares*	*Mean square*	*P value*
Angle variation	34	1774	52.2	<0.0001
Grain angle	4	1660	415.1	<0.0001
Ring angle	6	39	6.4	<0.0001
Grain x Ring	24	75	3.1	<0.0001
Error	134	133	0.989	
Total	168	1906		

Figure III.12a demonstrates the stress-strain behavior of compression-parallel-to-the-grain specimens by the North American species. In *Figure III.12b* the characteristics of compression perpendicular to the grain at 15° ring orientation can be seen. The long horizontal part of the diagram is the result of subsequent cellular collapse of early-wood followed by late-wood layers. The stabilized stresses in this region were considered as strength values if the specimen did not fail in shear prior to densification. *Figure III.12c* demonstrates the intense compression strength decrease as a function of grain orientation.

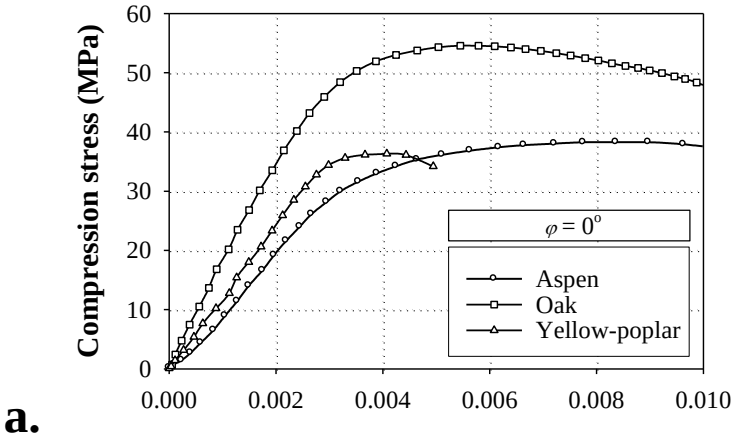

a.

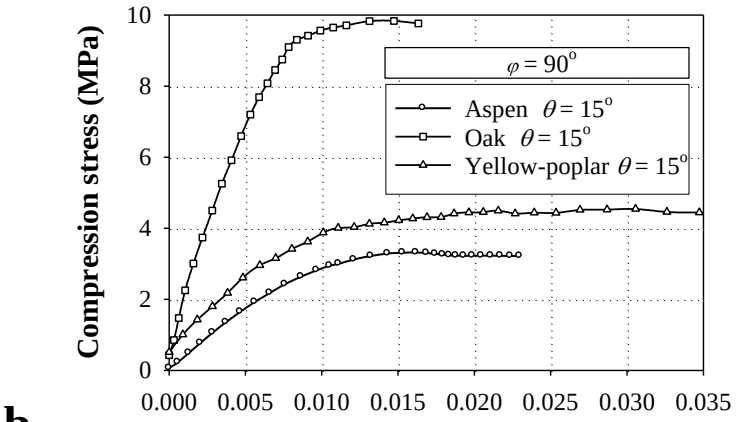

b.

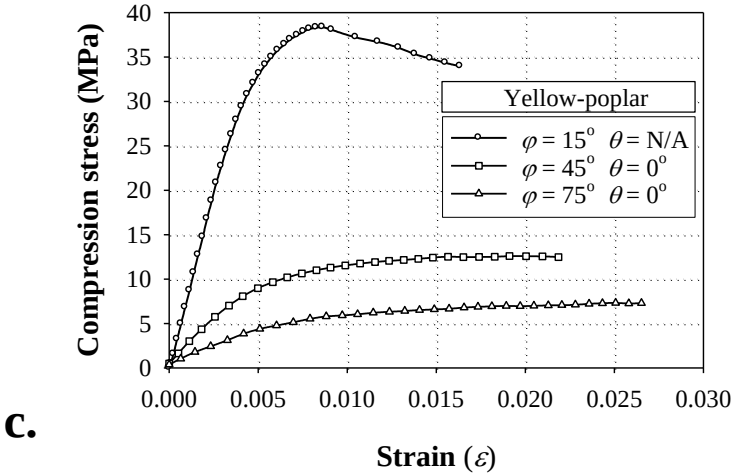

c.

Figure III.12. *Typical stress-strain diagrams of hardwoods under compression.* ***a.*** *– parallel to the grain;* ***b.*** *– perpendicular to the grain;* ***c.*** *– the effect of grain orientation.*

The orthotropic nature of compression strength and elasticity can be studied on *Figures III.13* to *III.15*, for the North American species. Details of ***a.*** and ***d.*** show the experimentally observed strength and E_c values, respectively. The nodes on the diagrams are the tabulated mean property values. The seven values, indicated at 15° grain angle, all correspond to the one average value of ten replications that were measured at this level at random ring orientations. The intermediate mesh data were interpolated using the inverse distance method (SPSS Inc., 1997).

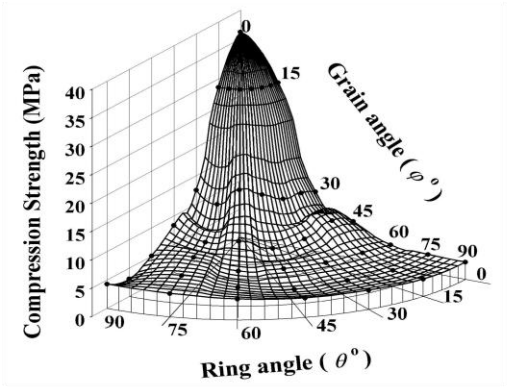

a. *– Experimental strength values*

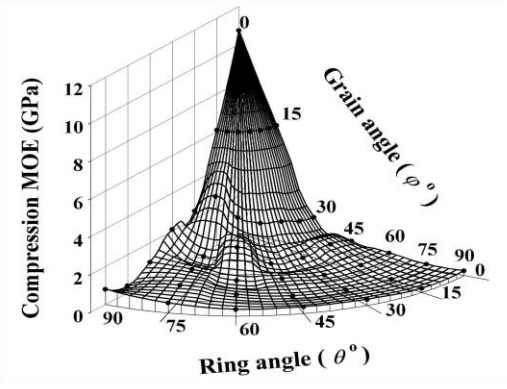

d. *– Experimental MOE values*

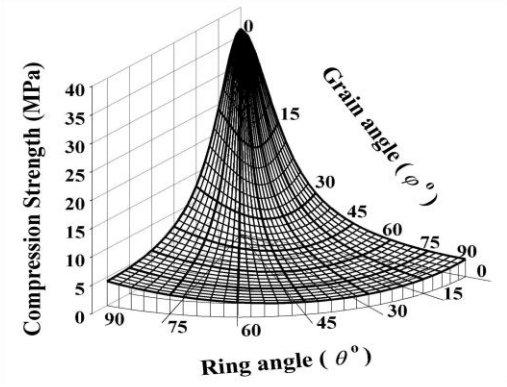

b. *– Predicted – 3D Hankinson formula*

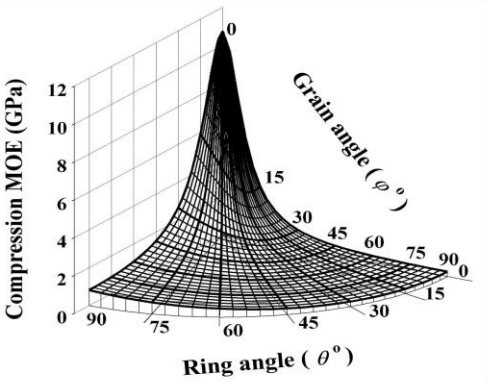

e. *– Predicted – 3D Hankinson formula*

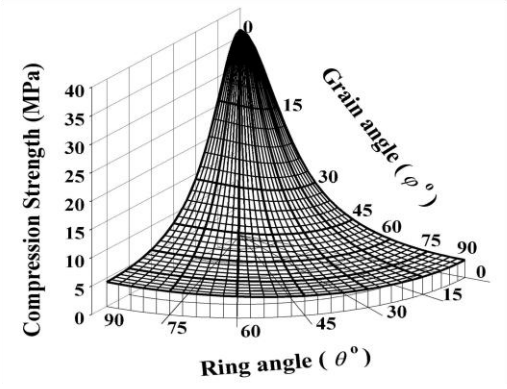

c. *– Predicted – Orthotropic tensor theory*

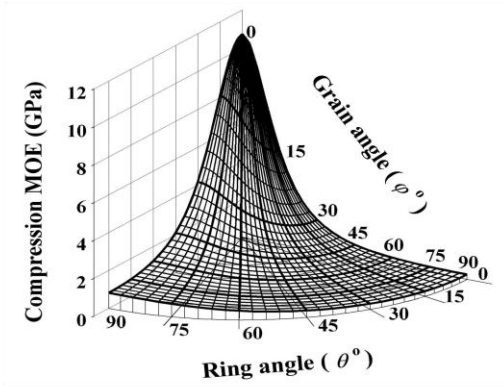

f. *– Predicted – Orthotropic tensor theory*

Figure III.13. *Observed and predicted compression strength and stiffness properties of* ***Quaking aspen*** *by orthotropic diagrams.*

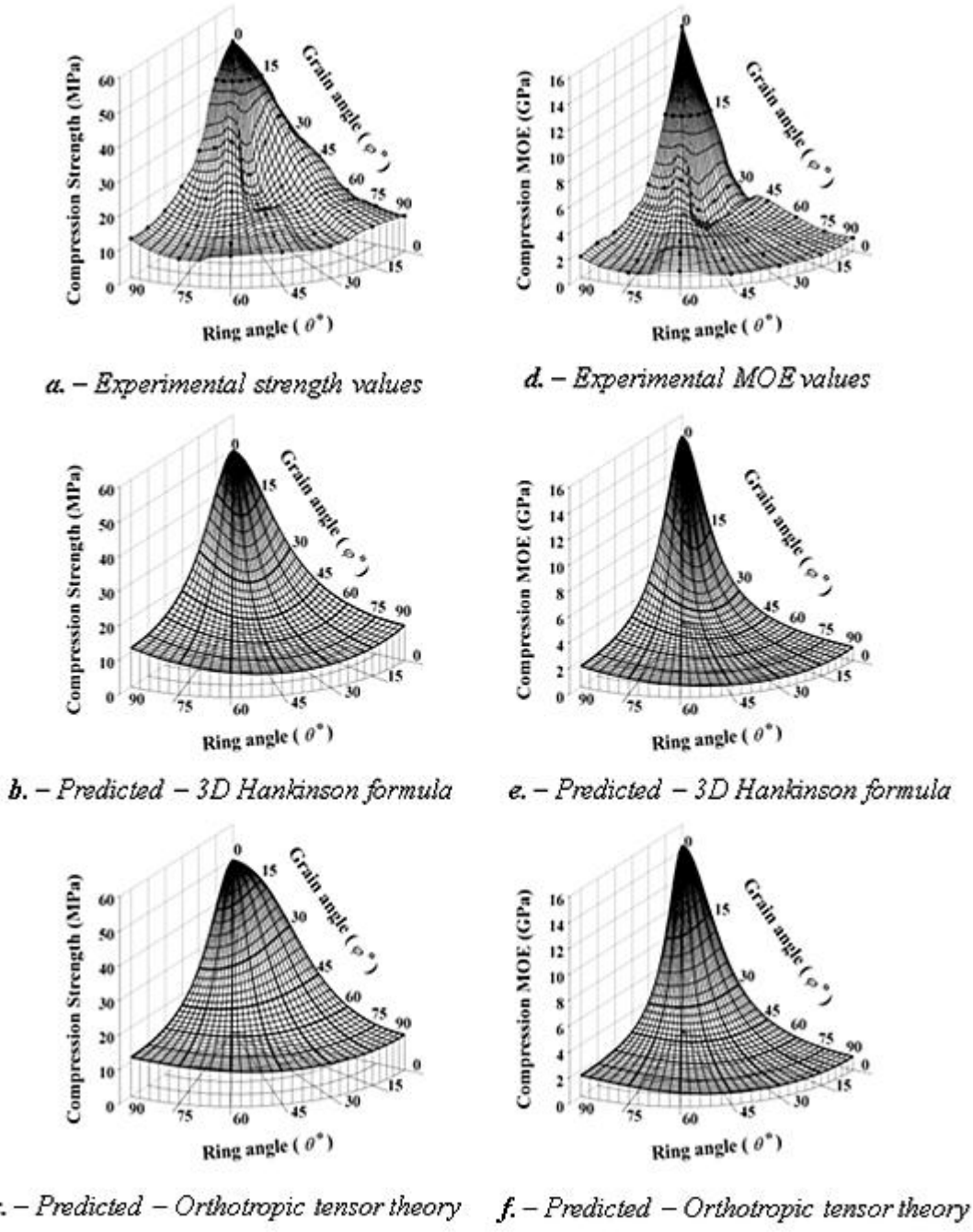

Figure III.14. *Observed and predicted compression strength and stiffness properties of* ***Red oak*** *by orthotropic diagrams.*

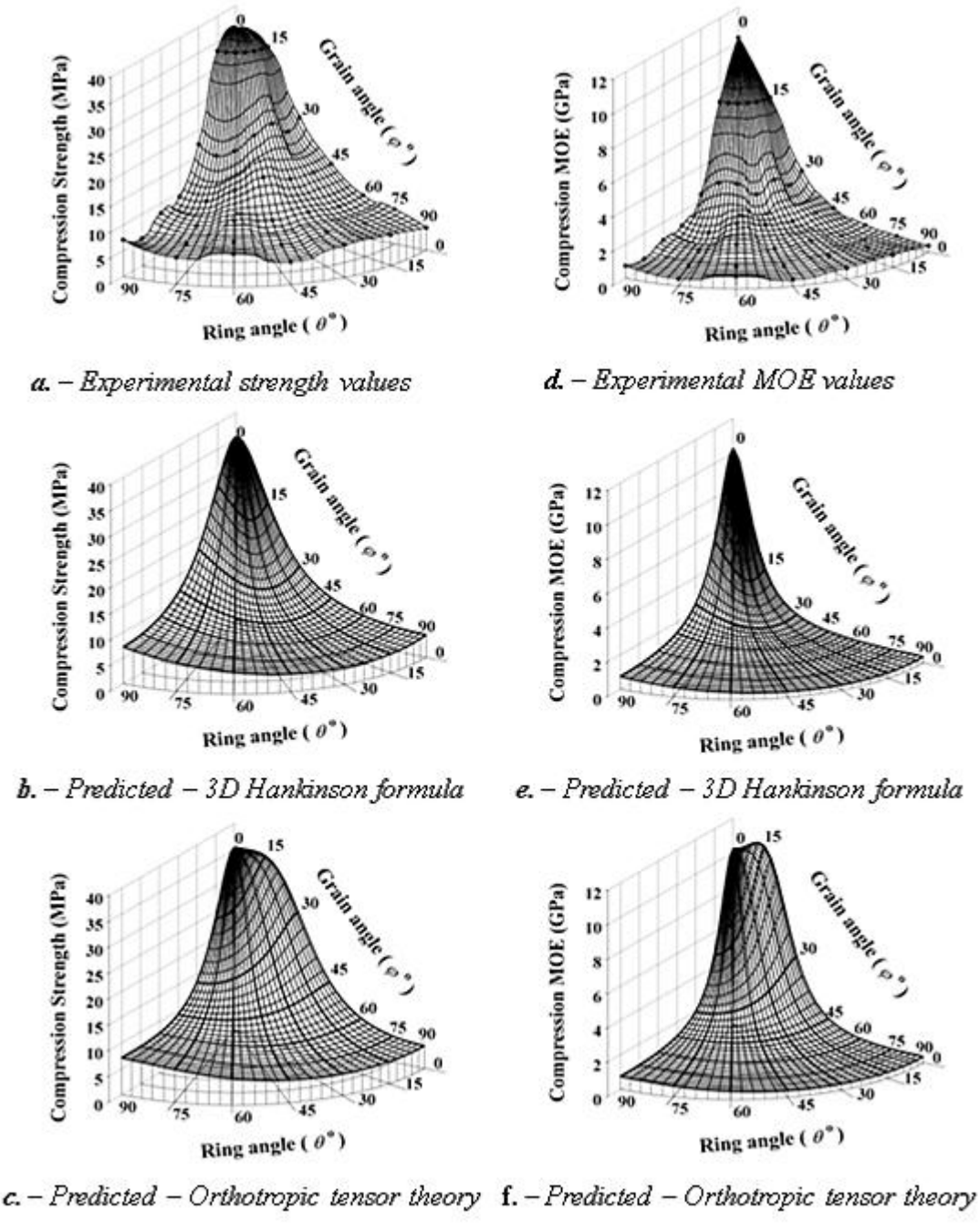

Figure III.15. *Observed and predicted compression strength and stiffness properties of Y**ellow-poplar** by orthotropic diagrams.*

PREDICTION OF THE COMPRESSION PROPERTIES

During the next step, the two discussed models were evaluated for the accuracy of their estimation. The required model inputs, specified earlier, were the average measured strength and E_c values. The model-generated property data were plotted as orthotropy diagrams for visual evaluation. *Figures III.13* to *III.15* provide examples for compression strength and E_c prediction of aspen, red oak and yellow-poplar, respectively. Diagrams marked as ***b*** and ***e*** show the predictions of the 3D Hankinson's formula, while ***c*** and ***f*** represent the predicted values derived from tensor analysis using *Equation III.11*. These diagrams clearly confirm the individual and interaction effect of φ and θ on the strength and E values in compression.

Statistical comparisons of experimental and predicted properties by curve fitting confirmed the applicability of these models. *Table III.5* contains the results of the analyses by species and model types. For aspen and red oak, in the cases of compression strength and E_c, both models demonstrated excellent agreement ($r^2 > 0.9$). For yellow-poplar, however, the prediction quality of the Hankinson's formula decreased, although the r^2 values remained on acceptable levels for both strength and stiffness. The phenomena may be explained by the sensitivity of the Hankinson's equation to small grain angle variations. This is particularly manifested during strength predictions where the effect of small grain deviation on the experimentally measured strength is less significant.

Table III.5. *- Coefficients of determination provided by the two prediction models for compression strength and MOE.*

	Coefficient of determination (r^2) values			
	Orthotropic tensor theory		***3-D Hankinson formula***	
Species	***Compression strength***	***Compression MOE***	***Compression strength***	***Compression MOE***
Aspen	0.93	0.94	0.91	0.91
Red oak	0.93	0.93	0.93	0.94
Yellow-poplar	0.92	0.93	0.72	0.83

FAILURE MODE ANALYSIS

In modeling the compression strength, a failure criterion developed by Ashkenazi (1978) was applied *(Eq. III.11.*). Nahas (1986) provided detailed evaluation of this criterion along with others. Although the criterion includes the interaction effect, the basic assumption of it is that the failure is independent from the deformation. Consequently, it can not provide information about the type of failure.

During the compression strength determination, several types of failure were observed. *Figure III.16* shows the most characteristic failure modes, where specimen *a* demonstrates a typical compression failure. Specimens *b* and *c* failed as a combination of cellular collapse and shear as indicated by the horizontal dislocation of certain parts of the blocks. Clear shear failures in the *LR* an *LT* planes are represented by specimens *d* and *e*, respectively. Most of the

perpendicular-to-the-grain specimens ($\varphi = 90°$) did not fail at all, due to the unique densification characteristic of solid wood. For safety reasons, tests were stopped as soon as the stress level explicitly stabilized in the plateau region.

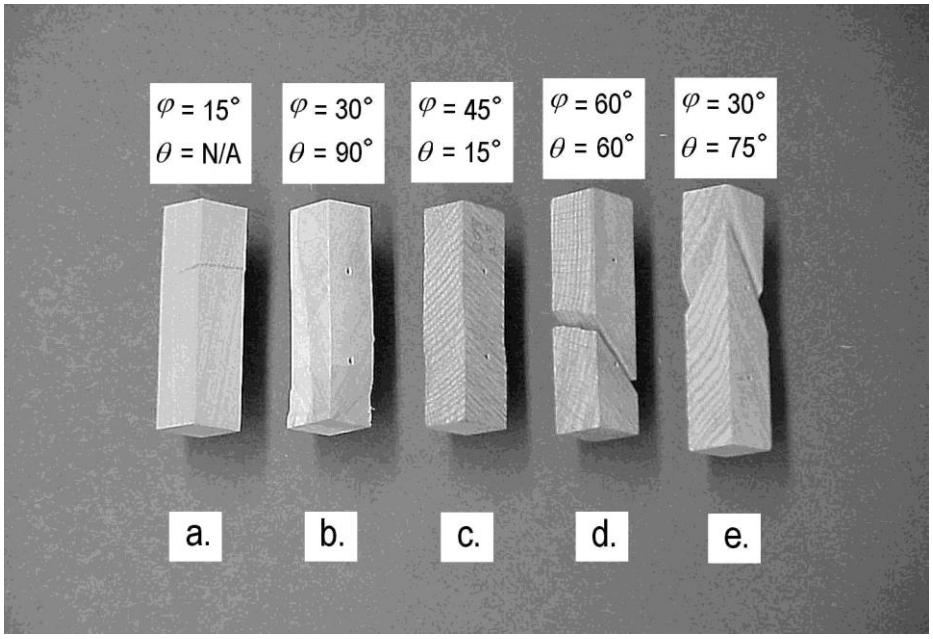

***Figure III.16**. Characteristic failure mode of compression specimens;*
***a.** – compression buckling; **b.** – combined buckling and shear; **d., e.** – shear failure.*

The complexity of failure mode prediction was addressed briefly in an earlier section. In further elaboration of this issue, *Figure III.17* demonstrates the assessment of shear failure's likelihood in the cases of two particular angle combinations under compression stress. First, consider a red oak specimen with $\varphi = 45°$ and $\theta = 15°$ grain and ring orientations under $\sigma_u = 23.24$ MPa compression stress in the global coordinate system. Note that σ_u is the average compression strength of oak for the particular φ/θ combination (*Table A.III.2*). In *Figure III.17*, the mesh represents the principal shear strength of oak in planes parallel to the grain (*Figure III.8c*). Possible combinations of φ and θ are defined by the inter-dependence of the grain orientation of F_V and the rotation angle of the parallel-to-the-grain sheared plane (see *Figure III.9* and explanation in *Appendix III*). The principal shear strength values at these angle combinations form the solid line within the strength surface, which denotes the possible shearing scenarios of the specimen. This line can be considered as the critical shear stress contour of the examined φ/θ compression specimen. The corresponding shear stresses, computed from $\sigma_u = 23.24$ MPa and the inclined sectional areas (A), are represented by the symbols and drop-lines. Solid symbols mark the compression-induced shear stresses that exceed the estimated shear strength, while the empty symbols mark the stresses that are below the strength values. Theoretically, the specimens should have failed in shear, however, because of the natural variability of wood and the presence of normal stresses in the sheared planes, usually a combined failure was observed as shown in *Figure 16c*. The interpretation of ϑ; Θ and the approximation of shear stresses under compression are discussed in more depth in *Appendix III*.

The second example demonstrates that compression may induce shear failure in a horizontally grained specimen too. For specimens with φ = 90° and θ = 45°, the average strength (σ_u) was 9.77 MPa. The critical shear stress contour, in this case, reduces to a single line (dotted in *Figure III.17*) along the lower edge of the shear strength surface because the direction of shear is always perpendicular to the direction of grain for this specimen configuration. The calculated stresses exceed the strength values in the range of 15° > Θ > 0°.

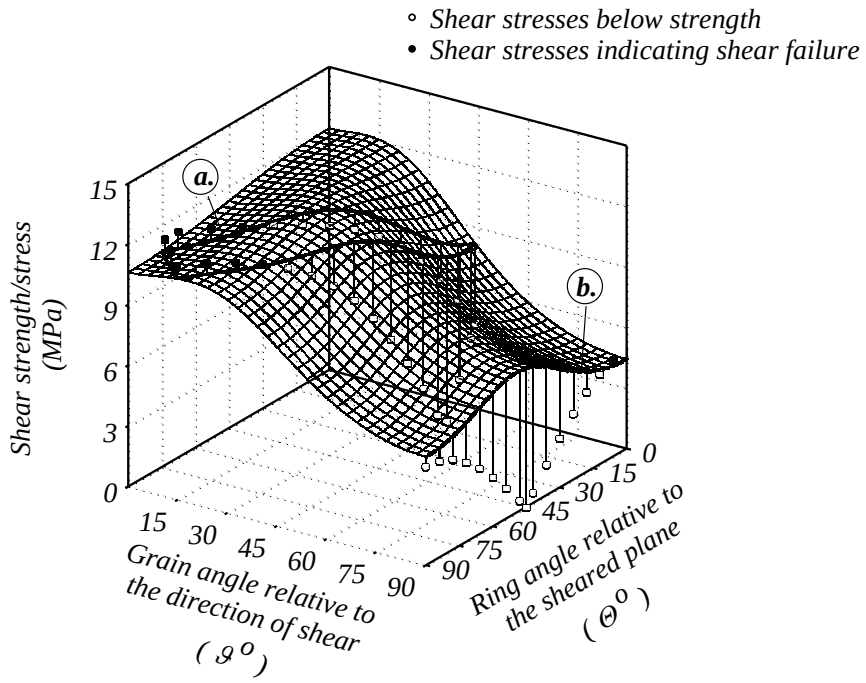

Figure III.17. *Likelihood of shear failure in compression specimens.*
a. *– critical shear stress contour of φ = 45° and θ = 15° specimen; σ_u = 23.24 MPa*
b. *– critical shear stress contour of φ = 90° and θ = 45° specimen; σ_u = 9.77 MPa*

This domain represents inclined planes around 45° relative to the length of the specimen in which shear failure may occur. At Θ = 45° the shear stress is zero because no shear can be induced along the vertical or horizontal planes in the global coordinate system by compression. Unfortunately, the practical application of such analysis is limited, because of the uncertainties in shear strength determination and variations in growth characteristics of natural wood. One might consider that more advanced failure theories like the Tsai-Wu or the von Mises criteria may provide better assessment of compression strength. However, the parameter determination of these criteria involves the same uncertainties due to inherent variability of wood. Some of the delicate experimental techniques used for assessing properties of synthetic composites are not

viable for solid wood. Nevertheless, it may be stated that there is no single failure theory that can be applied to all species and wood-based composites and to all loading conditions.

Up to this point, for practical reasons, the mechanical properties were evaluated and modeled using solid wood specimens. The next section discusses the properties of furnish materials for structural composites. These includes structural and decorative veneers in some forms i.e., strands, veneer ribbons and clippings.

III.6 The Orthotropy of MOE for Structural and Decorative Veeneers

III.6.1 Objectives and theoretical background

The work discussed in this section was aimed at exploring the orthotropy of modulus of elasticity (MOE) in tension for structural and decorative veneers. The research involved *1.)* the experimental determination of MOE of veneer sheets using an ultrasonic technique; *2.)* the development and methodical evaluation of models that address the effect of grain orientation on the changes of MOE; and finally *3.)* experimental validations to screen out the best prediction equations for further modeling purposes. Theoretical considerations were as follows:

The propagation velocity of longitudinal stress-waves in a material is directly related to the modulus of elasticity and the bulk density of the substance:

$$E_d = \mathrm{v}^2 \rho \qquad (III.14)$$

where: E_d – dynamic Modulus of Elasticity (Pa)
v – propagation velocity (m/s)
ρ – density (kg/m^3)

The above equation holds true for so-called one-dimensional bodies only, that is, where the dimensions perpendicular to the wave propagation are at least one order of magnitude smaller than the wave length. In veneer sheets, where one cross-sectional dimension is larger than the wave length (two-dimensional body), the above equation is modified with the Poisson's ratio:

$$E_d = \mathrm{v}^2 \rho \, (1-\nu_{xy}^2) \qquad (III.15)$$

where: ν_{xy} = Poission's ratio (*x* – propagation direction; *y* – perpendicular in-plane direction).

Unfortunately, reliable information concerning ν_{xy} is seldom available. In past investigations, stress-wave MOE measured on veneer was invariably calculated using *Equation III.14*. The results of Jung's investigations (1979) indicate that the correction introduced in *Equation III.15* appears to be negligible in red oak wood veneers. Other researchers also reported the negligible effect of Poisson's ratio in evaluation of thin wooden plates (Divos and Tanaka 2000).

Because of the viscoelastic nature of wood, measured dynamic MOE depends on the rate of stress-development. During dynamic testing, stresses develop much faster than they do during static testing and the difference between the resulting MOE values is significant. For this reason, MOE calculated from longitudinal or transverse vibration characteristics is called dynamic MOE. Divos and Tanaka (2000) proposed the following empirical equation to calculate the ratio of dynamic and static MOE:

$$\frac{E_d}{E_s} = 1 + 0.017 \log\left(\frac{t_s}{t_d}\right) \qquad (III.16)$$

where: E_d ; E_s – dynamic and static MOE, respectively
t_d ; t_s – characteristic time of the dynamic and static MOE determination, respectively.

Note that t_d is the period (T) of the applied stress wave when vibration method is used to determine dynamic properties and t_s is the elapsed time to develop 10 % of failure stress level by any applicable static testing procedure.

III.6.2 Prediction models

As it was already mentioned, several models and theories were developed for estimating the direction dependent properties of orthotropic materials. Many of these approaches include hard to measure material constants like modulus of rigidity or Poisson's ratios. The model selection criteria for this segment of the research included: simplicity, reliability and easy adaptability. The following three models were involved in this investigation.

TENSOR APPROACH

The compliance matrix of an orthotropic material can be converted into a four-dimensional tensor (Szalai, 1994). Transforming the first element of this tensor results in an equation that can be used to estimate the stiffness of the material in any direction inclined to its principal material coordinates. The general equation applied to MOE in the LT plane only, where the grain angle (φ) controls the property, reduces to the following form:

$$\hat{E}_\varphi = \frac{1}{\frac{1}{E_L}\cos^4\phi + \frac{1}{E_T}\sin^4\phi + \left(\frac{4}{E_{LT}^{R45^\circ}} - \frac{1}{E_L} - \frac{1}{E_T}\right)\sin^2\phi\cos^2\phi} \qquad (III.17)$$

where: $\hat{E}_\varphi$ – predicted MOE at grain angle φ;
E_i – experimentally determined MOE in the principal anatomical directions ($i = L,T$);
$E_{LT}^{R45^\circ}$ – experimentally determined MOE in the LT plane, at $\varphi = 45°$.

Equation III.17 needs three predetermined E values for predicting the modulus of elasticity in the LT plane. Besides its demonstrated theoretical basis, the experimentally determined midpoint (i.e., $E_{LT}^{R45^\circ}$) may provide improved accuracy compared to other models.

HANKINSON'S FORMULA

The most widely used equation for predicting the effect of sloping grain on unidirectional strength and MOE is the experimental Hankinson's formula (*Hankinson, 1921*). For MOE in the LT plain, the equation can be written as follows:

$$\hat{E}_H = \frac{E_L E_T}{E_L \sin^2 \varphi + E_T \cos^2 \varphi} \qquad (III.18)$$

where $\hat{E}_H$ is the predicted MOE at grain angle φ and the other notations are as in *Equation III.17*. The Hankinson's formula, though empirical, is simpler than the tensor approach and uses only two predetermined MOE values for the estimation.

HYPERBOLIC FORMULA

Woodward and Minor (1988) reported that a hyperbolic formula provides excellent fit to tensile strength data. Although no experimental data were provided regarding the stiffness prediction, it may provide reasonable estimation of elasticity values. The equation applied in the LT plane takes the following form:

$$\hat{E}_H = \frac{2E_T E_L}{e^{0.01\phi}\left(E_T + E_L\right) + e^{-0.01\phi}\left(E_T - E_L\right)} \qquad (III.19)$$

where *e* is the base of the natural logarithm, and the other notations are as in *Equation III.18*. Similar to that of Hankinson's formula, it represents a simple approach that requires only two predetermined elastic contants. During this research, the applicability and prediction accuracy of these models were investigated by the following exparimental and analytical methods.

III.6.3 Materials and methods

Experimental material consisted of 3.2 mm thick structural veneer sheets of three Appalachian hardwood species: quaking aspen (*Populus tremuloides*), red oak *(Quercus rubra*), and yellow-poplar (*Liriodendron tulipifera*), and two European species: Turkey oak (*Quercus cerris*), and true poplar (*Populus x. Euramericana cv. Pannonia*). Structural composite plants in West Virginia and in Europe prepared the veneer sheets from logs. The veneer sheets used for specimen fabrication were processed as in actual manufacturing including peeling, drying and clipping. Consequently, specimens included all the random discrepancies such as cracks, compression set, etc. that may develop during structural veneer manufacturing. However, studying the effects of further composite manufacturing processes such as densification and resin penetration on the mechanical properties was beyond the scope of this investigation.

Dynamic MOE was determined using a stress wave measuring equipment. The device consisted of an ultrasonic timer and two piezoelectric accelerometers. The transducers used a 127 V, 45 kHz impulse that lasted for 30 μs. The subsequent impulses were generated at one second intervals. Surface pressure of 3-4 MPa between the transducers and the veneer sheets provided adequate coupling, using sandpaper as a coupling material.

Figures III.18a and *III.18b* show the details and schematic of the ultrasonic equipment, respectively. The distance between the transducer and the receiver was 160 mm. The material was clamped on a special table, which was covered with a 4 mm thick rubber sheet, to avoid bridging of the signal between the transducer and the receiver. A commercial hand-clamp provided adequate surface pressure between the transducers and the material.

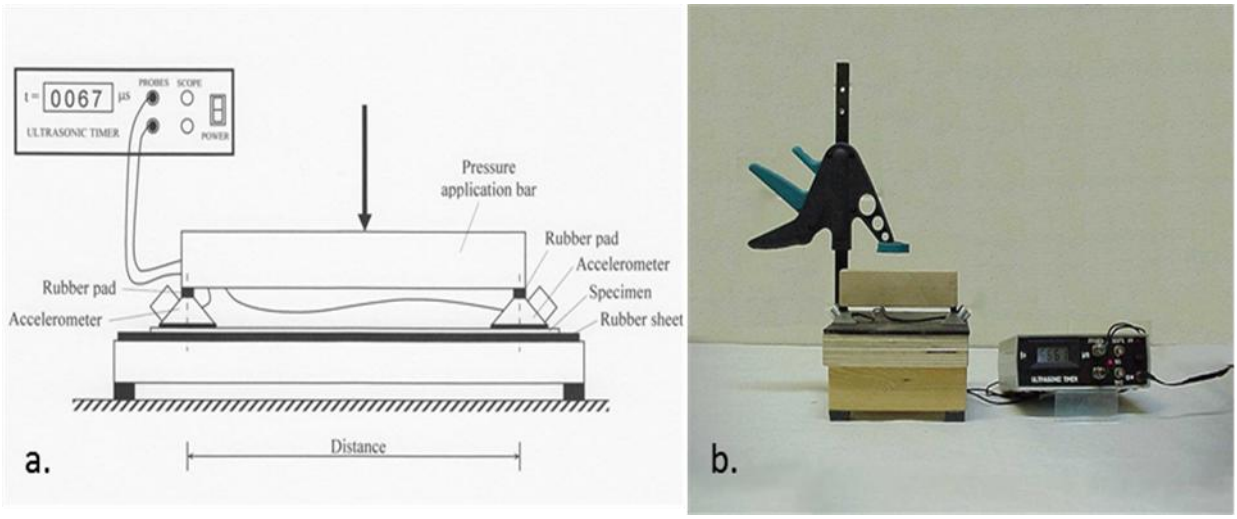

Figure III.18. *Schematic of the ultrasonic timing device (**a.**) and the actual setup (**b.**).*

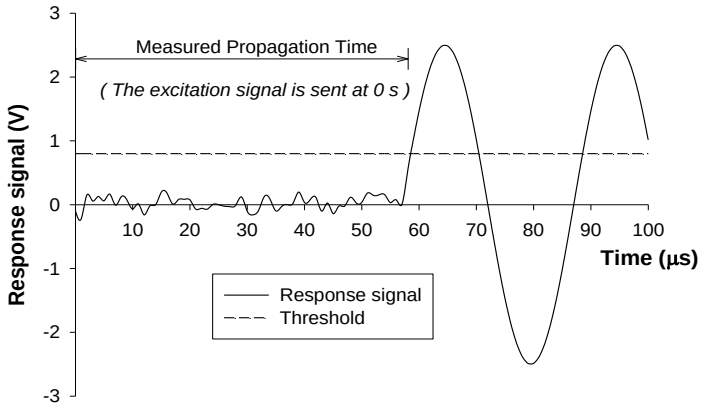

Figure III.19. *The operation principle of the ultrasonic timer. Explanation of the propagation time and the threshold limit.*

Figure III.19 demonstrates the operation principle of the ultrasonic timer. Timing starts when the excitation impulse rises, and stops when the received signal reaches a threshold value above the noise level. The advantage of this method is that there is minimal delay between the reception of the signal and the stoppage of the timer. The measured time was corrected to account for travelling time in the transducer housing.

Because peeled structural veneers represent two-dimensional bodies, the applicability of *Equation III.14* or *III.15* was investigated comparing measurements on wide and narrow strips of the same veneer. Results indicated that *Equation III.14* is sufficient for dynamic MOE determination.

Material preparation for the exploration of dynamic MOE started with the splitting of large veneer sheets along the grain. This provided a base line for cutting the 200 mm x 200 mm specimens using a large paper shear. Furthermore, the split-side of the specimen served as the 0° grain direction to which the inclined directions could be measured and marked. Both sides of the specimens were marked by 15° increment of grain orientation using a precision protractor having ±1° of accuracy. The pre-cut and marked specimens were conditioned in a controlled environment of 21° C and 65 % relative humidity. Approximately six days of conditioning resulted in constant weight of the veneer sheets. Twenty control specimens were used to establish the physical properties of the experimental materials. *Table III.6* contains the summary statistics of these properties obtained by standard measurements (ASTM D-2394 and ASTM D-4442). The comparatively low standard deviations of physical properties indicate that the natural variability wood was limited by selecting defect free and straight-grained veneer specimens.

After conditioning and immediately prior to dynamic MOE evaluation, the exact dimensions and weight of the specimens were measured and recorded for bulk density calculations. The accuracies of dimension and weight measurements were 0.01 mm and 0.01 g, respectively. The ultrasonic propagation time was assessed in the marked directions on both faces of each specimen.

Table III.6. *Summary statistics of the measured physical properties of structural veneers.*

Species		***Moisture Content (%)***		***Specific gravity***		***Bulk Density (kg/m^3)***	
	n [a]	$\bar{x}$ [b]	***Std.*** [c]	$\bar{x}$	***Std.*** [c]	$\bar{x}$	***Std.*** [c]
Aspen	20	11.8	0.32	0.37	0.01	385	18.0
Red oak	20	10.5	0.38	0.50	0.01	523	19.5
Yellow-poplar	20	11.5	0.61	0.42	0.02	450	17.3
True poplar	20	11.3	0.59	0.38	0.04	397	17.6
Turkey oak	20	11.7	0.45	0.65	0.03	670	19.4

a – sample size;
b – mean value;
c – standard deviation.

Data evaluation started with calculating the density of the specimens, and the propagation time (average of two sides) in each direction on each sheet. The propagation velocity was calculated by dividing the transducer distance by the corrected propagation time. Finally, *Equation III.14* provided the E_d values in each direction for each specimen. Because every specimen was tested in each direction, this situation corresponds to a randomized complete block (RCB) design.

Figure III.20. *The experimental setup for static MOE measurements.*

A relationship between the dynamic and static MOE was established by testing veneer and solid wood specimens of each species (conditioned the same way as above), at four grain angle levels (0°, 15°, 30° and 45°). Sample sizes were set to 5 for these analyses for each variable combination. The target dimensions were 300 mm in length and 25 mm in width. Solid wood specimens had the same dimensions except the thickness was set to 12 mm. Dynamic MOE was measured in a similar manner as described above. During static MOE assessment the MTS servo-hydraulic testing machine collected load and strain values using a data acquisition system. The frequency of the data registration was 1 second. The top tension-grip of the experimental setup had a self-aligning, rotational free coupling to the load cell (*Figure III.20*). Thus, the majority of bias introduced by the twisting of angle-to-grain specimens has been alleviated. Testing speed and other testing parameters were in accordance with the relevant ASTM standard (ASTM D 143 – 94).

III.6.4 Results

Table III.7 shows the summary statistics of the dynamic MOE of each species at different grain angle levels. *Figure III.21* demonstrates these data by box plots as a function of grain orientation (φ).

In general, measured dynamic MOE values decreased sharply with increasing grain angle, up to 45°. Above this angle of grain orientation, MOE leveled off, and there was little additional decrease. These observations agree well with the results of orthotropic compression MOE determination as discussed in section *III.5.4.*

Table III.7. *Summary statistics of the measured dynamic MOE values.*

Species		***Grain angle (ϕ°)***							***n***
		0°	***15°***	***30°***	***45°***	***60°***	***75°***	***90°***	
		Dynamic Modulus of Elasticity (GPa)							
Quaking aspen	***Mean***	***11.976***	***7.056***	***2.658***	***1.279***	***1.048***	***1.035***	***1.030***	***20***
	Std.	*0.888*	*0.752*	*0.287*	*0.135*	*0.045*	*0.045*	*0.047*	
Red oak	***Mean***	***10.651***	***5.770***	***1.997***	***1.396***	***1.387***	***1.383***	***1.382***	***23***
	Std.	*1.201*	*0.827*	*0.348*	*0.046*	*0.039*	*0.039*	*0.044*	
Yellow-poplar	***Mean***	***13.529***	***7.631***	***2.589***	***1.254***	***1.149***	***1.145***	***1.142***	***21***
	Std.	*1.020*	*0.735*	*0.254*	*0.112*	*0.050*	*0.060*	*0.062*	
Turkey oak	***Mean***	***12.221***	***8.435***	***3.989***	***1.878***	***1.158***	***0.807***	***0.685***	***11***
	Std.	*0.852*	*0.897*	*0.417*	*0.258*	*0.195*	*0.071*	*0.125*	
True poplar	***Mean***	***10.638***	***7.208***	***3.476***	***1.850***	***1.158***	***0.870***	***0.750***	***12***
	Std.	*0.839*	*0.825*	*0.371*	*0.159*	*0.154*	*0.106*	*0.132*	

n – sample size.
Std. – standard deviation

One-way ANOVA revealed that grain orientation significantly affects the MOE of each species. Tukey's multiple comparison tests, however, failed to detect statistically significant differences between the MOE values above 45° and 60° grain angles for the Appalachian and European species, respectively.

As a first approach to evaluating the prediction models, correlation analysis was used on the data, without regard to blocking. *Table III.8* lists the r^2 values by species and model types. In all but one case, the hyperbolic formula provided less precise prediction than either of the other two models. Thus, it was eliminated from further evaluations. The fit of Hankinson's formula

resulted in higher r^2 values in the cases of aspen and yellow poplar, while the orthotropic tensor approach (*Equation III.17*) seems to work better for red oak and for the Hungarian species. For the Appalachian species, the former appears to work better in the lower grain angle region, while the latter is very accurate in the higher range.

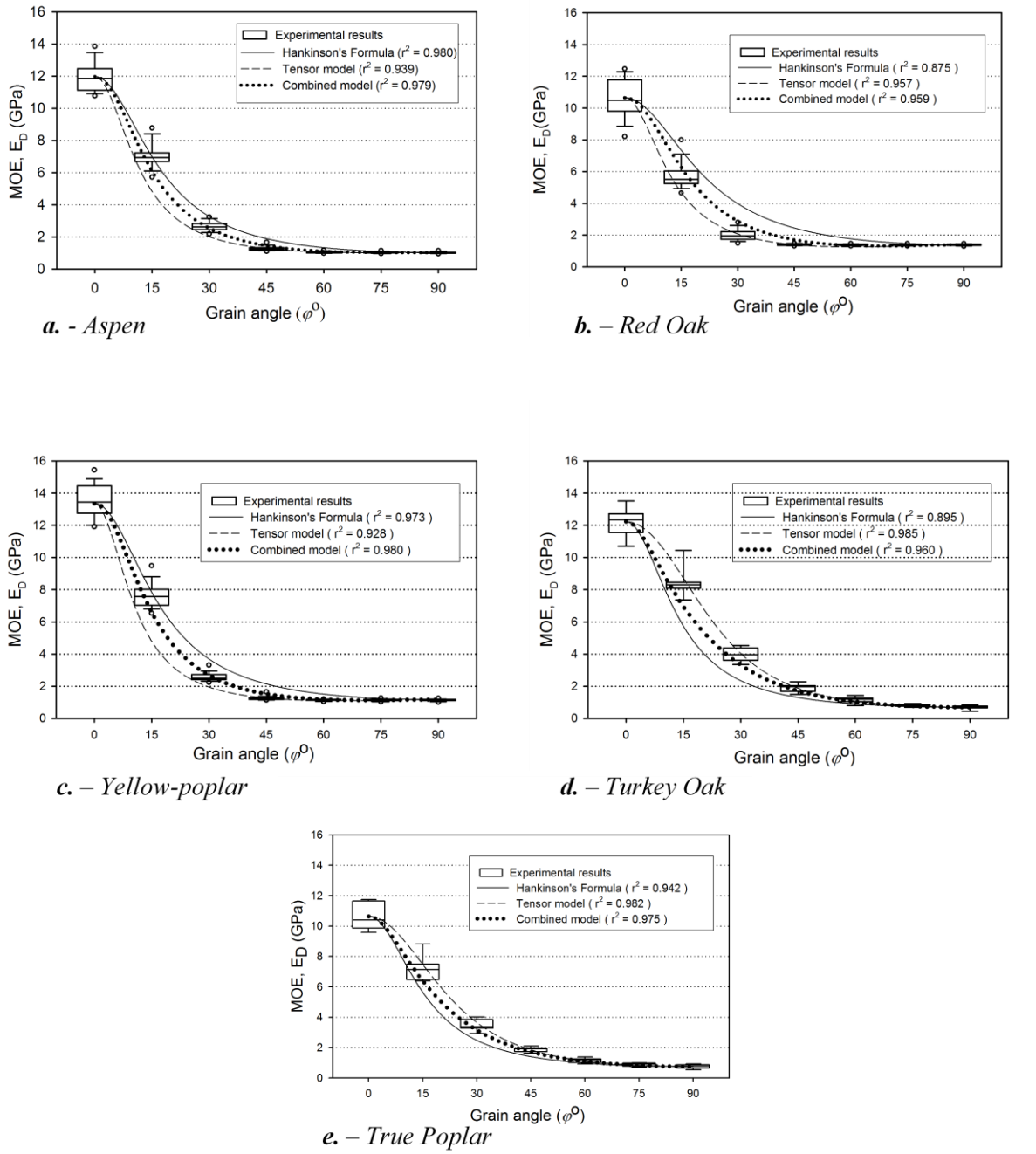

Figure III.21. *Model predicted and experimental dynamic modulus of elasticity values (E_d) as a function of grain orientation (φ°) for the listed species:* ***a.*** *–* ***e.***

Table III.8. *Coefficients of determination (r^2) values provided by the different prediction models.*

Species	***Hankinson's formula***	***Orthotropic tensor model***	***Hyperbolic formula***	***Combined model***
Quaking aspen	0.98	0.94	0.92	0.98
Red oak	0.88	0.96	0.93	0.95
Yellow-poplar	0.97	0.93	0.93	0.98
Turkey oak	0.90	0.99	0.72	0.96
True poplar	0.94	0.98	0.79	0.98

In complex modeling that requires several input parameters, the calculated results can be seriously impaired if the uncertainties of the parameters are high. Our goal was to screen out the possible best prediction equation for MOE determination of structural veneers as a function of grain orientation for further modeling purposes. Thus, the procedure introduces only limited uncertainties that propagates into the final model prediction. Based on the above discussion, a combination of the two models appeared to improve the MOE prediction throughout the whole range. Following is one possible combination that works well:

$$\hat{E}_C = \hat{E}_H \frac{\sqrt{\pi/2} - \sqrt{\varphi}}{\sqrt{\pi/2}} + \hat{E}_O \frac{\sqrt{\varphi}}{\sqrt{\pi/2}} \qquad (III.20)$$

where: $\hat{E}_H$, $\hat{E}_O$ and $\hat{E}_C$ are the dynamic MOE values predicted at grain angle φ, by the Hankinson formula, the orthotropic tensor approach, and the above combination, respectively. It is obvious that the value of $\hat{E}_C$ will be close $\hat{E}_H$ at lower grain angles, and approaches $\hat{E}_O$ rapidly, as ϕ increases. *Figures III.21a* through *III.21e*, along with r^2 values given in *Table III.8*, show that the combined model provides improved prediction for almost all examined species. One should note that *Equation III.20* does not provide a new approach to predict the direction dependent MOE of structural veneers. Rather, it exploits the fact that the evaluated two models have different accuracies over the lower and higher grain angle domains. Furthermore, bias analyses revealed that the combination model significantly reduces uncertainties in forecasting dynamic MOE properties. While it was not always the best model, the combined formula provided consistently good performance, in terms of both r^2 values and bias. With the exception of red oak, the bias remained below 20%. It does appear that this model offers satisfactory predictions for each species, and might be more useful for dynamic MOE estimation for further model developments.

Figure III.22 shows the association between the experimentally measured dynamic and static MOE. This graph includes the data points measured both on veneer and on solid wood, for all North American species. It was assumed, that the relationship should depend only on the characteristic time of the test procedure (*Equation III.16)*. Because the ratio of t_s to t_d is

independent from species or orientation, the relationship should be linear with uniform slope for every species, and the regression line should pass through the origin.

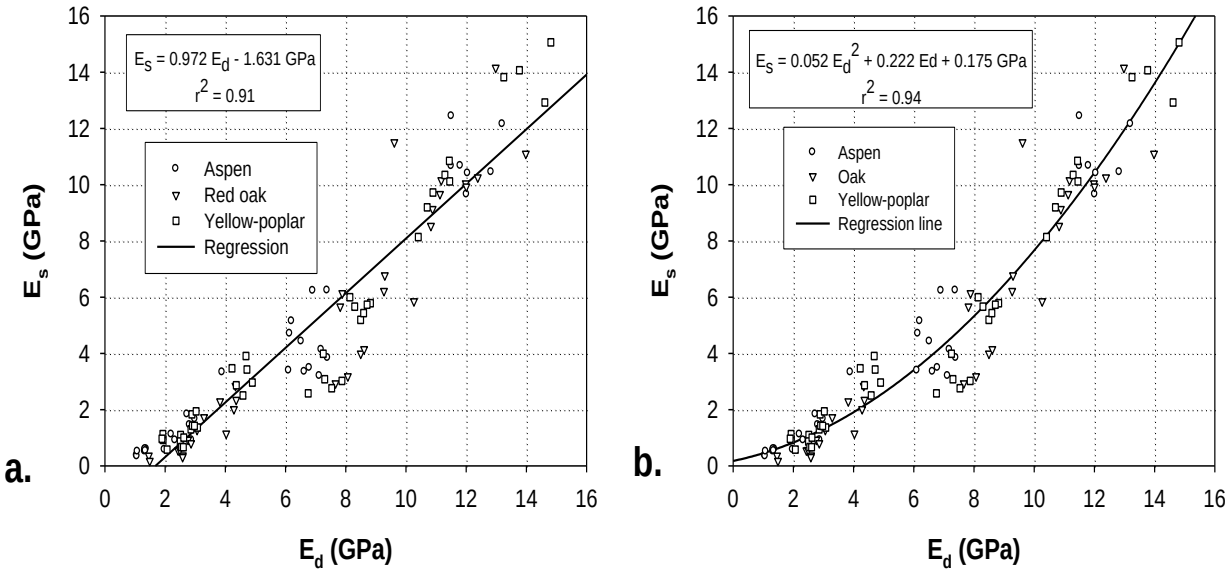

Figure III.22. *Association between experimentally measured dynamic and static MOE values.* ***a.*** *– first-order,* ***b.*** *– second-order regression models.*

From *Figure III.22a* it is apparent that this is not so. The regression line does not pass through the origin, and the linearity of the data is questionable. The cause of this anomaly is most likely the high damping effect in veneer and wood in non-longitudinal directions, which might have influenced the measurements. A serious problem with the first order regression model depicted on *Figure III.22a* is that, according to its equation, dynamic MOE values measured at higher grain angles correspond to negative static MOE.

Figure III.22b shows the scatter plot to which a second order polynomial was fitted. As the improved r^2 value indicates, this model describes the relationship significantly better than did the linear regression. It is also noticeable that, using the quadratic model, positive static MOE values are calculated for any dynamic MOE value. While there is no real justification for using a second order regression model, it appears that this equation might be better for estimating the static MOE from its dynamic counterpart.

III.6.4 The three dimensional orthotropy of MOE for sliced veneers

The furnish material of engineered wood products (EWPs) is usually peeled structural veneer with about 2.5 ~ 3 mm thickness. Ideally, these veneers represent thin wooden plates in the longitudinal and tangential (LT) planes and the thickness of the plate is in the radial (R) direction. On the other hand decorative veneers are about 0.5 ~ 1.0 mm thick and produced by slicing operation from a half log or flitch. Due to the nature of slicing, the principal planes of the veneer sheets vary between LT and LR as the slicing proceeds toward the center of the log (*Figure III.23*). Consequently, the location of the veneer within the flitch should have significant effect on the elastic properties. The purpose of the side study was to investigate the effect of transition between LT and LR anatomical planes on the modulus of elasticity of decorative veneers.

The two species involved were red oak (*Quercus rubra*) and black cherry (*Prunus serotina*) veneers obtained from a West Virginia plant. We used the same stress wave timing to assess the dynamic MOE of the substrates. Specimen preparations were the same as discussed earlier in this chapter, except conditioning. We measured the veneers "*as is*" after transportation to the laboratory of WVU, Division of Forestry. *Table III.9* contains the measured physical properties. Species selection was limited by the industrial partner veneer slicing schedule.

Table III.9. *Summary statistics of the measured physical properties of decorative veneers.*

Species & Groups	***n***	***Moisture Content (%)***		***Bulk Density(kg/m^3)***	
		Mean	***Std.***	***Mean***	***Std.***
Red Oak					
Gr.1	*8*	*6.3*	*0.55*	*743*	*113.5*
Gr.2	*12*	*6.5*	*0.68*	*752*	*66.0*
Gr.3	*9*	*4.5*	*0.42*	*600*	*48.9*
Gr.4	*16*	*3.6*	*0.37*	*671*	*33.6*
Gr.5	*15*	*4.4*	*0.16*	*615*	*16.2*
Black Cherry					
Gr.1	*13*	*6.2*	*0.27*	*565*	*29.5*
Gr.2	*15*	*6.0*	*0.42*	*592*	*33.2*
Gr.3	*23*	*5.5*	*0.39*	*590*	*20.1*
Gr.4	*17*	*5.3*	*0.75*	*596*	*47.0*
Gr.5	*15*	*6.9*	*0.41*	*652*	*21.9*

n – sample size

Five groups from different assumed locations within a flitch - as shown on *Figure III.23* -were selected for each species. Although the exact locations of the veneers within the log can not be identified, we assumed that this approximation would give at least an indication of trends about the spatial orthotropy of MOE in diverse anatomical planes.

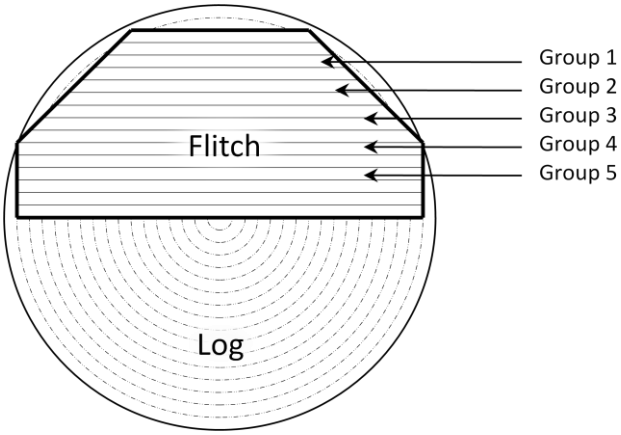

Figure III.23. *The approximated location in the flitch of the decorative veneer sheets by group designations.*

For an ideal orthotropic material such as carbon or glass fiber composites, measurements between 0° and 90° could have been sufficient to describe the effect of fiber directions on the modulus of elasticity. However, natural grain deviations in wood called for 0° to 180° evaluations that we performed with 15° augmentations. The experimental technique was the same as discussed in Section *III.6.3* and demonstrated on *Figure III.18* and *III.19.* The dynamic MOE measurements within a group were averaged by species, and basic statistical features were recorded.

In *Appendix III Table A.III.3* summarizes the experimentally obtained dynamic modulus of elasticity (E_d) values for both species. One-way analysis of variance (ANOVA) revealed significantly higher E_d values for red oak compared to black cherry. Both species exhibited significant loss of stiffness as grain angle increased reaching the minimum values at or near to 90° of grain deviation as it was expected. As φ increased an increasing variance of the data was observed; however, to a lesser extent for cherry. This may be explained by the more homogenous cellular structure of cherry. *Figures III.24* and *III.25* demonstrate the in plane orthotropic nature of E_d values for red oak and black cherry, respectively. On the diagrams the different curves represent the different locations from which the groups were obtained. One can realize that the two species showed different trends in E_d as a function of location. At φ=0° oak had the maximum E_d of 17.4 MPa for Group 3. The location effect was fairly consistent. Cherry had the highest E_d in Group 5 (@ φ=0°) and along the grain it consistently decreased toward the bark (Group 1). However, other than 0° grain angle this species showed somewhat erratic behavior demonstrated by the intersections of E_d curves and the asymmetry between the 0-90° and 90-180° grain angle domains.

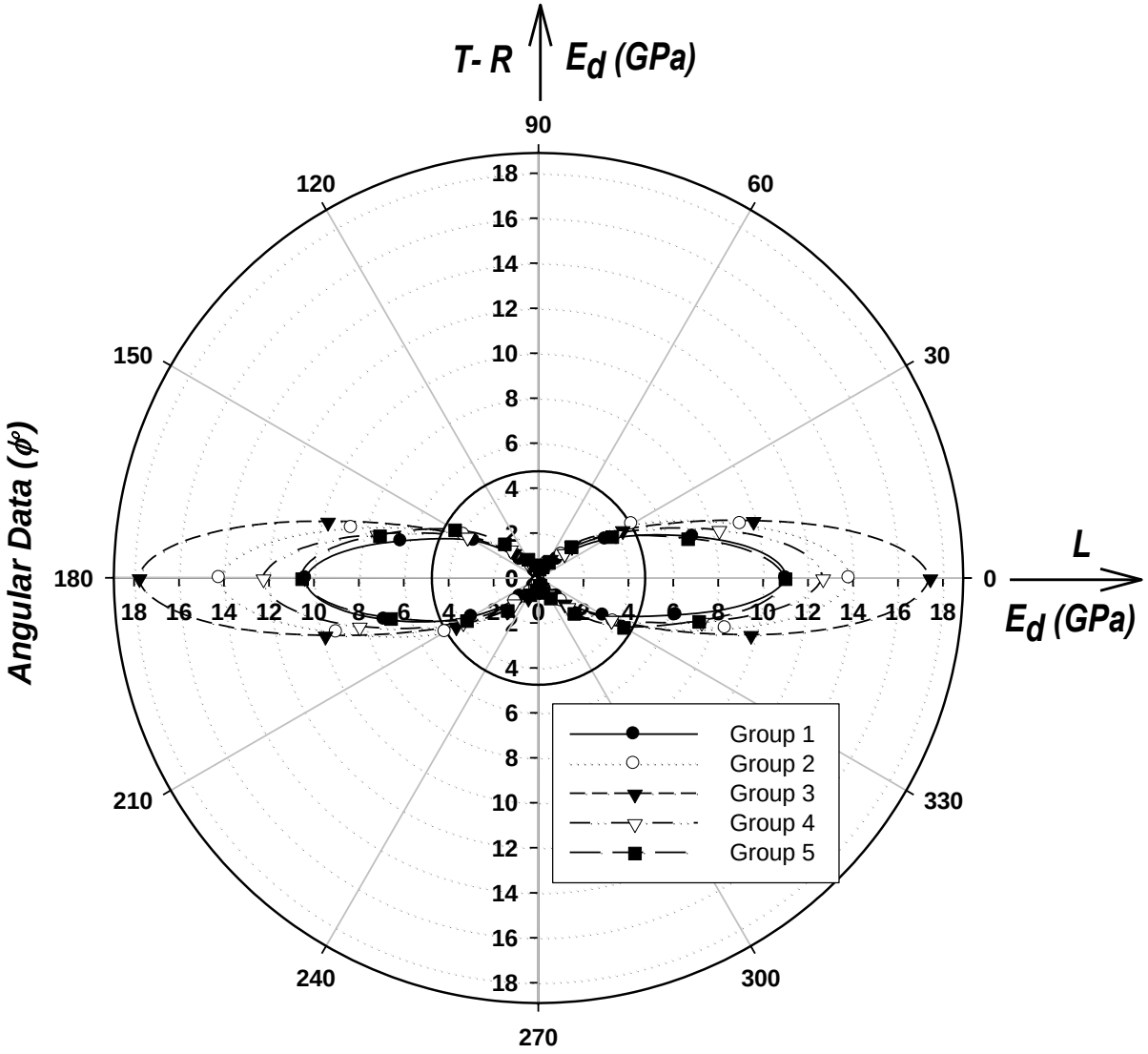

Figure III.24. *Polar plot of dynamic modulus of elasticity for* ***Red Oak*** *veneers as a function of grain angle (φ) and location within the flitch. Groups 1-5 are from bark to the pith, respectively.*

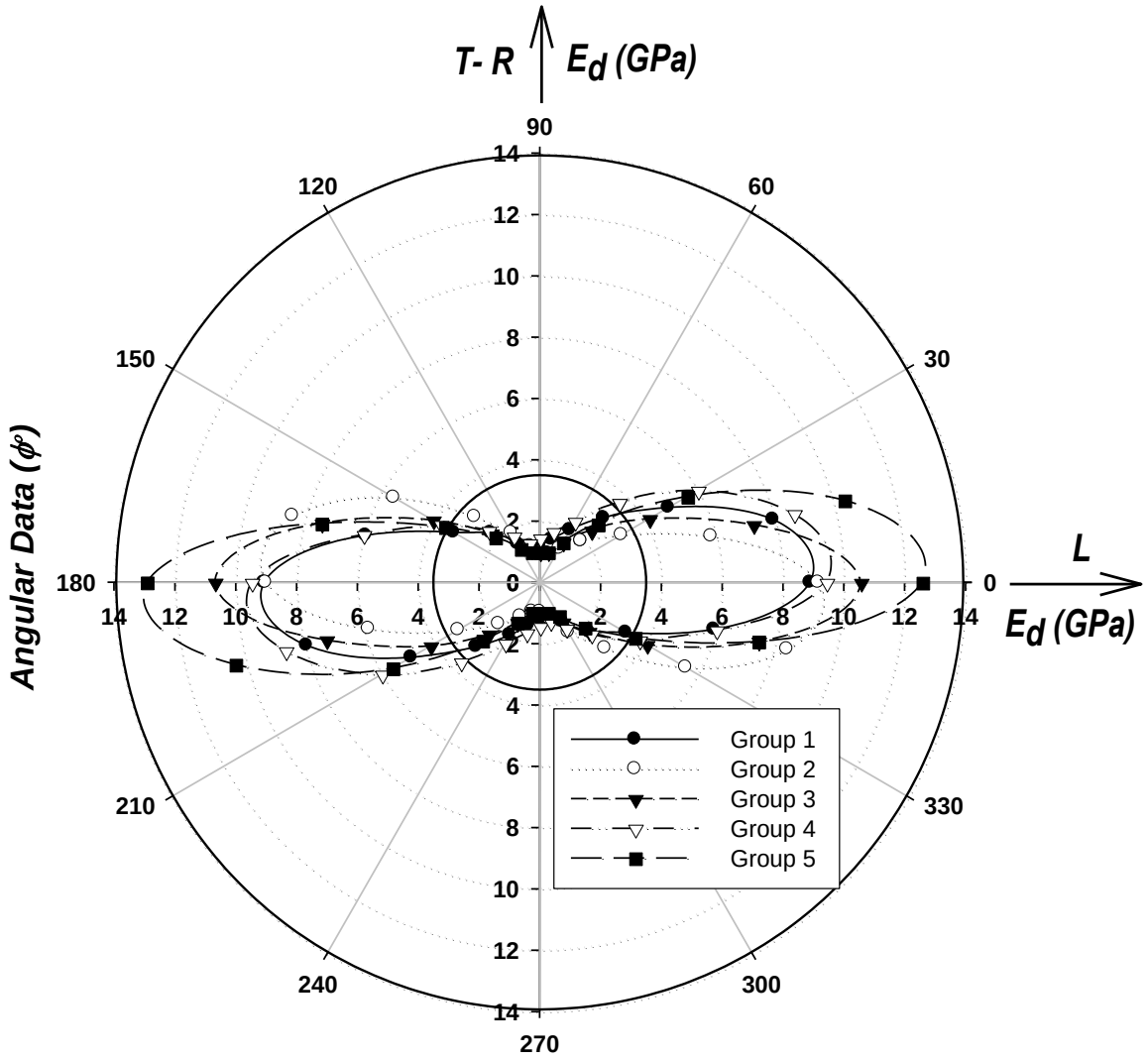

Figure III.25. *Polar plot of dynamic modulus of elasticity for* ***Black Cherry*** *veneers as a function of grain angle (φ) and location within the flitch. Groups 1-5 are from bark to the pith, respectively.*

III.7 Summary and Conclusions

The analytical and experimental works devoted to explore the orthotropic nature of mechanical properties for solid wood and veneers were outlined in this Chapter. On selected species the orthotropy of shear and compression strength, dynamic and compression moduli of elasticity were modeled and predicted as functions of grain and ring angle orientations. One might easily realize that not all the species and mechanical properties could be addressed because of the vast number of species and property combinations. Consequently, the findings of this research have limited universal values. Care should be taken in extrapolation of results for wood species and testing conditions other than specified in this Chapter. Some of the essential conclusions may be listed as follows:

1. In general, the well-known orthotropic nature of wood's mechanical properties was confirmed; and the assumption that the cylindrical orthotropy of wood may be reasonably approximated in an orthogonal, three-dimensional Cartesian coordinate system proved to be valid as well.
2. Shear strength of solid hardwood species can be modeled based on an orthotropic tensor theory. However, a combination of tensor approach and the modified Hankinson's formula proved to be the best predictor of the apparent shear strength as a function of grain and ring orientations.
3. The direction dependent compression properties can be modeled equally well by tensor analysis or by the three dimensional Hankinson's formula. Analytical works and failure analyses revealed that shear failure under compression is likely for certain grain/ring angle combinations. The developed critical shear stress contour in compression may be practical for failure prediction for straight grained homogeneous species.
4. For structural and decorative veneers the discussed non-destructive testing procedure is a convenient approach to experimentally determine the modulus of elasticity. For structural veneers the grain angle effect is best described by a combined model which incorporates a tensor approach at the lower grain angle region and the Hankinson's formula over approximately 45° grain orientation.
5. The effect of the location in the flitch for decorative (sliced) veneers was clearly indicated. Although, the examined two species demonstrated different trends regarding the location effect, the grain angle influenced the modulus of elasticity similarly to that of structural veneers. Consequently, the evaluation may be viable by the described combination model. To explore the true nature of orthotropic behavior of sliced veneers a more rigorous analysis is still needed.
6. Results from the developed experimental methods and the outcome of prediction models served as input parameters for modeling the mechanical properties of existing, structural composites. Furthermore, the gained insight of orthotropic nature of wood and veneers provided guidance for innovative product developments. The next couple of chapters bestow descriptions of these works.

III.8 Closure of Chapter III

The research outlined in this Chapter resulted in a Ph.D. Dissertation (Bejo 2001), and five peer reviewed publications in international journals having impact factors (Lang 1997; Lang et al. 2000; Lang and Kovacs 2001; Lang et al 2002 and Lang et al. 2003.) Furthermore, results were published in Hungarian as well (Bejo et al. 2003a; Bejo et al. 2003b; Denes et al. 2002a and Denes et al. 2002b). The international cooperation has been made possible through the North Atlantic Treaty Organization (NATO), Cooperative Research Grant, CRG.LG 973967. Additionally, results were presented at four international, scientific conferences. The publications mentioned above received international interests and were cited just about twenty times in scientific journals of the profession.

We do feel that the developed experimental and analytical procedures would help researchers in better understanding the orthotropic nature of wood and wood products. The resulting extensive data base can be useful for design and development of wood based composites.

References III

1. American Society for Testing and Materials. 1996. Standard Methods of Testing Small Clear Specimens of Timber ASTM D 143 – 94. ASTM, West Conshohocken, Pa.
2. American Society for Testing and Materials. 1996. Standard Test Methods for Specific Gravity of Wood and Wood-base Materials ASTM D 2395 – 93. ASTM, West Conshohocken, Pa.
3. American Society for Testing and Materials. 1996. Standard Test Methods for Direct Moisture Content Measurement of Wood and Wood-base Materials ASTM D 4442 – 92. ASTM, West Conshohocken, Pa.
4. Arcan, M., Hashin, Z. and Voloshin, A. 1978. A Method to produce Uniform Plane Stress States with Applications to Fiber-reinforced Materials. Experimental Mechanics 18(4): 141-146
5. Ashkenazi, E. K. 1959. On the Problem of Anisotropy of Construction Materials (in Russian). Sov. Phys. Tech. Vol 4. 1959 pp. 333-338.
6. Ashkenazi, E. K. 1976. Anisotropy of Wood and Wood-Base Materials. 1st edition.(in Russian) Izdatelstvo Lesnaja Promuslennosty. Moscow, USSR.
7. Bejó, L., Láng E., Szalai J., Kovács Zs. és Divós F. 2003b. Lombos fafajok ortotrop szilárdsága és rugalmassága. II. rész.: Kísérleti eredmények és következtetések. FAIPAR, 51(4):8-15.
8. Bejó L., Láng E., Szalai J., Kovács Zs. és Divós F. 2003a. Lombos fafajok ortotrop szilárdsága és rugalmassága. I. rész: Elméleti alapok és kísérleti módszerek. FAIPAR, 51(2):19-25.
9. Bendsten, B. A. and S. Porter 1978. Comparison of Results From Standard 2-Inch With 1-1/2-Inch Shear Block Tests. Forest Prod. J. 28(7):54-56
10. Bendsten, B. A., J. H. Haskell, W. L. Galligan 1978. Characteraizing the Stress-Compression Relationship of Wood In Compression Perpendicular to Grain. Wood Sci. 10(3):111-121.

11. Bindzi, I. and M. Samson. 1995. New Formula for Influence of Spiral Grain on bending stiffness of Wooden Beams. ASCE, Journal of Structural Engineering, 121(11):1541-1546.
12. Bodig, J. 1965. The Effect of Anatomy on the Initial Stress-Strain Relationship in Transverse Compression. Forest Prod. J. 15(4):197-202.
13. Bodig, J. and B. A. Jayne. 1982. Mechanics of Wood and Wood Composites. Van Nostrand Reinhold Company Inc. New York, NY 712 pp.
14. Breyer, D. E. 1980. Design of Wood Structures. McGraw-Hill Book Company. New York, N.Y. 542 pp.
15. Cowin, S. C. 1979. On the Strength Anisotropy of Bone and Wood. J. of Applied Mech. 46(12):832-838.
16. Dénes, L., Kovacs, Zs., Balint Zs. és Láng E. 2002b. Szinfurnérok rugalmasságának anizotrópiája - II. – Rész. FAIPAR 50(3):21-24.
17. Dénes L., Kovács Zs., Balint Zs. és Láng E. 2002a. Színfurnértok rugalmasságának anizotrópiája - I. Rész. FAIPAR, 50(2):3-7.
18. Divos, F., I. Daniel, L. Bejo. 2000. Defect Detection in Timber by Stress Wave Technique. *In:* Proc. Int. Conf. on Wood and Wood Fiber Composites, Stuttgart, Germany, 13-15 April, 2000.
19. Divos, F., T. Tanaka. 2000. Effect of creep on Modulus of Elasticity determination of wood. ASME J. of Vibration and Acoustics 122(1):90-92.
20. Dowdy, S. and S. Wearden. 1991. Statistics for Research. 2nd ed. John Wiley and Sons, New York, NY. 259 pp.
21. Ethington, R. L., V. Eskelsen, and R. Gupta 1996. Relationship between compression strength perpendicular to grain and ring orientation. Forest Prod. J. 46(1):84-86.
22. Gerhards, G. C. 1988. Effect of Slope of Grain on Tensile Strength. Forest Prod. J. 38(7/8):39-40.
23. Goodman, J. R., and J. Bodig 1972. Orthotropic Strength of Wood in Compression. Wood Science. 4(2):83-94.
24. Hankinson, R. L. 1921. Investigation of Crushing Strength of Spruce at Varying Angles of Grain. Air Service Information Circular No. 259, U.S. Air Service.
25. Hunt, M. O., M. H. Triche, G. P. McCabe and W. L. Hoover. 1989. Tensile Properties of Yellow-Poplar Veneer Strands. Forest Prod. J. 39(9):31-33.
26. Jung, J. 1979. Stress-Wave Grading Techniques on Veneer Sheets. Gen. Tech. Rep. FPL-GTR-22. USDA Forest Service, Forest Products Laboratory, Madison, WI.
27. Jung, J. 1982. Properties of Parallel-Laminated Veneer Lumber from Stress-Wave-Tested Veneers. Forest Prod. J. 32(7):30-35.
28. Kaiserlik, J. H. and R. F. Pellerin. 1977. Stress-Wave Attenuation as an Indicator of Lumber Strength. Forest Prod. J. 27(6):39-43.
29. Kimmell, J. D. and J. J. Janiowak. 1995. Red Maple and Yellow-Poplar LVL from Ultrasonically Rated Veneer. Forest Prod. J. 45(7/8):54-58.
30. Koch, P. and G. E. Woodson. 1968. Laminating Butt-Jointed, Log-Run Southern Pine Veneers into Long Beams of Uniform High Strength. Forest Prod. J. 18(10):45-51.
31. Kollman, F. P. and W. A. Cote. 1968. Principles of Wood Science and Technology, I. Springer-Verlag, New York, 1968 pp. 326 and 340.
32. Kovacs, Zs., F. Divos, V. Szabadhegyi, E. M. Lang, B. Zombori and T. Fodor. 1997. ELVE Final Report: An Investigation and Evaluation of Laminated Veneer Lumber (LVL)

Manufactured from European Hardwoods. Final Report to the EUCC Commission of Cooperation in Science and Technology. 79 pp

33. Kunesh, R. H. 1968. Strength an Elastic Properties of Wood In Transverse Compression. Forest Prod. J. 18(1):65-72.
34. Lang, E. M. 1997. An Alternative Method for Shear Strength Assessment. Forest Prod. J. 47(11/12):81-84.
35. Lang, E. M., L. Bejo, J. Szalai and Zs. Kovacs. 2000. Orthotropic strength and elasticity of hardwoods in relation to composite manufacture. Part I. Orthotropy of shear strength. Wood Fiber Sci 32(4):502-519.
36. Lang, E.M. and Zs. Kovacs., 2001. Size effect on shear strength measured by the ASTM method. Forest Products Journal, 5(3):49-21.
37. Lang, E. M., L. Bejo, J. Szalai, Zs. Kovacs and R. B. Anderson. 2002. Orthotropic Strength and Elasticity of Hardwoods in Relation to Composite Manufacture. Part II. Orthotropy of compression strength and elasticity. Wood and Fiber Science, 34 (2):350-365.
38. Lang, E. M., L. Bejo, F. Divos, Zs. Kovacs and R. B. Anderson. 2003. Orthotropic Strength and Elasticity of Hardwoods in Relation to Composite Manufacture. Part III. Orthotropic elasticity of structural veneers. Wood and Fiber Science, 35 (2):308-320.
39. Liu, J. Y. 1984. New Shear Strength Test for Solid Wood. Wood and Fiber Sci. 16(4):567-574.
40. Liu, J. Y. and Floeter, L. H. 1984. Shear Strength in Principal Plane of Wood. Journal of Engineering Mechanics, 110(6):930-936.
41. Norris, C. B. 1950. Strength of Orthotropic Materials Subjected to Combined Stresses. Forest Products Laboratory, Report No. 1816. USDA , Forest Service. 49 pp.
42. Norris, C. B. 1957. Comparison of Standard Block-Shear Test with the Panel-Shear Test. Forest Prod. J. 7(9)299-301.
43. Okkonen, E. A., and B. H. River 1989. Factors Affecting the Strength of Block-shear Specimens. Forest Prod. J. 39(1):43-50.
44. Pellerin, R. F. 1965. Vibrational Approach to Nondestructive Testing of Structural Lumber. Forest Prod. J. 15(3):93-101.
45. Pu, J. and R. C. Tang. 1997. Nondestructive Evaluation of Modulus of Elasticity of Southern Pine LVL: Effect of Veneer Grade and Relative Humidity. 29(3):249-263.
46. Pugel, A. D. 1990. Angle-to-Grain Tensile Strength Specimen for Thin Wood Samples. Forest Prod. J. 40(2):49-51.
47. Radcliffe, B.M. 1965. A theoretical evaluation of Hankinson formula for modulus of elasticity of wood at an angle to the grain. Quarterly Bull. Michigan Agr. Exp. Station. 48(2):286-295.
48. Riccati, J. 1747. Verae et Germanae virim elasticarum leges ex phaenumenis demonstratae. De Bononiensi Schientarium Academia Commentarii 1:523. Bogona.
49. Rippy, R. C., F. G. Wagner, T. M. Gorman, H. D. Layton, T. Bodenheimer. 2000. Stress-Wave Analysis of Douglas-Fir Logs for Veneer Properties. Forest Prod. J. 50(4):49-52.
50. Riyanto, D. S., and R. Gupta. 1996. Effect of Ring Angle on Shear Strength Parallel to the Grain of Wood. Forest Prod. J. 46(7/8):87-92.
51. Ross, R. J., S. W. Willits, W. von Segen, T. Black, B. K. Brashaw, R. F. Pellerin. 1999. A Stress Wave Based Approach to NDE of Logs for Assessing Potential Veneer Quality. Part 1. Small Diameter Ponderosa Pine. Forest Prod. J. 49(11/12):60-62.

52. Sharp, D. J., 1985. Non-Destructive Techniques for Manufacturing LVL and Predicting Performance. Proc. Fifth Symp. on Nondestructive Testing of Wood, Washington State Univ., Pullman, Wash. pp. 100-108.
53. Shuppe, T. F., C. Y. Hse, L. H. Groom, E. T. Choong. 1997. Effect of Silvicultural Practice and Veneer Grade Layup on Some Mechanical Properties of Loblolly Pine LVL. Forest Prod. J. 47(9):63-69.
54. SPSS Inc. 1997. SigmaPlot® 4.0 for Windows. SPSS Inc. Chicago, IL.
55. Suhling, J.C., R.E. Rowlands, M.W. Johnson and D.E. Gunderson. 1985. Tensorial Strength Analysis of Paperboard. Experimental Mechanics. Vol. 42, 75-84.
56. Szalai, J. 1994. Anisotropic Strength and Elasticity of Wood and Wood-Based Composites. (in Hungarian) Private ed. Sopron, Hungary. 398 pp.
57. Tsai, W. S. and E. M. Wu. 1971. A General Theory of Strength for Anisotropic Materials. Journal of Composite Materials. 5(1):58-80.
58. Wang, J., J. M. Biernacki, F. Lam. 2001. Nondestructive Evaluation of Veneer Quality Using Acoustic Wave Measurements. Wood Sci. Technol. 34(2001) 505-516.
59. Woodward, C. B. and J. Minor. 1988. Failure Theories for Douglas-Fir in Tension. Journal of Structural Engineering 114(12):2808-2813.
60. Wu, E. M. 1974. Phenomenological Anisotropic Failure Criterion. In Composite Materials, Vol. II entitled: Mechanics of Composite Materials. Sendeckyj, G. P. ed., Academic Press.
61. Ylinen, A. 1963. A Comparative Study of Different Types of Shear Tests of Wood. Paper presented on the Fifth Conference of Wood Technology. U.S. Forest Products Laboratory, Madison, Wisconsin, September 16-27, 67 pp.

List of Figures III

Figure III.1. *Orthotropy of solid wood in principal and global coordinate systems.*

Figure III.2. *Shear in the principal anatomical planes and notation of the corresponding shear stresses.*

Figure III.3. *The principle and interpretation of the combined model.*

Figure III.4. *Schematic of the specimen manufacturing practice from straight-grained blanks.*

Figure III.5. *Schematic of the testing apparatus (**a.**) and the experimental setup (**b.**).*

Figure III.6. *Comparison of the experimental and three model predicted shear strength data. Species: aspen (Populous tremuloides).*

Figure III.7. *Comparison of experimental and model predicted shear strength data by orthotropy diagrams. Species: poplar (Populous x. Euroamericana) **a.** & **c.**; yellow-poplar (Liriodendron tulipifera) **b.** & **d.***

Figure III.8. *Comparison of experimental and model predicted shear strength data by orthotropy diagrams. Species: R. oak Quercos rubra) **a.** & **c.**; T. oak (Quercus cerris) **b**. & **d**.*

List of Tables III

Table III.6. *Summary statistics of the measured physical properties of structural veneers.*

Table III.7. *Summary statistics of the measured dynamic MOE values.*

Table III.8. *Coefficients of determination (r^2) values provided by the different prediction models.*

Table III.9. *Summary statistics of the measured physical properties of decorative veneers.*

Nomenclature III

Uppercase letters:

ANOVA	*analysis of variance*
ASTM	*American Society for Testing and Materials*
COV	*coefficient of variation*
E_d	*dynamic modulus of elasticity*
E_c	*compression*
E_s	*static modulus of elasticity*
EWP	*engineered wood products*
F	*force*
K	*constant*
L, T, R	*material coordinates*
LT, LR, RT	*anatomical planes*
N	*newton*
MC	*moisture content*
MOE	*modulus of elasticity*
MSS	*maximum shear stress*
RCB	*randomized complet block design*
SG	*specific gravity*
RH	*relative humidity*
WHU	*West Hungarian University*
WVU	*West Virginia University*

Lower case letters:

df	*degree of freedom*
e	*base number of natural logarithm*
m	*resolution number*
n	*power; sample size*
n, p ,q	*compression properties at* $\varphi°; 0°$ *and* $90°$ *of grain angle*

r^2	*coefficient of determination*
t_s; t_d	*static; dynamic characteristic times*
T	*period, temperature*
x_1, x_2, x_3	*global coordinates*

Greek letters:

α	*probability type-I error*
β	*regression coefficient*
ε	*strain*
φ	*grain angle*
v	*propagation velocity*
ν_{xy}	*Poisson's ratio*
π	*Ludolf's number*
σ	*stress*
ρ	*density*
θ	*ring angle*
Θ	*rotation angle of sheared plane*
ϑ	*shear force orientation*
τ	*shear strength*

Subscripts/superscripts:

1, 2, 3	*global coordinate indexes*
i, j, q	*running indexes*
H	*Hankinson's or hyperbolic*
L, T, R	*material coordinate indexes*
LT, LR, TR	*in principal material planes*
u	*ultimate*
O	*orthotropic*
φ,θ	*at ring and grain angle*

Symbols:

‘	*prime; transformed values or coordinates*
¯	*bar-over; average value*
ˆ	*hat; predicted value*
°	*degree*

CHAPTER IV

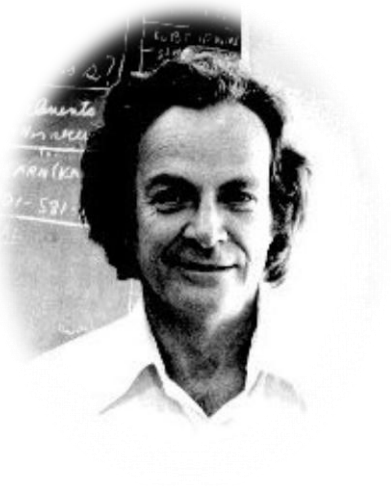

"IT DOESN'T MATTER HOW BEAUTIFUL YOUR THEORY IS. IF IT DOESN'T AGREE WITH THE EXPERIMENT IT'S WRONG."

RICHARD FEYNMAN

(1918 – 1988)

IV. Models for Wood-based Composites: Modeling the Mechanical Properties

IV.1 Introduction and Objectives

Structural wood-based composite (SCL) materials are excellent substitutes for solid wood in many aspects: they are lightweight, strong and durable. Moreover, some of the species/products combinations exhibit higher and more consistent mechanical properties due to the densification during the consolidation process; and, demonstrate better dimensional stability than those of solid wood. Many of their properties can also be engineered to a certain extent.

During the traditional development the trial-and-error approach is costly, time-consuming and often not feasible. A better alternative is using simulation modeling to optimize the various manufacturing parameters (Law and Kelton 1991). Using a reliable probability-based simulation model, one can demonstrate the effects of changing properties or relative position of the constituting materials on the final performance of the products without having to run actual manufacturing trials.

As described previously, we explored the key orthotropic mechanical properties of five hardwood species. The developed data base may provide reasonable opportunities to extend the pool of raw materials for structural composite manufacture.

As the concluding part of the comprehensive project, the objectives of this study were to develop and validate probability-based simulation models that can describe the bending and orthotropic compression MOE of Parallel Strand Lumber (PSL) and Laminated Veneer Lumber (LVL), based on the geometry and orthotropic elastic parameters of their constituents. The stochastic parameters of three North American species were incorporated into simulation models. Such simulation routines may provide an inexpensive tool for evaluating the effect of novel raw materials or other modifications on the expected performance of these structural composite products. Moreover, the models were validated by comparing their predictions to properties measured on commercial LVL and PSL produced from yellow-poplar structural veneers.

IV.2 Literature Review

Modeling physical and mechanical properties requires a thorough understanding of spatial structure of the composites. An early simulation model described the structure of paper as consisting of several layers of fibers and interfibrillar spaces or pores (Kallmes and Cote 1960; Kallmes et al. 1961). This work provided a basis for developing a mathematical model that depicts randomly packed, short-fiber-type wood composites (Steiner and Dai 1993; Dai and Steiner 1994a, 1994b). Results of this investigation were used in a Monte Carlo simulation program that can model different types of mats, and analyze them for various important geometric characteristics (Lu et al. 1998). The program can also determine the effect of sampling zone size on the measured density distribution. Harris and Johnson (1982) dealt with

the characterization of flake orientation in flake-boards. They pointed out that unbounded distributions are not appropriate for this purpose and suggested a bounded distribution to provide angles between 0 and π radians.

Physical and mechanical properties of wood based composites are closely related to density. Vertical and horizontal density distribution (VDD and HDD) generated much research interest. Suchsland and Xu (1989, 1991) developed physical models to examine the effect of HDD on thickness swelling and internal bond strength. They concluded that the durability of flakeboard is substantially affected by the severity of the horizontal density distribution. Xu and Steiner (1995) presented a mathematical concept for quantifying the HDD. Another study (Wang and Lam 1998) linked a simulation program with an experimental mat through a robot system that deposited flakes in the simulated positions. Predicted and actual HDD showed good agreement.

Harless et al. (1987) created a very comprehensive simulation model that can regenerate the VDD of particleboard as a function of the manufacturing process. Other research in this area included the characterization of VDD using a trigonometric density function (Xu and Winistorfer 1996*)*, and a simplified physical model to examine how the number of flakes, face flake moisture content and press closing time affect VDD (Song and Ellis 1997).

Zombori (2001) formed a series of linked simulation and finite element models that could, in turn, recreate the geometric structure, compression behavior, and heat and mass transfer of oriented strand board. These models could predict the inelastic stress-strain response, environmental conditions, moisture content and density at different points within the panel. His results – some of which are applicable to other composites, like particleboard, too – were in reasonable qualitative agreement with laboratory test data.

Xu and Suchsland created most of the models simulating physical and mechanical properties of wood composites. They dealt with the linear expansion of particleboard (1997), followed up by a study discussing the effect of out-of-plane orientation (1998a.) In these works, they made use of the off-axis MOE, determined by the Hankinson formula. Results of these studies helped to develop another model (Xu and Suchsland 1998b) to simulate the uniaxial MOE of composites with uniform VDD, based on the total volumetric work. Xu (1999) modified this simulation to investigate the effect of VDD on the bending MOE of composites, using the summation of stiffness values of discrete layers. This model was applied to evaluate the effect of percent alignment and shelling ratio on the MOE of OSB (Xu 2000). Simulation results agreed well with experimental and literature data.

Triche and Hunt (1993) modeled parallel-aligned wood strand composites using finite element analysis. They created small scale, parallel-aligned strand composites that can be considered as physical models for LVL or PSL. The applied model accounted for the effect of densification, adhesive penetration and crush-lap joints, and estimated the tensile strength and MOE of the specimens with excellent accuracy. In a previous study, Barnes (2001) modeled the strength properties of oriented strand products. He introduced the concept of stress transfer angle

to assess the effect of strand length and thickness on the mechanical properties of composites. He found good agreement between experimental and model-predicted MOE, MOR and tensile strength values.

Wood based composite lumbers, such as LSL, LVL or PSL, are relatively new products that generated less research interest than did composite panels. Results of research works on composite panels can be applied to these products with care. Meanwhile, available literature does not seem to contain simulation studies that are directed specifically towards modeling the geometric structure and mechanical properties of these structural composites.

IV.3 Theoretical Background

Although the structure of the two composite types involved in this study is largely different, the fundamental principles used in the simulation of their elastic properties are the same. The effective bending modulus of composites is defined by the stiffness summation of discrete layers (Bodig and Jayne 1982) as follows:

$$E = \frac{\Sigma E_i I_i}{I} \qquad (IV.1)$$

where: E, I – composite MOE and 2nd order moment of inertia of the cross-section, respectively;

E_i, I_i – layer MOE and moment of inertia of the i^{th} layer with respect to the 100omposite's neutral axis, respectively.

This theory assumes equal compression and tension stiffness and pertains directly to layered composites like glued-laminated beams, LVL and plywood. However, it can be applied to non-layered systems, such as PSL, as well. In this case, the above summation involves individual strands, rather than layers. The compression and tension modulus of elasticity may be different for some wood species depending on the moisture content as reported by Conners and Medvecz 1992. Therefore, the MOE of a constituent depends on whether it is located in the compression or the tension zone. Some elements are subjected to both compression and tension stresses and the orthotropic response of woody materials depends on their orientation relative to the principal material coordinates of the composite. Furthermore, the inherent densification and resin penetration may significantly alter the modulus of elasticity, thus impairing the computed results. These points are important to consider during any model development.

The determination of compression MOE is based on the calculation of the external work applied to a body and the internal energy stored therein. These quantities are equal in the linear elastic region. Xu and Suchsland (1998b) derived the following equation from this equality:

$$E = \frac{\Sigma E_i V_i}{V} \qquad (IV.2)$$

where: E, V - compression MOE and total volume of the composite;

E_i, V_i - compression MOE and volume of the i^{th} constituent.

The above-discussed simple theories govern the behavior of SCL materials in many loading applications. However, the stochastic nature of spatial arrangement of the constituents, the natural variability of wood properties and the unpredictable effects of manufacturing processes represent real challenges in forecasting mechanical properties of the final products. Without pursuing absolute precision, our goal was to reasonably model the elastic behavior of LVL and PSL on the basis of the properties of their constituents.

IV.4 Model Development

In general, models developed during this study include three major modules that provide electronically stored information for validation and further computations. First the spatial geometric structure of the composite in question is characterized using empirical probability distributions and/or deterministic variables. In the second step, an appropriate routine allocates stochastic MOE values to each constituent in the principal anatomical directions as input variables for the orthotropic models. The computed direction-dependent stiffness quantities are then modified by randomly assigned densification values. Finally, the modulus of elasticity in bending or in compression can be calculated using *Equations IV.1* or *IV.2*.

Although the mechanical and physical properties of structural composites are more consistent than those of solid wood, still a vast array of interacting variables governs their properties and behavior under load. To maintain the mathematical tractability of the models, several simplifying assumptions had to be made. The major hypothesis of this research was that a single cross section might represent the entire beam or column reasonably well. This assumption allowed the reduction of the three-dimensional problem to a much simpler in-plane modeling. Further simplifications used in the models included the following:

- Composites are treated as prismatic beams;
- Veneers used for layers and strands are peeled perfectly tangential to the annual ring (i.e., their plane is LT);
- A continuous glue-line provides perfect adhesion between the layers or strands;
- The applied glue does not alter the MOE of the layers or strands significantly;
- The grain orientation of an LVL layer is always parallel with the longitudinal axis of the beam; the grain orientation of a PSL strand is always parallel with the longitudinal axis of the strand;
- The layup is random; the MOE values of the layers or strands are independent of their position. In practice for LVL, the stress wave sorting for face and core designation is visually overridden because of defects. Thus, this assumption may be justified;
- The thickness of a layer in LVL is constant. Irregularities, such as crushed-lap joints that connect two veneer sheets and the inherent voids have counteracting effects on strength and stiffness, and are disregarded;
- PSL strand cross-sections are rectangular in shape; strands are not bent or distorted;
- PSL strand width is constant (25 mm);
- The densification of a PSL strand is independent from its position within the billet.
- The neutral plane in bending coincides with the symmetry axis of the cross-section.

IV. 3.1 Simulation of the geometry of the composites

Figure 1 shows the geometric features of LVL and PSL. The composites are placed in an orthogonal coordinate system, where *x* is the longitudinal axis of the beams, *y* is the main cross-sectional orientation of the constituents, and *z* is perpendicular to both *x* and *y*. One can easily realize that *x*, *y* and *z* are correspondingly equivalent to the *L*, *T* and *R* principal anatomical directions in solid wood. Using these axes, it is possible to define *load orientation* (*θ'*) and *strand/layer orientation* (*φ'*) relative to normal stresses acting in the beam. These angles are analogous to grain and ring angle in solid wood, respectively.

For LVL, the simulation of the geometric properties included the following steps:

- Establishing the number of layers. This is a deterministic variable that depends on the particular material being simulated. In the present case, the number of layers was 15;
- Assigning original and final thickness values to each layer from their respective probability distributions. The two outer layers (face) at each side and the rest (core) were treated differently because of the different densification during the pressing process;
- Calculating cross-section (A_i), 2nd order moment of inertia around the symmetry axis of the composite (I_i), and volume fraction (V_i) for each layer.

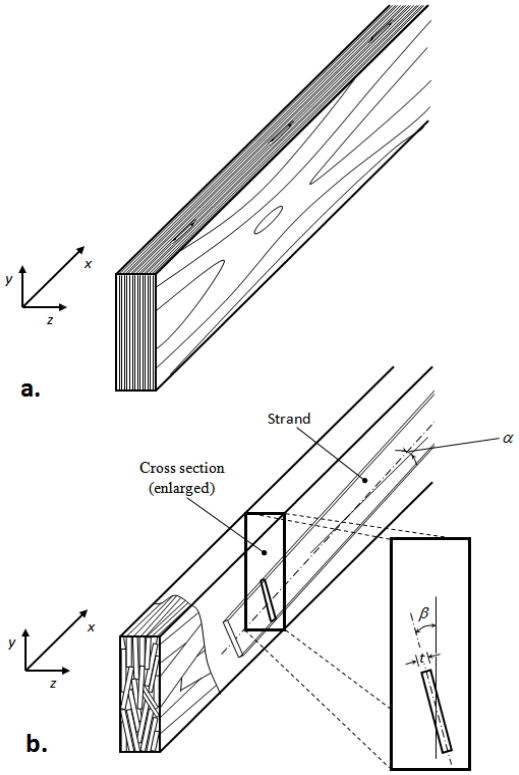

Figure IV.1. *The geometric structure of LVL (a) and PSL (b).*

Figure IV.2a shows the comparison of actual and simulated cross sections for LVL. The stochastic parameters of the spatial structure are the thickness of the layers and their locations within the cross section.

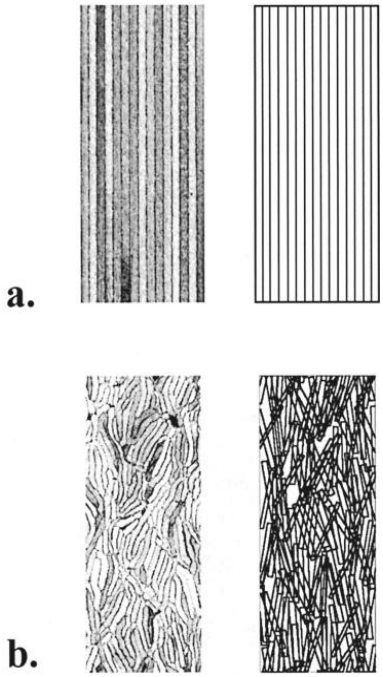

Figure IV.2. *Actual and simulated cross-sections of LVL (a) and PSL (b).*

To electronically recreate the spatial structure of PSL, we developed an inverse, iterative simulation routine. The method is inverse, because it generates the projected-densified thickness of strands first. Randomly assigns original thickness values in the second step, and then it computes the projected width and projected cross-sectional area according to the orientation and preserves the densification of the strands. The process is repeated until a pre-established area coverage criterion is satisfied. Note that the densification, affecting the MOE of the strand, is defined by the original and non-projected densified thickness.

Steps of the simulation process included the following:

- Choosing the *y* and *z* cross-sectional dimensions;
- Simulating the number of strands. In PSL, the number of constituents is a random variable, established by generating the number of strands per in^2, cca. 6.45 cm^2 (u), and multiplying this number by the cross-sectional area of the beam;
- Assigning projected-densified and original strand thickness (t and t_o), longitudinal *strand angle* (α), and a cross-sectional *strand deviation* (β) values to each strand. The model neglects the deviation of the strands' longitudinal axis from the *x-y* plane. The original width of the strands is 25 mm, except for one strand, which has a smaller width This strand reflects the fractional part of the strand number (u);
- Calculating densifications from t and $t_{0;}$
- Summation of projected-densified strand areas and checking the area coverage criterion;
- Arranging strands in both the *y* and the *z* directions. To achieve an even coverage, strand centroids are distributed uniformly in a systematic way, rather than randomly.
- Calculating A_i ,V_i and I_i (flatwise and edgewise), for each constituent. Strands that protrude beyond the boundary of the beam cross section are handled according to the torus convention (Hall, 1988).

The strand deposition process results in overlapping strand areas and holes as demonstrated on *Figure IV.2b*. These overlapping areas and holes represent distorted strands that fill the sectional area of PSL in reality. Note, that the horizontal dislocation of strands has no effect on the stiffness of the composite or a particular individual strand in bending. In case of compression, the location of a strand within the cross-section is indifferent regarding the composite MOE. In the simulated cross section, a projected area, two angles and the position of the strand's centroid represent each constituent.

Stochastic parameters, mentioned above, were generated using probability density functions fitted to experimental databases. *Table A.IV.1* in Appendix IV summarizes the type and parameters of each function. *Figure IV.3* shows two sample histograms, created from experimental data. The diagrams include the overlaid probability density functions, along with a histogram of 1000 simulated random deviates. Visual appraisal and standard statistical tests (Kilmogorov-Smirnov; χ^2) helped to identify the best fitting probability density functions.

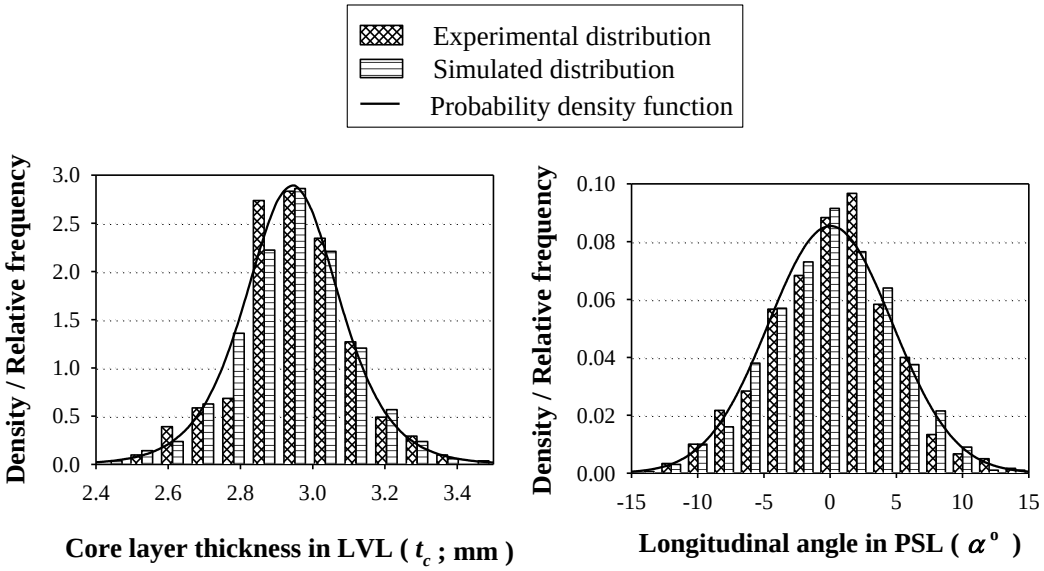

Figure IV.3. *Sample histograms of the geometric input parameters with the probability density functions overlaid.*

VI.3.2 Modeling the elastic parameters of the constituents

The MOE of the constituents were generated in a three-step process which included:

1. Determining the orientation of the constituents relative to the direction of stresses.
2. Assigning compression and/or tension MOE values to the constituents in the given orientation. This involves the use of orthotropic theories, which require MOE values in various anatomical directions, as input parameters. Experimental determination of these parameters and the validation of the orthotropic models have been presented in the previous chapter. The model simulates compression and tension MOE using the three-dimensional Hankinson formula (Lang et al. 2002) and a combination of the Hankinson's formula and the orthotropic tensor theory (Lang et al. 2003), respectively. The elastic input parameters for these formulas are generated assuming normal distribution.

3. Modifying the constituents' MOE values to account for the effect of densification. The model increases the MOE denomination of the veneers or strands, due to density increase during hot pressing, based on experimental, second order densification curves.

We developed the simulation routines using the FORTRAN 90 programming environment. The source code includes four programs, as well as several different functions to generate random data from different distributions, so as to simulate the orthotropic tensile and compression MOE along with the densification effect. A sample flowchart is included in *Figure IV.4,* demonstrating the simulation process for PSL.

A module stores the species-specific input parameters for quaking aspen (*Populus tremuloides*), red oak (*Quercus rubra*) and yellow-poplar (*Liriodendron tulipifera*). These parameters include the summary statistics and probability density functions of input E values, density and sectional dimensions. The routine can be easily extended to cope with new species by adding their parameters to this module.

IV.4 Experimental Validation of the Models

IV.4.1 Materials and methods

Materials used for validation of the models were commercial LVL and PSL. While the LVL had only yellow-poplar veneers, PSL contained approximately 25 % Southern yellow pine (*Pinus spp*.) strands. Note that the input elastic properties in the principal material directions are generated randomly from probability density functions. The obvious overlap of the probability density functions of MOE for the two species may introduce only a few outliers into the model. Consequently, the effect of mixture of species was neglected. All testing materials were kept in a temporary environmental chamber at approximately 21º C temperatures and 65 % relative humidity (RH) during the entire duration of the project. Moisture contents of the test materials were periodically checked on control specimens using standard ASTM procedure (ASTM 1996c). In the first phase of the validation, twenty simulated cross sections for both LVL and PSL were compared to actual sections of the materials. The links between the actual and simulated sections were the number of layers and the number of strands per in^2 (u) for LVL and PSL, respectively. Assigning unit length to the generated cross sections, the density of the simulated composites could be calculated and compared to actual values. Experimental densities were measured and calculated using structural size composites. Additionally, for LVL the total simulated thickness of the beam was compared to actual thickness; and, for PSL the cumulative, projected strand areas (ΣA_i) and the cumulative moment of inertia (ΣI_i) of the strands were measured up to target quantities.

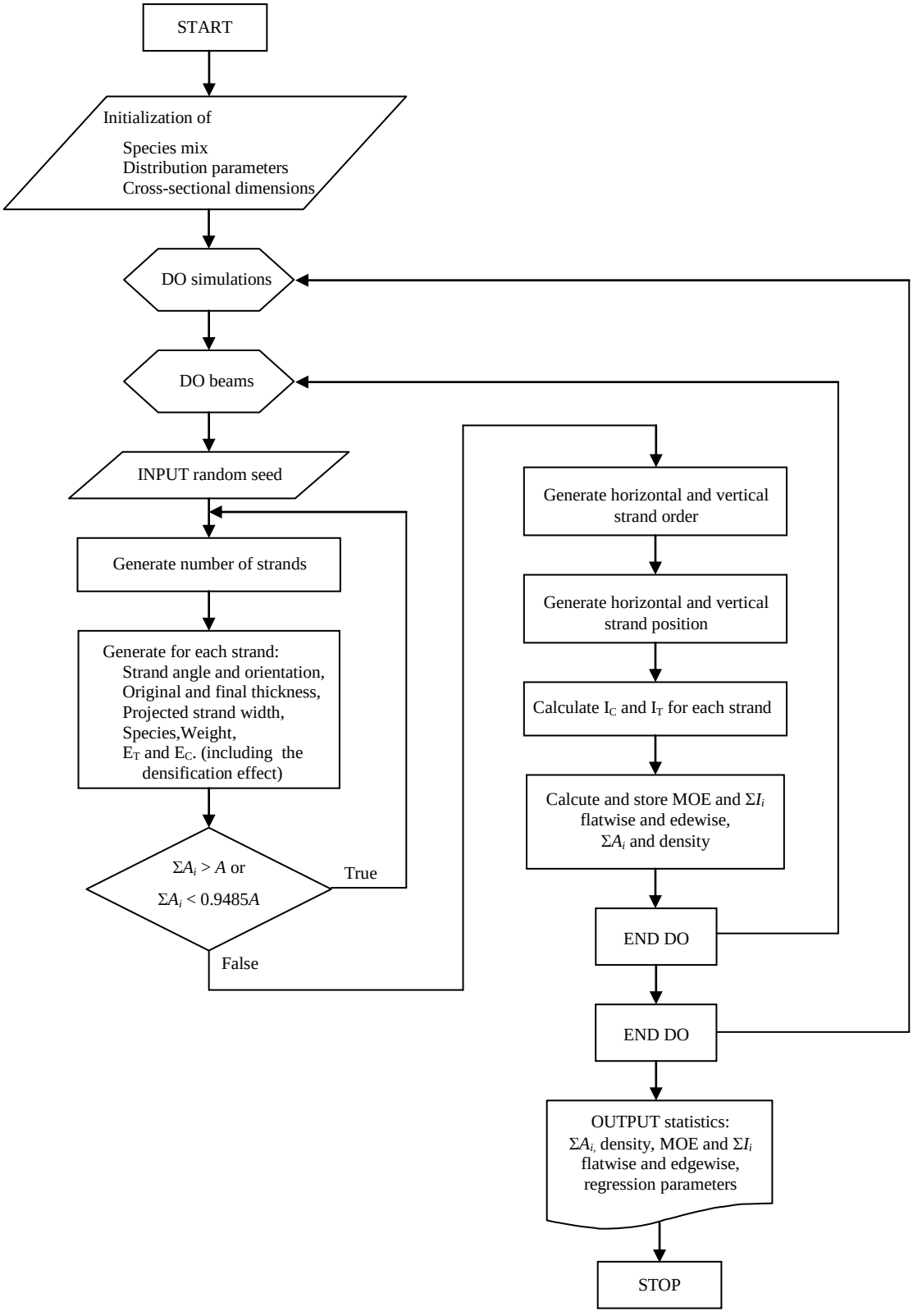

Figure IV.4. *Flowchart of the bending MOE simulation of PSL.*

Twenty structural size beams of LVL and PSL, tested both edgewise and flatwise using a 4-point bending setup over 2.44 m span, provided experimental bending MOE data. The nominal cross sections were 45 mm x 95 mm and 75 mm x 140 mm for LVL and PSL, respectively. The procedure strictly followed the specification of the relevant ASTM standard (ASTM 1996a). The Baldwin type testing apparatus had a load cell with 180 kN capacity. A linear potentiometer having ± 0.01 mm accuracy measured the relative deflection of the shear free section of the beam. Load-deflection data were collected in real time using a computerized acquisition system.

Compression MOE determination followed the specification of ASTM standard D 143-94, secondary method. Accordingly, specimen dimensions were: 25 x 25 x 100 mm. For evaluation of the orthotropic nature of the composites, the principal dimensions of the specimens were rotated systematically by 45º increments, which resulted in six groups of load and strand orientation (φ' and θ'). Note that φ' and θ' are analogous to grain and ring angle of solid wood specimens. When a particular combination of load/strand orientation required, LVL sections were glued side-to-side to provide 100 mm of specimen length. Measurements of ten replications for each combination provided the experimental compression MOE data. Compression load application and the double–sided strain measurements were conducted on an MTS servo-hydraulic universal testing machine, equipped with a 10 kN ±1N load cell. Pairs of strain data were obtained continuously using two MTS clip-on gauges as described in Chapter III. Both for bending and compression, the collected load-deformation data were within the linear elastic region.

Bending MOE simulation consisted of generating twenty LVL and PSL beams, and calculating their MOE both in flatwise and edgewise orientations. The cross-sectional dimensions of the simulated beams were the same as the nominal dimensions of the tested specimens. The entire Monte Carlo simulation was repeated twenty times resulting 400 cross sections where each represented a particular composite beam edge- or flatwise.

Compression model validation was similar to the above procedure, but it involved 20 replications of only 10 simulated specimens in each of six orientations per composite types. This process resulted in a total of 2400 simulation runs.

Standard statistical procedures including t-test, Mann-Whitney Rank Sum Tests helped to evaluate the differences between experimental and simulated results. All tests were conducted at 95 % confidence level ($\alpha = 0.05$).

IV.5 Results and Discussion

To confirm the validity of the first module, the simulated physical properties, including density and geometrical characteristics, were compared to experimental data. *Table A.IV.2* contains the summary statistics of the results. Simulated quantities are average values of the mean, standard deviation, minimum, maximum and skewness calculated from the twenty Monte Carlo simulations, containing twenty beams for each composite type.

For LVL, good agreement between actual and predicted thickness values could be detected. It means that the selected probability density functions described the variations in face and core veneer thickness reasonably well. In contrast, the model significantly underestimated the density when the simulated values were compared to actual densities measured on 2.44 m long LVL beams. Our initial hypothesis was that the overlapping veneer joints and the coupling through-the-width voids have no effect on the mechanical properties of LVL. Apparently, this is not true regarding density because the volume of dense LVL containing an extra layer is significantly bigger than that of void volume in the beam. However, the comparison of model predicted densities to measured ones on joint-free LVL sections demonstrated excellent agreement.

As it was expected, the model slightly under-predicted the simulated cross-sectional area of PSL strands (ΣA_i) because of the built-in area coverage constraint. In reality, PSL contains longitudinal voids due to the imperfect packing of strands. See *Figure IV.2b* where the black and white areas represent through-the-length holes of a 10 mm long PSL section on the actual and simulated cross sections, respectively. These voids have technological advantage in releasing internal steam pressure from the billet after high-frequency die consolidation. The approximately 97.4 % average area coverage resulted from the simulation is a good approximation of a real PSL cross- section. The model under-predicted the 2nd order area moment of inertia of the beam (ΣI_i) by approximately 5 % on average basis. The target or actual cross-sections contain voids that cannot be handled during the experimental determination of bending MOE. This is an inherent bias of the testing procedure that we have accepted. Conversely, the simulated density, which showed excellent agreement with actual values, encouraged the acceptance of this simulation routine.

In Appendix IV, *Table A.IV.3* contains the summary statistics of simulated and experimental bending MOE of LVL and PSL. Note that the data of simulation results are the average of twenty batches of twenty runs; and, not the standard deviation of averages but the average of standard deviations are listed. We do believe that this method provided better estimation of expected minimum and maximum values. *Figure IV.5* provides a quick visual overview of the results. The simulated bending MOE values of LVL in both directions were slightly lower compared to observed data. The differences, however, were not significant, especially in flatwise application and resulted mainly from the higher standard deviation of test results. It does appear that the effect of overlapping veneer joints (their presence/absence and location) manifested in higher variability.

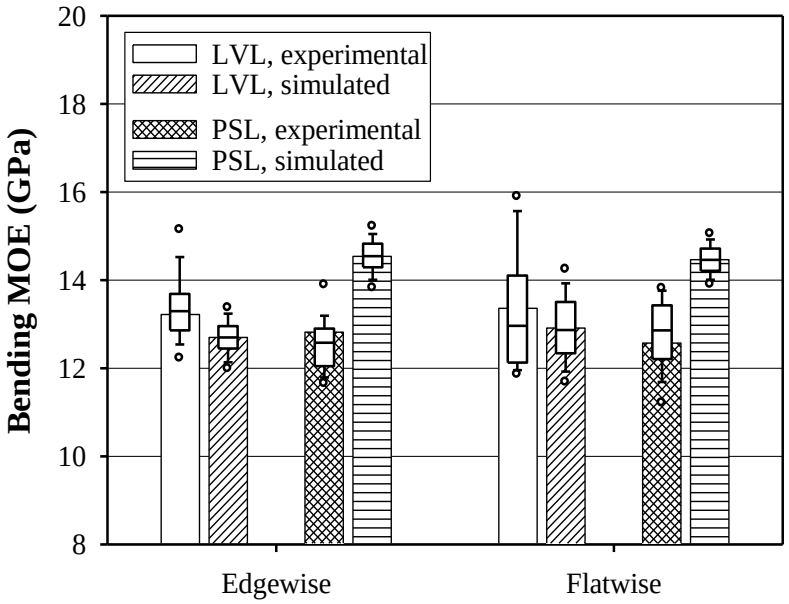

Figure IV.5. *Experimental and simulated bending MOE of LVL and PSL.*

The model significantly and consistently overestimated the bending MOE of PSL beams. There are several plausible explanations for this phenomenon related to the manufacturing technology of the product. However, based on the results of the compression MOE simulation and experimental data, we believe that the inaccuracy of the orthotropic model to estimate the MOE of composites, and neglecting the out of *x-y* plane deviation of strands are the major reasons for these overestimations.

The compression MOE simulation routine was run 2400 times to provide an adequate predicted database. *Table A.IV.4*, in Appendix IV, contains the average statistical parameters of the twenty compression MOE simulations in the six selected combinations of orientation, along with the experimental statistics per product type. *Figure IV.6* offers a quick comparison between observed and simulated results in each direction for LVL and PSL.

Excellent fit of predictions to observed values were identified for both LVL and PSL at 0º/-; 45º/0º; 90º/0º *φ'/θ'* angle combinations. This indicated that the orthotropic models described the changes of MOE in the *x-y* plane exceptionally well; and the inherent shear deformations, mostly in the LT anatomical plane of the constituents, had no explicit effect on the elastic performance of the products.

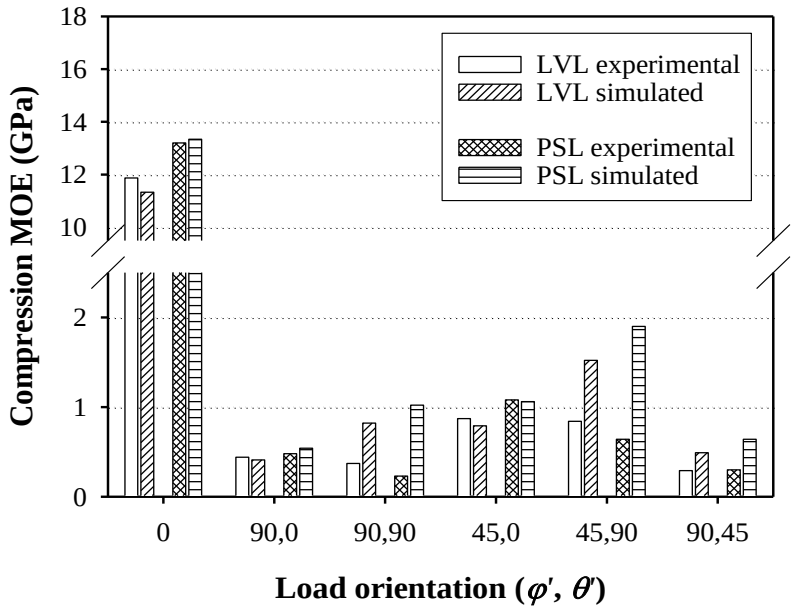

Figure IV.6. *Experimental and simulated compression MOE of LVL and PSL in the selected six combinations of directions.*

Once the direction of normal stresses deviated from the principal *x-y* plane of the composites, the model consistently and significantly overestimated the modulus of elasticity. This fact indicated that neither the 3D Hankinson's formula nor the 3D orthotropic tensor approach could model the true elastic response of three dimensionally oblique, consolidated wood strands or veneers properly over the entire spatial domain.

Figures IV.7 a and b show the orthotropic compression diagrams generated from the average simulated and experimental compression MOE of LVL, respectively, using the orthotropic tensor theory (Szalai 1994). Details **c** and **d** on this figure depict similar diagrams for PSL. The simulated and actual compression MOE values apparently coincide in the *x-y* plane. However, as the layer or strand orientation (θ') increases over approximately 25º, the trends of the model predictions are reversed compared to trends observed. No such deviations in trends could be observed when the orthotropic models were validated using solid wood specimens (Lang et al. 2002). The veneer manufacturing process may have introduced cracks, compression sets that altered the rolling shear resistance of the veneers; or, the densification affected the out-of plane deformation under compression. This phenomenon needs further investigation.

Nevertheless, these models have practical importance because they can predict the expected elastic response of LVL and PSL with excellent accuracy from the mechanical properties of their constituents in the majority of structural loading conditions. These include support reactions, columns, edgewise beam and rafter applications where the direction of normal stresses generated by external loads usually coincides with the *x-y* plane of the composites.

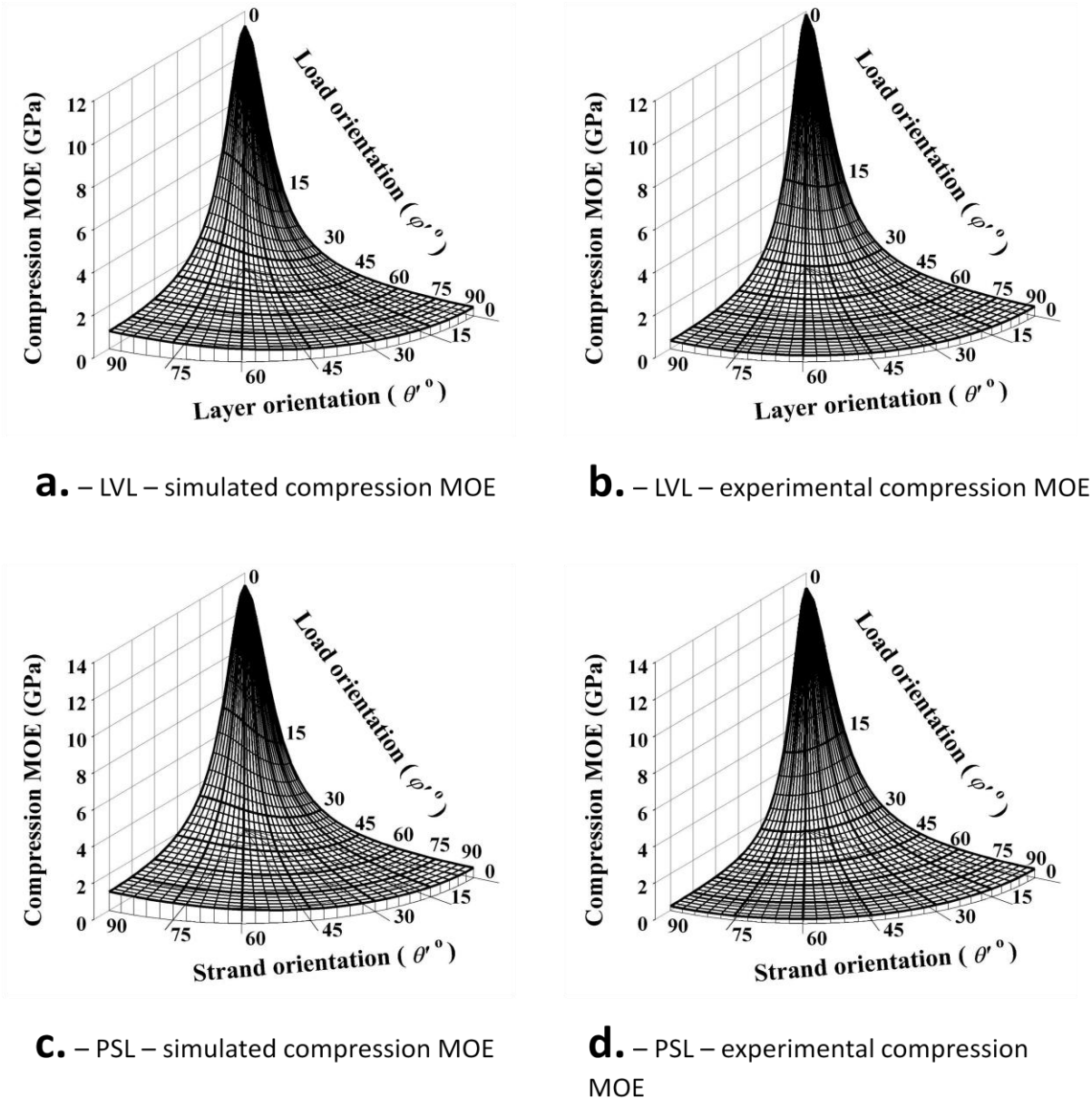

a. – LVL – simulated compression MOE

b. – LVL – experimental compression MOE

c. – PSL – simulated compression MOE

d. – PSL – experimental compression MOE

Figure IV.7. *Orthotropic diagrams of the simulated and experimental compression MOE of the composites.*

Sensitivity analysis was performed to further demonstrate the practicality of the developed simulation models. The analysis consisted of simulating the flatwise-bending MOE of PSL, while progressively reducing the scale parameter (standard deviation) of the distribution of strand angle (α) and strand deviation (β). The examined ranges were between 100% and 0% of the scale parameters, i.e., decreasing the variance of α and β from their original level to no variation at all. Other parameters (e.g., strand thickness, the number of strands and the mean value of α and β) were kept constant.

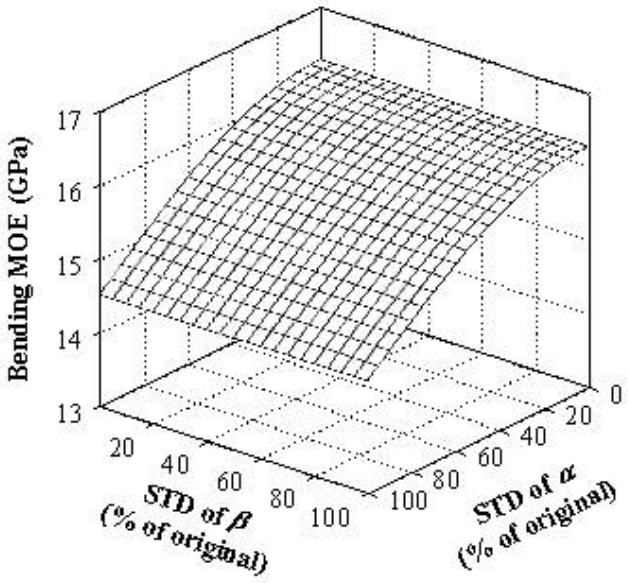

Figure IV.8. *The effect of decreasing variation of α and β on the flatwise, bending MOE of PSL.*

Figure IV.8 shows the bending MOE of PSL, as a function of the standard deviation of α and β expressed by percent of the original standard deviations. As this diagram shows, decreasing the deviation of β from its mean value has little effect on the MOE of PSL. On the other hand, the changes in variance of α, affects the MOE significantly. Bending MOE improves more than 12 % (nearly 2 GPa), if the variation is completely eliminated. This is unfortunately not possible for PSL. However, if by some innovative means, the standard deviation could be reduced by 50%, it would still increase the bending MOE by 8.5 %, provided that the other parameters do not change.

IV.6 Summary and Conclusions

The bending and orthotropic compression MOE of LVL and PSL have been modeled through simulating the cross-sectional geometry of the composites and the elastic parameters of the constituents. In general, good agreements have been found between simulated and experimental characteristics.

Despite their simplicity, the models reconstructed the geometric structure and density of the composites reasonably well. Analytical works revealed the difficulties in modeling the modulus of elasticity of spatially oblique wood constituents. It has been concluded that the rolling shear in spatially off-axis strands and veneers may significantly influence the apparent modulus of elasticity in compression or in bending. Further research is needed to enhance existing orthotropic models to address the rolling shear deformation and its effect on the elastic response of wood based composites. On the other hand, it can be concluded that the elastic performance of the examined composites is predictable with excellent accuracy if the normal stresses are parallel to the principal *x-y* plane of the structural elements.

IV.7 Closure of Chapter IV

The model development, described above, resulted in a chapter of a Ph.D. Dissertation (Bejo 2001) one peer reviewed publication in English (Bejo and Lang 2004). Our models were presented at two international conferences or symposia (Bejo and Lang 2004a; Bejo and Lang 2004b.) Other independent researchers extended our prediction approach for PSL to a three dimensional, structural model (Arwade et al. 2009 and Arwade et al. 2010). These improvements of our model were published in highly regarded journals dealing with experimental mechanics.

References IV

1. American Society for Testing and Materials. 1996a. Standard methods of static tests of lumber in structural size. ASTM D 198 – 94. ASTM, West Conshohocken, Pa.
2. American Society for Testing and Materials. 1996c. Standard test methods for direct moisture content measurement of wood and wood-base materials ASTM D 4442 – 92. ASTM, West Conshohocken, Pa.
3. American Society for Testing and Materials. 1996d. Standard methods of testing small clear specimens of timber. ASTM D 143 – 94. ASTM, West Conshohocken, Pa.
4. Arwade, A.R., P.L. Clouston and R. Winanas. 2009. Measurement and stochastic computational modeling of the elastic properties of parallel strand lumber. J. Engrg. Mech. 135(9):897-905.
5. Arwade, A.R., R. Winanas and P.L. Clouston 2010. Variability of the compressive strength of parallel strand lumber. J. Engrg. Mech. 136(4):405-412.
6. Barnes, D. 2001. A Model of the effect of strand length and strand thickness on the strength properties of oriented wood composites. Forest Prod. J. 51(2):36-46.
7. Bejo, L. 2001. Simulation based modeling of the elastic properties of structural composite lumber. Ph.D. Dissertation, Virginia University, Division of Forestry and natural Resources, Morgantown, WV, U.S.A. pp. 224.
8. Bejo, L. and E. M. Lang., 2001. Simulation based modeling of the flexural properties of structural composites. 55th Annual Meeting of the Forest Products Society, Baltimore, MD. (Előadás). In Biographies & Abstracts p. 22.
9. Bejo, L. and E. M. Lang. 2001. Elastic properties of structural composite lumber products. A simulation model. New Research Results of Wood and Fiber Science Conference, Sopron, Hungary, November 7, 2001. (Előadás, angolul)
10. Bejo, L. and E.M. Lang. 2004. Simulation based modeling of the elastic properties of structural composites. Wood and Fiber Science. 36(3):395-410.
11. Bodig, J., and B. A. Jayne. 1982. Mechanics of wood and wood composites. Van Nostrand Reinhold Co., N.Y.
12. Conners, T. E. and P. J. Medvecz. 1992. Wood as a bimodular material. Wood and Fiber Sci. 24(4):413-423.
13. Dai, C. and P. R. Steiner. 1994a. Spatial structure of wood composites in relation to processing and performance characteristics. Part 2. Modelling and simulation of a randomly-formed flake layer network. Wood Sci. Technol. 28:135-146.

14. Dai, C. and P. R. Steiner. 1994b. Spatial structure of wood composites in relation to processing and performance characteristics. Part 3. Modelling the formation of multi-layered random flake mats. Wood Sci. Technol. 28:229-329.

15. Harless, T. E., F. G. Wagner, R. D. Seale, P. H. Mitchell, D. S. Ladd. 1987. A model to predict the density profile of particleboard. Wood Fiber Sci. 19(1):81-92.

16. Harris, R. A. and J. A. Johnson. 1982. Characterization of flake orientation in flakeboard by the Von Mises probability distribution function. Wood and Fiber 14(4):254-266.

17. Humphrey, P.E. and A.J. Bolton. 1989. The hot pressing of dry-formed wood-based composites. Part II. A simulation model for heat and moisture transfer, and typical results. Holzforschung 43:199-206.

18. Kallmes, O. and H. Corte. 1960. The structure of paper. I. The statistical geometry of an ideal two-dimensional fiber network. TAPPI 43(9):737-752.

19. Kallmes, O., H. Corte. And G. Bernier. 1961. The structure of paper. II. The statistical geometry of a multiplanar fiber network. TAPPI 44(7):519-528.

20. Lang, E. M., L. Bejo, J. Szalai, Z. Kovacs and R. B. Anderson. 2002. Orthotropic strength and elasticity of hardwoods in relation to composite manufacture. Part II: Orthotropy of compression strength and elasticity. Wood and Fiber Sci. 34(2):350-365.

21. Lang, E. M., L. Bejo, F. Divos, Z. Kovacs and R. B. Anderson. 2003. Orthotropic strength and elasticity of hardwoods in relation to composite manufacture. Part III: Orthotropic elasticity of structural veneers. Wood and Fiber Sci. 35(2):308-320.

22. Law, A.M. and W.D. Kelton. 1991. Simulation modeling and analysis. 2nd ed. McGraw-Hill, Inc. New York. pp. 759.

23. Lu, C., P. R. Steiner, F. Lam. 1998. Simulation study of wood-flake composite mat structures. Forest Prod. J. 48(5):89-93.

24. Song, D. and S. Ellis. 1997. Localized properties in flakeboard: A simulation using stacked flakes. Wood and Fiber Sci. 29(4):353-363.

25. Steiner, P. R. and C. Dai. 1993. Spatial structure of wood composites in relation to processing and performance characteristics. Part 1. Rationale for model development. Wood Sci. Technol. 28:45-51.

26. Suchsland, O. and H. Xu. 1989. A simulation of the horizontal density distribution in a flakeboard. Forest Prod. J. 39(5):29-33.

27. Suchsland, O. and H. Xu. 1991. Model analysis of flakeboard variables. Forest Prod. J. 41(11/12):55-60.

28. Szalai, J. 1994. Anisotropic strength and elasticity of wood and wood based composites. Private ed. Sopron, Hungary. Pp. 398.(in Hungarian.)

29. Triche, M. H. and M. O. Hunt. 1993. Modeling of parallel-aligned wood strand composites. Forest Prod. J. 43(11/12):33-44.

30. Wang, K. and F. Lam. 1998. Robot-based research on three-layer oriented flakeboards. Wood and Fiber Sci. 30(4):339-347.

31. Xu, W. 1999. Influence of vertical density distribution on bending modulus of elasticity of wood composite panels: A theoretical consideration. Wood and Fiber Sci. 31(3):277-282.

32. Xu, W. 2000. Influence of percent alignment and shelling ratio on modulus of elasticity of oriented strandboard: A Model investigation. Forest Prod. J. 50(10):43-47.

33. Xu, W. and P. R. Steiner. 1995. A statistical characterization of the horizontal density distribution in flakeboard. Wood Fiber Sci. 27(2):160-167.

34. Xu, W. and O. Suchsland. 1997. Linear expansion of wood composites: A model. Wood Fiber Sci. 29(3):272-281.

35. Xu, W. and O. Suchsland. 1998a. Influence of out-of-plane orientation of particles on linear expansion of particleboard: A simulation study. Forest Prod. J. 48(6):85-87.

36. Xu, W. and O. Suchsland. 1998b. Modulus of elasticity of wood composite panels with uniform vertical density profile: A model. Wood and Fiber Sci. 30(3):293-300.

37. Xu, W. and P. M. Winistorfer. 1996. Fitting an equation to density profile data using Fourier analysis. Holz Roh- Werkst. 54(1):57-59.

38. Zombori, B. G. 2001. Modeling the transient effects during the hot-pressing of wood-based composites. Ph.D. Dissertation, Virginia Polytechnic Inst. And State University, Blacksburg, VA. Pp. 212.

List of Figures IV

Nomenclature IV

Uppercase letters:

A	*cross sectional area*
ANOVA	*analysis of variance*
ASTM	*American Society for Testing and Materials*
E	*modulus of elasticity*
HDD	*horizontal density distribution*
I	*moment of inertia*
L, T, R	*anatomical directions*
LT, LR, TR	*anatomical planes*
LVL	*laminated veneer lumber*
MC	*moisture content*
N	*newton*
MOE	*modulus of elasticity*
PSL	*parallel strand lumber*
RH	*relative humidity*
SG	*specific gravity*
V	*volume*
VDD	*vertical density distribution*

Lower case letters:

t; t_o	*thicknesses*
u	*strand number per unit volume*
x, y, z	*coordinates*

Greek letters:

α	*probability type-I error; strand angle*
β	*strand deviation*
χ^2	*test statistics*
φ'	*strand orientation*
π	*Ludolf's number*
ρ	*density*
θ'	*load orientation*

Subscripts/superscripts:

$_o$	*initial value*
$_i$	*strand/layer index*

CHAPTER V

"THE WEALTH OF NATIONS IS BASED ON TAKING RAW MATERIALS AND TURNING THEM INTO SOMETHING USEFUL."

ADAM SMITH
(1723 – 1790)

V. Development of New Wood-based Composites

V.1 Introduction

More than a decade ago Smulski (1997) assembled an up-to-date compendium of wood based structural composite manufacturing practices; and demonstrated the current significance and prosperous future of the industry. Furthermore, Winandy (2002) identified four critical issues that the forest products industry has to deal with at the beginning of the third millennium. These include: demand for engineered systems; demand for durability; forest resources and management; public and user perceptions. This report argued that the above issues will mandate the increased use of SCL products including recycled composites, wood-cement systems and structural fiberboards. Another study by the APA, The Engineered Wood Association predicted 4% annual increase through 2008 in demand for structural composite materials (Adair 2003). ***They all were wrong!*** Unforeseen social, political and economical circumstances resulted in a global recession. Demand for wood-based structural composites declined along with the diminishing construction industry.

From the early seventies, research on wood and wood composites went through several trendy periods including matrix structural analysis, finite element modeling, wood plastic composites, nano-technology, etc. Currently (in 2011) the CO_2 retention is the up-to-the-minute research topic. This phenomenon, coupled with the emphasized sustainable forestry idea, created an unfriendly environment for wood researchers. The lack of support from the struggling forest products industry along with the politically motivated grant distributions resulted in limited number of products or technology development regardless of countries on all of the four habitable continents and in Australia as well. However, sooner or later the industry will gain momentum again and production enterprises without innovative product development and technologies will not survive.

The next session of this Dissertation describes the manufacturing feasibility of strand type structural and non-structural composites. Detailed development and technological steps are intentionally omitted because of some confidential information.

V.2 Rationale

Decorative (face) veneer manufacturing processes convert high quality half or quarter logs, with an average length of 3 – 4 m, into thin (0.5-0.8 mm) veneer sheets, sometimes referred to as veneer "leafs" by slicing or eccentric rotary peeling. *Figure V.1a* schematically illustrates the slicing process. After drying and stacking, a clipping operation (*Figure V.1b*) sets the final rectangular dimensions of the veneer bundles that contain 15 to 20 sheets.

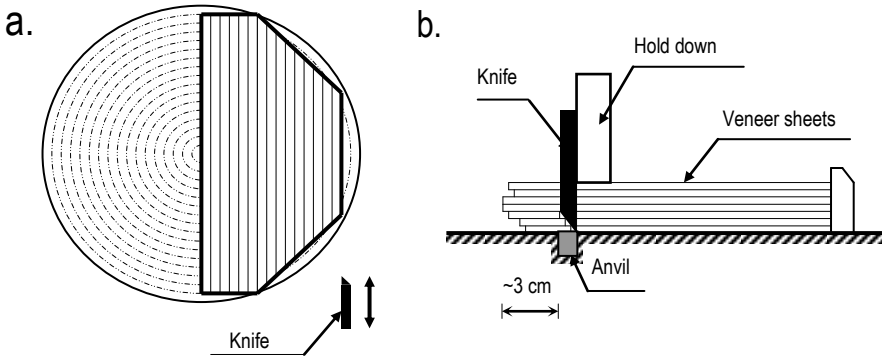

Figure V.1. *Schematic of the decorative veneer manufacturing process. a. – Slicing. b. – Clipping operation.*

During this operation, residual side-clippings, with an average length of 1 – 4 m and width of 25 to 40 mm, are produced. Moreover, the end clipping operation generates rectangular shaped cutoffs that can be easily converted into strand-type raw furnish for further composite manufacture. *Figure V.2* shows these typical veneer residues obtained from local mills in West Virginia. Surprisingly, these wastes are habitually used as fuel for energy generation -- usually with low efficiency -- or are being further processed to create landscaping mulch. Only ten percent of the clippings are being converted into fiber.

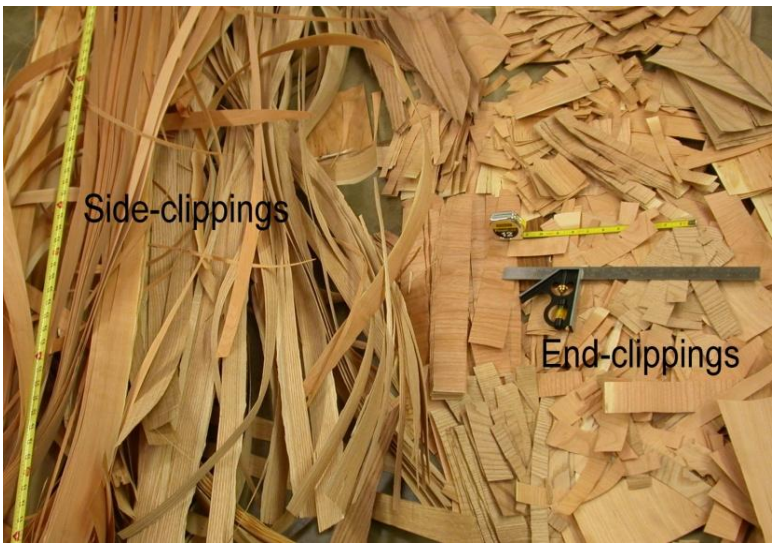

Figure V.2. *Residues of clipping generated during decorative veneer manufacture.*

A professional survey (Hassler 2002) revealed that in the central Appalachian region, 15 veneer mills generate approximately 60,000 metric tons of clipping residues annually. This volume corresponds to 92,000 m^3 wood based composite materials on a 650 kg/m^3 average density basis. More than half of the responding companies use dry clipping procedures yielding residuals that have about 8 to 11% moisture content. The rest of the clippings have moisture contents around and above the fiber saturation point (FSP ~28%). Assuming the Appalachian mills are representative of all veneer mills in U.S. and Canada, it can be roughly estimated that more than a quarter of million tons of veneer residues are produced annually at almost one hundred veneer mills in North America.

The experimental and development parts of a comprehensive study resulted in two characteristic structural composites designated as veneer strip panels (VSP) and veneer strip lumber (VSL). Side- and end-clippings were reconstituted into discrete composite panels and load-supporting SCL slabs by traditional hot pressing consolidation processes. The resin application happened through roller coating and drum blending using conventional phenol-formaldehyde (PF) and polymeric diphenylmethane-diisocyanate (pMDI) resins common in structural panel and SCL manufacturing. Standard ASTM testing procedures (ASTM D-1037 1996 and ASTM D-143 1996) on limited sample sizes included apparent modulus of elasticity (MOE) and bending strength (MOR) determinations. Furthermore, internal bond (IB) tests demonstrated excellent strength values in the direction perpendicular to the principal plane of the materials (Lang and Denes 2002).

For engineered load supporting composites, a corrugated web panel is being developed. (Lang 2007, Denes et al. 2010, Denes et al. 2010, McGraw 2010 and McGraw et al. 2010) This I-joist element, named, CorPan is designed to improve the concentrated load bearing capacity of the beam. I-joists, formulated with CorPan web, have improved resistance against lateral buckling. The exploration of panel properties and the parameters of pressing operation have already been established. Currently, the optimum waveform and dimensions are under investigation.

Additionally, a typical core material was developed, named as UreStrand. The product intends to replace high density (particle board, MDF) core materials for doors, countertops, etc. Consequently, the critical attributes: density and compression strength were evaluated extensively.

The innovative new products, from one segment of the forest products industry, demonstrate tremendous potential in waste management via residual utilization. Their energy efficient production technologies and carbon storage capabilities contribute to the environment protection and sustainable forest management.

V.3 Product's Range and Properties

This section provides some information about the above mentioned products without getting into detailed discussion of their development. Please note, that the innovation processes, included the results of material property assessment discussed in the previous chapters.

V.3.1 Veneer strip panels (VSP)

VSP is a high performance structural panel made of parallel and angle-to-length side clippings. The average modulus of elasticity and bending strength along with the density are as follows:

E = 14.0 GPa; MOR = 92 MPa; Density = 730 kg/m^3

Figure V.3. *Veneer strip panels formulated from side clippings.*

These three–layer, high performance structural panels are made of side and end clippings and are designed for specific applications where the flatwise bending strength is particularly important. The average modulus of elasticity and bending strength along with the density are as follows:

E = 16.0 GPa; MOR = 120 MPa; Density = 800 kg/m^3

Figure V.4. *Three-layer structural composites, designed for flatwise application.*

V.3.2 Veneer strip lumber (VSL)

VSL is a single layer, high performance structural lumber made of shredded side clippings. The composite was designed for both edge- and flatwise applications. The average modulus of elasticity and bending strength along with the density are as follows:

E = 17.0 GPa; MOR = 146 MPa; Density = 750 kg/m^3

Figure V.5. *Structural composite lumber formulated from shredded side clippings.*

V.3.3 CorPan, a web element for I-joists

CorPan is made of side clippings and/or rejected, low quality decorative veneers. The physical and mechanical properties are similar to that of VSP without having angle-to-length layers. The dimensional stability is achieved by the corrugation which additionally provides the buckling resistance of the edge-loaded web elements.

E = 14.0 GPa; MOR = 92 MPa; Density = 730 kg/m^3

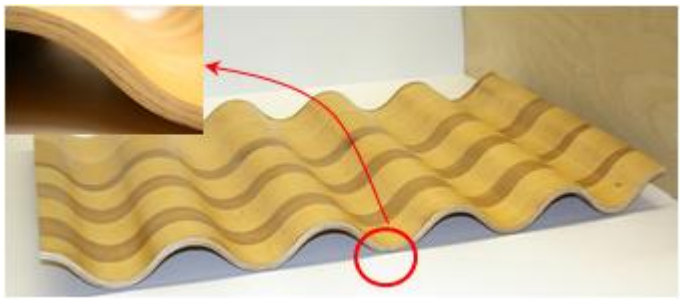

Figure V.6. *Corrugated panel (6.4 mm thick) produced from side clippings of decorative veneers.*

Corrugated panels were manufactured in two thicknesses, namely 3.2 and 6.4 mm. The CorPan application is viewed in *Figure V.7*, while *Figure V.8* demonstrates the proof testing procedure.

Figure V.7. *I-joists with 3.2 mm thick CorPan web elements. Flanges (left to right) are: pine, yellow-poplar PSL and LVL composites.*

Figure V.8. *Testing the newly developed I-joists for effective MOE and bending strength by four-point loading.*

V.3.4 UreStrand core materials

The third product group of our innovations included the development of a light weight, veneer strand – foam combination. The product has considerable compression strength and excellent heat insulation properties. Thus, it is very desirable substitute of core materials in layered composite panels. The innovation lies in the application of polyurethane foaming agent to veneer strands. Density and thickness of the slabs can be controlled by the spread of foaming agent and by the openings of the forming press. *Figure V.9* illustrates the medium and low density sections of the UreStrand core materials.

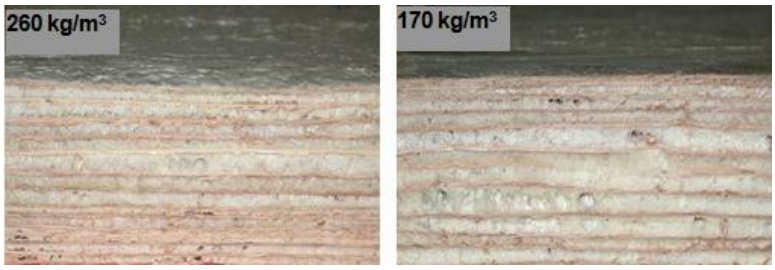

Figure V.9. *Cross sections of medium and low density, urethane – veneer strand composites.*

The application possibilities may be studied on *Figures 10* and *11*, where the former shows panels for door leaves or countertops and the second demonstrates structural insulation panels. The initial core slabs can be further manipulated (i.e., cut, rotate and re-glue) to achieve specific panel properties.

Figure V.10. *Variety of panel products with UreStrand core material.*

Figure V.11. *Medium density UreStrand core in structural insulated panels.*

V.4 Statistical Process Control in Wood-based Composite Manufacture

V.4.1 Introduction and theoretical considerations

Design of new products or development of existing ones, play a vital role in most industrial organizations. Besides the thorough knowledge of the constituting raw materials, the manufacturing parameters, ratios of additives and technological sequences have significant influence on the final performance of the products.

Many of the problems, related to the quality properties of the products, originate from the erratic variability of different factors. Thus, minimizing any controllable variability would improve the performance of the products. The manufacturing processes are influenced by numerous deterministic or stochastic factors that may drastically affect the performance characteristics of any new product. Some of these factors are controllable while others are not. These uncontrollable ones are referred to as noise factors. In this context optimizing product/process performance means: a./ identifying the key variables which influence the quality characteristics; b./ determining the levels of controllable factors that optimize process or performance; c./ selection of a combination of control variables at which the system is insensitive to variation in the noise factors. A product or process improved in this way is called robust and the methodology is known as robust parameter design (RPD). The technique was introduced by Taguchi (Taguchi 1987) to improve the quality of a product through minimizing the effect of the noise factors by changing the setting levels of controllable variables.

The method is related to the design of experiment (DOE) theory using orthogonal arrays to study the parameter space. Taguchi proposed the use of separate designs for the two types of variables: the controllable factors are placed in a so-called inner array and the uncontrollable ones comprise an outer array. Experiments are completed according to the Cartesian product of these designs. To reduce the number of the experimental runs, one can use a combined array (Nair et al. 1992) which incorporates both controllable and noise factors. Depending on the

setting levels of the variables, a first or second order response model is fitted through the experimentally obtained data. Sufficient degrees of freedom in the model allow the investigation of the curvilinear effect of the factors. The general regression model of a full-quadratic response surface is given as follows:

$$y = \beta_0 + \sum_{i=1}^{k} \beta_i x_i + \sum_{i=1}^{k-1} \sum_{j=i+1}^{k} \beta_{ij} x_i x_j + \sum_{i=1}^{k} \beta_i x_i^2 + \varepsilon \qquad (V.1)$$

where y represents the predicted property, k is the number of variables (x_i), β's are the least square regression coefficients, and the term ε denotes the random error assumed to be normally and independently distributed with mean zero and variance σ^2 ($N(0, \sigma^2)$). *Equation V.1* stands for a quadratic surface in the k-dimensional space of input parameters where β_i, β_{ij} contribute to the deviations from average values (*Montgomery 2005, 1999*).

After dividing the variables into controllable and noise factors (Montgomery 1997) the model in matrix form becomes:

$$y(x,z) = \beta_0 + \{x'\}\{\beta\} + \{x'\}[B]\{x\} + \{z'\}\{\gamma\} + \{x'\}[\Delta]\{z\} + \varepsilon \qquad (V.2)$$

where:

β_0 – the overall mean effect**;**

x' – row vector of control factors $x' = \{x_1, x_2, \ldots x_{n1}\}$;

z' – row vector of noise factors $z' = \{z_1, z_2, \ldots z_{n2}\}$;

x and z – transpose (column) vectors of x' and z', respectively;

β - column vector containing the regression coefficients of the control factors;

$[B]$ – an $n_1 \times n_1$ matrix whose diagonals are the regression coefficients associated with the pure quadratic effects, off-diagonals represent the interaction effects;

γ – vector of regression coefficients for the main effects of the noise factors;

Δ – an $n_1 \times n_2$ matrix of the control factors by noise factor interaction effects;

ε – random error.

This model doesn't contain the pure quadratic effects of the uncontrollable variables because of the general assumption that they play little role in making a product robust (Nair et al. 1992). After selecting the control and noise factors that affect the quality characteristics of the product, an appropriate experimental matrix is developed according to the orthogonal design generation rules (Adler et al.1977). The specified experimental runs in the design matrix then will be completed in random order and may be repeated if necessary.

Data processing begins with the analysis of variances (ANOVA) to determine the significance of factors and interactions. Taguchi's philosophy assumes that the interactions are unimportant. Thus, he proposes design matrices with low resolution. However, if the design matrix is not saturated some interaction effects may be expected. The model parameters are quantified using regression analysis. Predicted response values, generated by the obtained regression model, can be represented as response surfaces and the optimal region or optimization direction (by steepest ascent) can be identified or assigned.

During this research, we first confirmed the viability of the above discussed statistical process control method for application in wood-base composite design and development (Denes et al. 2006). Later selecting the critical parameters of technology and materials, the method was applied to screen out the optimum performance of these new composites. The next session briefly discusses one of the typical evaluation results.

V.4.2 An example of the viability of the Taguchi's method

V.4.2.1 Materials and Methods

Referring to *Figure V.3*, panels comprising side clippings only, were evaluated. To test the general applicability of the method; in phase one the furnish contained a mix of three dominant species. These included about 60% black cherry (*Prunus serotina*), 35% red oak (*Quercus rubra*) and 5% maple (*Acer spp*.) for all panel types. *Table V.1* summarizes the three experimental factors and their levels.

Table V.1. *Experimental factors and their levels.*

FACTORS			***FACTOR LEVELS***		
Symbol	***Description***	***Unit***	***1***	***2***	***3***
A	*Resin content*	*%*	*5*	*8*	*11*
B	*Target density*	*kg/m^3*	*650*	*700*	*750*
C	*Ratio of end clippings*	*%*	*0*	*25*	*50*

Results of this L_9 type analysis confirmed the applicability of the method and were published in a separate publication (*Denes at al. 2006*). More information about this pilot study is compiled in *Appendix V* in tabulated or graphic forms.

In a different run of the analysis, an industrial, phenol-resorcinol formaldehyde type adhesive (*50% solid content*) provided adhesion between the constituents. The resin application took place in a laboratory, rotary-drum blender. The spread of adhesive was set to 8.0% of the dry furnish mass, with target density for all panels as 700 kg/m^3. For this particular phase, seven technological parameters were selected with two levels for each factor according to *Table V.2.*

General methodology for both segments of this work included the investigation of the effects of processing parameters on the bending strength (MOR) and modulus of elasticity (MOE) of the products using design of experiments (DOE) and robust parameter design (RPD) as discussed above.

In the second phase, sixteen factor/level combinations were repeated three times resulting in 48 experimental panels for edge and flat-wise evaluations. Modulus of rupture and apparent MOE measurements followed the specifications of relevant ASTM standards. Data processing included analyses of variances (ANOVA) and the model parameters were quantified by regression techniques.

Table V.2. *Processing variables and setting levels.*

Code	Factors	Level -1	Level +1
X_1	*Wood species*	*Beech*	*Maple*
X_2	*Average strand width*	*15 mm*	*35 mm*
X_3	*Strand staggering*	*0 %*	*50 %*
X_4	*Number of layers*	*35*	*75*
X_5	*Strand orientation*	*15°*	*30°*
X_6	*Consolidation pressure*	*2.16 MPa*	*3.14 MPa*
X_7	*Consolidation temperature*	*130°C*	*160°C*

V.4.2.2 Results and Discussion

Results of these 2_{IV}^{7-3} fractional, factorial design analyses are graphically presented by *Figures V.12* and *V.13*, where the solid horizontal lines mark the overall mean values of the predicted property, dashed lines indicate ± 2 standard errors and the symbols denote the observed values at the indicated setting levels of the factors.

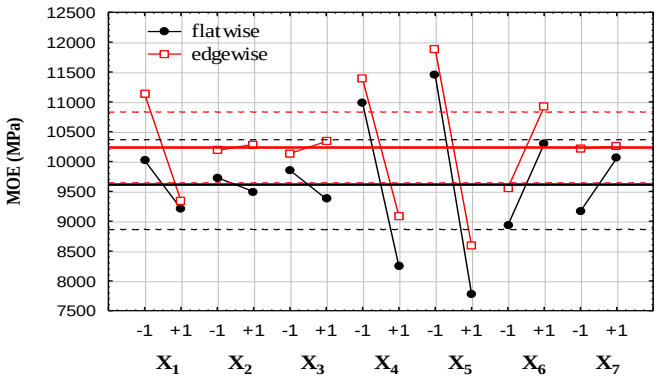

Figure V.12. *The effect of factors on the modulus of elasticity (MOE).*

The effect of a factor can be regarded statistically significant if the observed property values at the setting levels are on or over the limits of the ± 2 standard error domain.

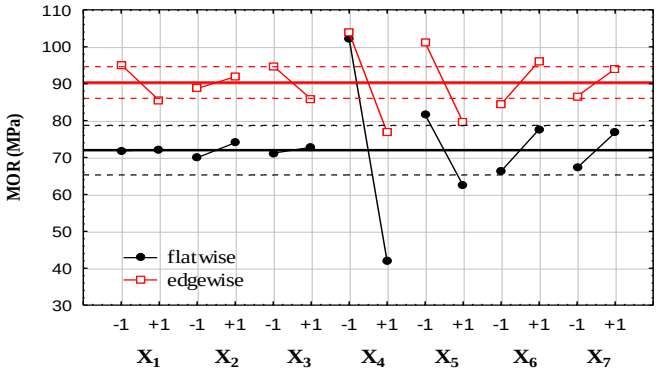

Figure V.13. *The effect of selected factors on the modulus of rupture (MOR).*

Accordingly, the MOE of the new composites in flatwise bending is affected by three factors: number of layers (X_4), strand orientation (X_5) and consolidation pressure (X_6).

Additionally, under edgewise bending, the effect of species factor (X_1) proved to be statistically significant too. Using the regression coefficients of the factors that demonstrated significant effects, linear models with the indicated adjusted R^2 values could be formulated as follows:

$$\hat{y}_{MOE_F} = 9613 - 1367x_4 - 1833x_5 + 684x_6 \quad R^2_{adj} = 0.73 \qquad (V.3)$$

$$\hat{y}_{MOE_E} = 10236 - 894x_1 - 1144x_4 - 1646x_5 + 681x_6 \quad R^2_{adj} = 0.83 \qquad (V.4)$$

Setting the factors at their optimal levels, the overall mean MOE may be exceeded by approximately 40%.

Similarly, *Figure V.13* shows the effects of factors on the modulus of rupture. It does appear that in edgewise bending only the X_2 (strand width) factor has negligible effect on the MOR.

$$\hat{y}_{MOR_F} = 72 - 30.1x_4 - 9.63x_5 + 5.7x_6 \quad R^2_{adj} = 0.87 \qquad (V.5)$$

$$\hat{y}_{MOR_E} = 90.3 - 4.8x_1 - 4.5x_3 - 13.5x_4 - 10.8x_5 + 5.8x_6 + 3.7x_7 \quad R^2_{adj} = 0.85 \qquad (V.6)$$

Again, setting the significant factors at optimum levels - according to the above linear models - the bending strength may be increased by almost 50% compared to the overall mean value. *Figure V.14* shows the effects of X_4 and X_5 (number of layers and strand orientation, respectively) on MOR in edgewise bending, for the two selected species.

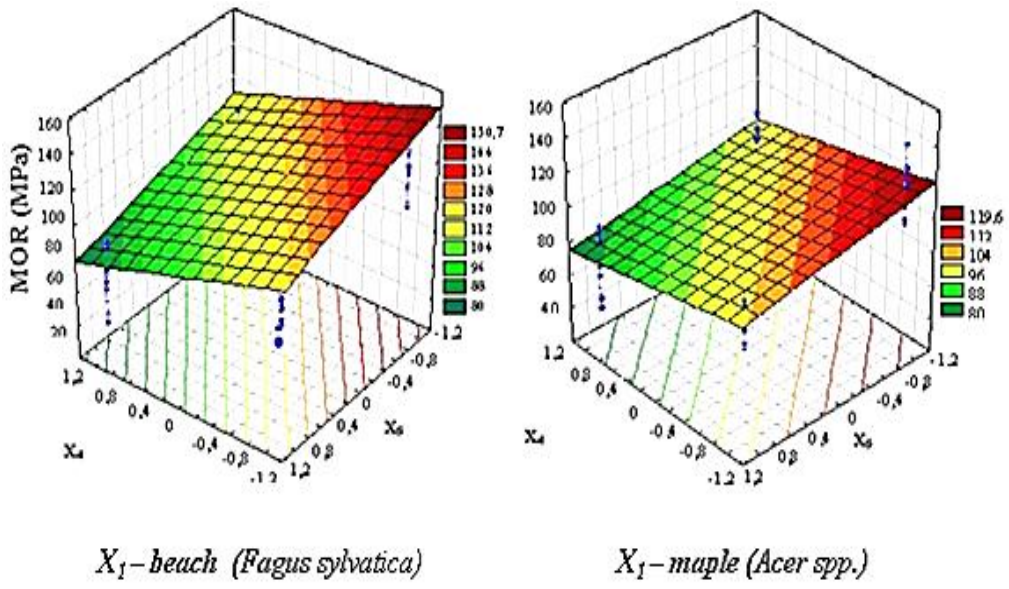

X_1 – beach (Fagus sylvatica) *X_1 – maple (Acer spp.)*

Figure V.14. *The effects of strand orientation (X_5) and the number of layers (X_4) on the edgewise bending strengths of beach and maple composites.*

V.5 Summary and Conclusions

Chapter V emphasized the significance of product development in the wood-based composite industry. The discussed novel products demonstrate that waste materials or residues may be successfully converted into value-added products. Additionally, besides the material property assessment models, deliberated in previous chapters, a statistical quality control process was briefly outlined. The viability of advanced statistical process control methods including RPD and the response surface methodology in strand-type wood composite development has been demonstrated. These methods provide sufficient information about influential processing parameters that may be used to optimize the flexural properties of the novel products.

The so called Taguchi's method is increasingly gaining importance in the forest products industry. On the other hand, response surface models are rarely used in the development of different wood based composites. However, expensive "*trial and error"* manufacturing runs can be avoided by screening out undesirable combinations of factors in the early stages of design and development.

V.6 Closure of Chapter V

Research described in this chapter resulted in a Ph.D. dissertation (Denes L. 2005), two peer-reviewed publications (Denes et al. 2010a; Denes et al. 2005) and one MSc Thesis in Forest Resource Management (B. McGraw 2008). Additionally, one MSc Thesis in Civil Engineering is in preparation with the expected date of defense in August, 2011.

Different segments of the research were presented at eight international conferences where the proceedings contain our paper (Denes et al. 2010b, Denes et al. 2010c, McGraw et al. 2010a, McGraw et al. 2010b, Denes et al. 2009, Denes et al. 2008, Lang et al. 2006, Denes et al. 2004). This research was partially financed by the Research Challenge Grant Program of West Virginia at West Virginia University during the academic year of 2001-2002 and the Hungarian National Science Foundation (OTKA), project number: T-25985. The continuation at WVU has been made possible through the Wood Utilization Research Program Task #8 and #21.

References V

1. Adair, C. 2003. Regional Production and Market Outlook: Structural Panels and Engineered Wood Products. 2003 – 2008. APA – EWS Mk0-E169.
2. Adler, P.J., V.E. Markova and V.J. Granovszkij 1977. Design of Experiments for Determination of Optimal Conditions (in Hungarian).Technical Publisher, Budapest. 252 pp.
3. American Society for Testing and Materials. 1996a. Standard Methods of Testing Small Clear Specimens of Timber ASTM D 143 – 83. ASTM, West Conshohocken, Pa
4. American Society for Testing and Materials. 1996b. Standard Test Methods for Evaluating Properties of Wood-Base Fiber and Particle Panel Materials. ASTM D 1037 – 94. ASTM, West Conshohocken, Pa.

5. Hassler, C. 2002.Veneer Residue Survey. Final Report to the Division of Forestry WVU. Balkan Tier Consulting Inc. Morgantown, WV. pp. 17.
6. Denes, L., E. M. Lang and Zs. Kovacs. 2004. Innovative Wood Composites from Veneer Residues. In Proceedings of the International Symposium on Advanced Timber and Timber-Composite Elements for Building. 27-29 October 2004, Florence, Italy pp. 169-175. ISBN 88-901660-1-0.
7. Denes, L., E.M. Lang and Zs. Kovacs. 2006. Product development from veneer mill residues: an application of the Taguchi's method. Wood and Fiber Science, 38(1):36-48.
8. Denes, L., B. McGraw, E. M. Lang, J. F. Davalos, 2009c. Engineered wood composite I-joists using corrugated Veneer–Polyurethane Foam Composite. In Proceedings of the 51st International Convention of Society of Wood Science and Technology. November 10-12, 2006 Conception, Chile. pp. WS 19:1-7.
9. Denes, L., B. McGraw, J. F. Davalos, E.M. Lang, 2010a. Development of a wooden I-joist using corrugated veneer web panels. Proceedings of the Conference on Processing Technologies and for Forest and Biobased Products Industries. PTF BP 2010, October 7-8. Salzburg University of Applied Sciences Kuchl/Austria, pp. 78-83.
10. Denes, L. Zs. Kovacs, E.M. Lang, J.F. Davalos, 2010b. Recycling the Sliced Veneer Clippings into Value-Added Products. An International Research Effort. Proceedings of the International Convention of Society of Wood Science and Technology and the United Nations Economic Commission for Europe – Timber Committee. October 11-14, 2010, Geneva, Switzerland. Paper WS–17: (1-7).
11. Lang, E.M. and L. Denes. 2002. Exploratory Research and Development of Veneer Strip Lumber (VSL) Using Clipping Residues. Unpublished Research Report to the WVU RCGP. West Virginia University, Division of Forestry. Morgantown, WV. pp.22.
12. Lang E. M., L. Denes and Zs. Kovacs. 2006. Development of strand-type composites using statistical process control methods. In the Proceedings of ICCE-14. International Conference on Composites/Nano Engineering. July 2-8, 2006. Boulder, CO. pp. 314-315 on CD
13. McGraw, B., Denes, L., Lang, E.M., Davalos, J.F., and Chen, A. 2010 Development of a Corrugated Wood Composite Web Panel for I-joist from Discarded Veneer-mill Residues, Proceedings of the 12th ASCE Aerospace Division International Conference on Engineering, Construction and Operations in Challenging Environments, Honolulu, Hawaii, March 14-17, 2010. 2 pp.
14. McGraw, B., Davalos, J.F., Chen A., Denes, L. and Lang, E.M. 2010. Corrugated Wood Composite Web Panel for I-joist using Discarded Veneer-Mill Residues, Proceedings of 16th US National Congress of Theoretical and Applied Mechanics (USNCTAM 2010), June 27 - July 2, 2010, State College, PA. pp. 452-462.
15. Montgomery, D.C. 1997. Introduction to statistical quality control, 3rd edition. John Wiley and Sons, Inc., New York. 677 pp.
16. Montgomery, D.C. 2005. Design and Analysis of Experiments, 6th edition. John Wiley and Sons, Inc., New York. pp 643.

17. Montgomery, D.C. 1999. Experimental design for product and process design and development. The Statistician. 48(2):159-177.
18. Nair, V.N. and panel discussants: Abraham, B. and Mackay, J.; Box, G.E.P.; Kacker, R.N.; Lorenzen, T.J.; Lucas, J.M.; Myers, R.H. and Vining, G.G.; Nelder, J.A.; Phadke, M.S.; Sacks, J. and Welch, W.J.; Shoemaker, A.C. and Tsui, K.L.; Taguchi, S.; Wu, C.F.J. 1992: Taguchi's Parameter Design: A Panel Discussion Technometrics. 34(2):127-161.
19. Smulski, S., editor 1997. Engineered Wood Products: A guide for Specifiers, Designers and Users. PFS Research Foundation, Madison, WI.
20. Winandy, J. E. 2002. Emerging Materials: What will durable materials look like in 2020? (PDF) In: Enhancing the Durability of Lumber and Engineered Wood Products; 11-13 February 2002, Kissimmee, FL. Forest Products Society, Madison, WI. p. 13-18.
21. Taguchi, G. 1987. Introduction to Quality Engineering: Designing Quality into Products and Processes. Asian Productivity Organization, Kraus International Publications, White Plains, N.Y.

List of Figures V

List of Tables V

Nomenclature V

Uppercase letters:

ANOVA	*analysis of variance*
ASTM	*American Society for Testing and Materials*
A, B, C	*factors*
[B]	*regression coefficients matrix*
DOE	*design of experiment*
IB	*internal bound*
MDF	*medium density fiberboard*
MPa	*mega Pascal*
MOE	*modulus of elasticity*
MOR	*modulus of rupture*
$N(0, \sigma^2)$	*normal probability distribution*
PF	*phenol-formaldehyde*
pMDI	*polymeric diphenylmethane-diisocyanate*
R^2	*coefficient of determination*
RPD	*robust parameter design*
SCL	*structural composite lumber*
VSL	*veneer strip lumber*
VSP	*veneer strip panel*
$X_{1,\ldots,7}$	*factor codes*

Lower case letters:

x, z	*transpose column vectors of x' and z'*
x', z'	*row vectors of control and noise factors*
y, $\hat{y}$	*regression*

Greek letters:

α	*probability type-I error;*
β	*regression parameters*
β_0	*overall mean effect*
ε	*random error*
Δ	*matrix of control factors by the noise factor interaction effects*
$\{\gamma\}$	*vector of regression coefficient of the main effects of noise factors*
σ^2	*variance*

Subscripts/superscripts:

i, j	*column and row indexes*
MOR, MOE	*for modulus of rupture and modulus of elasticity*
E, F	*edgewise and flatwise*

CHAPTER VI

LINUS CARL PAULING

(1901 – 1994)

"FACTS ARE THE AIR OF SCIENTISTS. WITHOUT THEM YOU CAN NEVER FLY."

VI. General Summary

This Dissertation compiled some of the author's research works on modeling the physical and mechanical characteristics of solid wood and wood-based composites. Additionally, development of innovative wood composites and their process modeling were also discussed. The study was divided into six chapters. *Chapter I* offered general introduction for the readers, who are less familiar with the uniqueness of wood and wood composites.

Given that wood and wood-based composites are materials of biological origin; many of their characteristics are governed by the unpredictable law of nature. Nonetheless, this natural cellular substance is widely used in its primary form as timber; or after different secondary transformations, it is utilized as furnish for a range of composites. The fact is that besides the volumetric decrease in production, for a variety of reasons, the dominance of the engineered wood products in any segment of the forest products industry increases yearly. Decades ago, the changes in available resources such as: use of small diameter trees, involvement of underutilized and non-traditional species resulted in the development of structural and non-structural wood composites. The backbone of this Dissertation described four connected projects in this area.

The essential parts (*Chapters II* thorough *V),* as stand-alone documents, provided descriptions of research works targeted to explore material properties, to investigate manufacturing processes and products' development possibilities via stochastic or deterministic modeling. The objectives of the analytical and experimental works, conclusions, and the new scientific achievements may be summarized as follows.

VI.1 Brief Rehearsal of the Objectives and Methodologies

Chapter II describes the development of a model that predicts the macro and micromechanical phenomena in OSB and/or LSL strand mats under consolidation in the press. The objective of the first part of this research was to virtually recreate the mat structure. Real mat parameters were assessed by measurements on yellow-poplar (*Liriodendron tulipifera*), manually formed strand mats. Following the data analyses, the probability distribution functions for the selected parameters were determined. Next, using a Monte Carlo simulation technique, from the appropriate distributions, the virtual mat structure was recreated.

The objective of the second phase was to develop a model for predicting the static stress – strain behavior of the mat under cold pressing. In the early stage of the consolidation we modeled the strands as simply supported beams under linearly distributed load. As the consolidation continues, and all the voids between the strands in an imaginary column are eliminated, the model computes the stress strain relations according to the developed non-linear strain function.

Chapter III deals with the exploration of orthtotropic mechanical properties of five underutilized wood species. The scientific literature is rather broad regarding properties of wood and wood based-composites. However, data on the anatomical direction-dependent mechanical properties is hardly available, especially for hardwoods. Our evaluations included shear and compression strength, as well as compression and dynamic moduli of elasticity analyses. The orthotropic nature of these properties was assessed at 15º increments of grain and ring angles. During this fundamental research new models and model combinations were developed and experimentally validated.

In Chapter IV simulation models for predicting the expected mechanical properties of laminated veneer lumber (LVL) and parallel strand lumber (PSL) are discussed. Inputs for these models, such as positions and properties of the constituents, were generated from experimentally and analytically determined probability functions. After the stochastic determinations of sectional properties and their summation, the models were verified and validated by comparing the predicted and experimental values of compression and bending muduli of elasticity. Both models provide possibilities to evaluate the effects of wood species, densification and technological parameters on the elastic constants of the products.

Finally, Chapter V delineates the development and manufacturing possibilities of new types of wood based composites. The described experimental and analytical works included the experiences gained during earlier research works that are partially given by this Dissertation. Furthermore, by using the methods of statistical process control and response surface methodology the optimization of products' performance and processing parameters can be achieved. Thus the raw material basis of wood based composite manufacture could be expanded that may result in additional innovation of value-added products.

VI.2 Summary of the New Scientific Results: Theses of the Dissertation[2]

VI.2.1 Modeling the consolidation of OSB mats

1. Using standard statistical methods we proved that the developed simulation routine adequately reconstructs the virtual strand mats. Critical parameters of the mats can be easily determined by measurements of actual mats. [II.10, II.12]

2. It has been confirmed that the acquired probability density and mass functions depend on the wood species, the size of the furnish and the methods of mat formation. [I.10, I.12]

3. As demonstrated by other researchers, the model based on the generation of stochastic variables is expandable, upgradeable and easy to modify [II.14, II.15, II.27, II.28].

4. We confirmed that the perpendicular to the grain compression modulus (E_c) and the non-linear strain function $\Phi(\varepsilon)$ determine the slope of the stress – strain function during the second phase of the consolidation; while the developed beam model follows the stress strain data reasonably well in the early stage of the consolidation. [II.10, II.12]

5. We experimentally verified of the applicability of the non-linear strain function, proposed by Gibson and Ashby (1988) and Wolcott et al. (1998, 1990) to the inhomogeneous, anisotropic and cellular wood strands. [II.10, II.12]

6. Our model, the first of a kind, is capable to predict the percentage of inadequate bonding areas and the horizontal density distributions within a panel. [II.10, II.11, II.13] Later models, worked out by others, provide results almost identical to our predictions. [II.27, II.28]

7. The developed stochastic/deterministic model provides reliable data over 0.01 MPa compression stress. The prediction of similar models, published in the same time frame, grants trustworthy data over 1.0 MPa [II.4, II,5, II.6].

8. This consolidation model helps the industry in elimination of the species and shape-dependent discrepancies in mat formation. The model may assist to reduce energy consumption and aids the manufacturing low density panels.

[2] *Publications discussing the results of the Dissertation are given by the corresponding chapter numbers and reference list numbers in superscripts. Other relevant works are cited similarly but aligned with the text.*

VI.2.2 Exploration of the orthotropic mechanical properties of hardwoods

9. It has been proven that the orthotropy of shear strength is best defined by the combination of the tensor theory and the Hankinson's formula for hardwoods. [III.37]

10. We experimentally verified that the newly developed method for shear strength assessment is equivalent to the standard ASTM procedure regardless of the differences in the size of sheared surfaces. [III.34, III.36]

11. It was confirmed that the tensor analysis and the three dimensional Hankinson's equation describe the orthotropy of compression strength equally well. [III.37]

12. The established critical shear stress contour provides possibilities to predict shear failure in compressed wood structures. [III.35, III.37]

13. After the evaluation of test results and analytical works we concluded that the direction-dependent dynamic modulus of elasticity (E_D) of structural veneers can be predicted by the combination of tensor approach and the original Hankinson's formula. [III.38]

14. Analyses revealed that the original position of sliced veneers in the flitch notably affects the dynamic MOE of the individual veneer leafs. The different effects on diffuse and ring porous wood were demonstrated as well. III.16, III.17]

During the course of this research extensive data base was developed regarding the orthotropic nature of underutilized hardwoods. Results of these tests and analyses may be used to introduce new species into the wood composite industry. In doing so, the sustainable forest management practices would improve.

VI.2.3 Modeling the properties of structural composites

15. Via experimental validations we demonstrated that on the basis of simulated cross sections and furnish properties the bending and compression MOE of LVL and PSL can be predicted with reasonable accuracy in the principal anatomical directions. [IV.7, IV.9, IV.10]

16. The simulated cross sections and their properties agreed well with the real ones. [IV.7, IV.10]

17. It was confirmed that in the inclined constituting elements, which deviate from the global coordinate system, the rolling shear induced deformations are significant. Such deformations impair the measurable elastic constants in bending and compression. [IV.7, IV.10]

18. It was demonstrated analytically that the better orientation of the PSL strands results in improved mechanical properties of the product. [IV.7, IV.9, IV.10]

The developed simulation models are seemingly two-dimensional. However, averaging several simulation runs an entire beam can be reasonably modeled. Our model for PSL has been extended to a three-dimensional one by other researchers [IV.4, IV.5].

VI.2.4 Innovation of new wood composites; optimization of the parameters by statistical methods

19. We demonstrated that the previously discarded clipping residues can be converted into value-added structural composite materials. [V.6, V.7, V.8, V.9, V.10]

20. Our research works resulted in the development and technology specifications of four new wood based products. [V.6, V.7, V.8, V.9, V.10, V.11, V.12, V.13, V.14]

21. Result of standard testing procedures confirmed that the mechanical and physical properties of the new products are comparable or are exceeding the properties of similar products on the market. [24,35,36,50,51,52,53]

22. We experimentally and analytically displayed that the optimal synthetic resin content is about 8%. [V.6, V.7, V.12]

23. It was confirmed that using statistical methods the optimization of products' properties can be done during the early stages of development. [V.6, V.7, V.12]

Commercial introduction of the new composites may aide the better utilization of natural resources; and may have positive effects on the CO_2 retention and forest harvesting practices.

VI.3 Final Closure

A large number of synthetic and natural origin composite materials have been developed since the first structural, wood-based composites, the commercial plywood, appeared in 1905 (McKay 1997). The definite advantages of composite materials are the abilities of the manufacturers to control the physical and mechanical attributes of their products. Thus specific demand can meet with specific supply.

Tailoring of wood-based composites to different specifications is limited by the uncontrollable mechanical/physical properties of the raw material. The lack of comprehensive knowledge about material properties and their interaction with processing parameters further hinder our ability to design and effectively manufacture such products. It does appear that still there is a great potential to further exploit the strength, stiffness, workability, warmth and beauty of *WOOD.*

The author sincerely hopes that the works presented here contributed, to a certain extent, to the better understanding and thoughtful utilization of wood and wood-based products.

Appendices

I - V

Appendix I

Mechanical and physical properties of selected hardwoods:

Table A.I.1. *Average literature values of elastic constants for selected hardwoods.*

Species	***SG*** *12 % MC*	***Moduli of Elasticity and Moduli of Rigidity (GPa)***					
		E_L	E_R	E_T	G_{LR}	G_{LT}	G_{RT}
Aspen *(Populus tremuloides)*	*0.38*	*8.90*	*0.73*	*0.31*	*0.57*	*0.41*	*0.13*
Cherry *(Prunus serotina*)	*0.50*	*10.30*	*0.824*	*0.52*	*0.74*	*0.69*	*0.07*
Red oak *(Quercus rubra)*	*0.63*	*13.82*	*1.28*	*0.66*	*0.99*	*0.74*	*0.23*
Turkey oak *(Quercus cerris)*	*0.72*	*14.00*	*1.10*	*0.83*	*1.32*	*0.91*	*0.44*
Yellow-poplar *(Liriodendron tulipifera*	*0.42*	*11.93*	*0.86*	*0.39*	*0.67*	*0.48*	*0.15*

Table A.I.2. *Average literature values of Poisson's ratios for selected hardwoods.*

Species	***Poisson's Ratios***					
	ν_{LT}	ν_{TL}	ν_{LR}	ν_{RL}	ν_{TR}	ν_{RT}
Aspen (Populus tremuloides)	*0.537*	*0.017*	*0.487*	*0.089*	*0.628*	*1.594*[1]
Cherry[2] *(Prunus serotina*)	*0.420*	*0.033*	*0.370*	*0.041*	*0.350*	*0.470*
Red oak (Quercus rubra)	*0.410*	*0.034*	*0.274*	*0.025*	*0.282*	*0.626*
Turkey oak[3] *(Quercus cerris)*	*0.410*	*0.090*	*0.430*	*0.070*	*0.340*	*0.790*
Yellow-poplar (Liriodendron tulipifera	*0.420*	*0.018*	*0.330*	*0.030*	*0.330*	*0.710*

1 – computed on the basis of symmetry;
2 – average hardwood values;
3 – average oak values.

Table A.I.3. *Average literature values of strength properties for selected hardwoods.*

Species	***Strength Poroperties*** ---------- *(MPa)* ----------				
	Bending // to the grain	*Tension ⊥to the grain*	*Compression // to the grain*	*Compression⊥ to the grain*	*Shear // to the grain*
Aspen *(Populus tremuloides)*	*58.0*	*1.80*	*29.3*	*2.60*	*5.90*
Cherry *(Prunus serotina*)	*85.0*	*3.90*	*49.0*	*4.80*	*11.7*
Red oak *(Quercus rubra)*	*99.0*	*5.50*	*46.6*	*7.00*	*12.3*
Turkey oak *(Quercus cerris)*	*94.0*	*---*	*44.0*	*---*	*9.00*
Yellow-poplar *(Liriodendron tulipifera*	*70.0*	*3.70*	*38.2*	*3.40*	*8.20*

Table A.I.4*. Average literature values of physical properties for selected hardwoods.*

Species	***Specific Gravity SG_b (Green)***	***Shrinkage from green to oven-dry MC***		
		Radial (%)	*Tangential (%)*	*Volumetric (%)*
Aspen *(Populus tremuloides)*	*0.35*	*3.5*	*6.7*	*11.5*
Cherry *(Prunus serotina*)	*0.47*	*3.7*	*7.1*	*11.5*
Red oak *(Quercus rubra)*	*0.56*	*4.0*	*8.6*	*13.7*
Turkey oak *(Quercus cerris)*	*0.60*	*4.4*	*9.8*	*16.1*
Yellow-poplar *(Liriodendron tulipifera*	*0.40*	*4.5*	*8.2*	*12.7*

Appendix II

Algorithms used to generate random deviates from specified probability distributions:

Normal distribution N(μ, σ^2)

Given X~N(0,1), we can obtain X'~ N(μ, σ^2) by setting X'= $\mu + \sigma$X

The polar method:

1. Generate U_1 and U_2 as IID U(0,1), let $V_i=2U_i -1$ for i=1,2 and let $W=V_1^2+V_2^2$.
2. If W>1 go back to step 1.
3. Otherwise, let $Y=\sqrt{(-2\ln W)/W}$ $X_1=V_1Y$ and $X_2=V_2Y$.
4. Then X_1 and X_2 are IID N(0,1) random variates.

Lognormal Distribution LN(μ, σ^2)

If Y~ N(μ, σ^2) , then e^Y ~ LN(μ, σ^2)

Procedure:

1. Generate Y~ N(μ, σ^2).
2. Return $X = e^Y$

Note: μ and σ are **not** the mean and variance of the LN distribution
To generate a LN distribution with a given μ_1 and σ_1^2 , the following relationships are used:

$$\mu = ln\left(\mu_1^2/\sqrt{\mu_1^2+\sigma_1^2}\right)$$

$$\sigma^2 = ln\left[(\sigma_1^2+\mu_1^2)/\mu_1^2\right.$$

Discrete deviates, Poisson (λ) Distribution

1. Let $a = e^{-\lambda}$, b = 1, and i = 0
2. Generate U_{i+1} ~ U(0,1) and replace b by bU_{i+1}. If b < a, return X = i. Otherwise, go to step 3.
3. Replace i by i+1 and go back to step 2.
4. Xs are Posisson(λ)random deviates.

Correlation structure of the spatial mat characteristics:

No statistically significant correlations were observed.

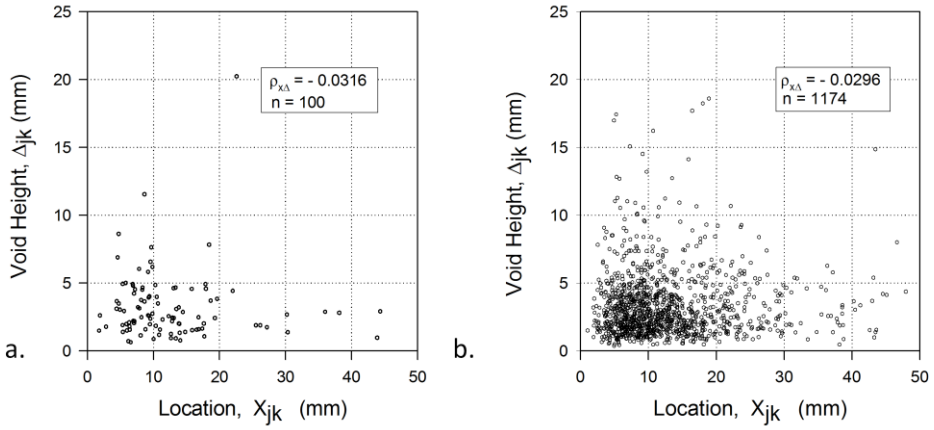

Figure A.II.1. *The correlation structure of void height versus location parameters. The correlation coefficients and sample sizes are listed.* ***a****. – observed;* ***b.*** *– simulated data.*

Solid strand columns in compression to evaluate ε_y and E_c:

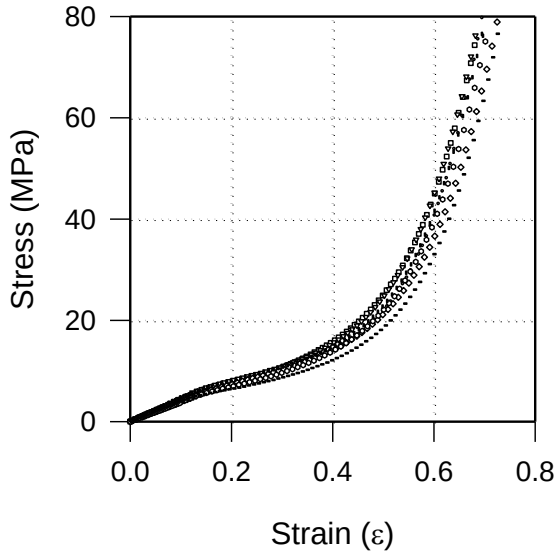

Figure A.II.2. *Stress-strain diagrams of nine experimental solid strand columns in compression.*

Environmental effects:

The effects of temperature and moisture content on the consolidation and stress relaxation were preliminary studied on low target density mats (400 kg/m^3). The same bulks were compressed to 19 mm target thickness and hold the press for approximately 170 seconds to observe the stress relaxation. Temperature and moisture content was set by a movable environmental chamber that could be fixed around the actuator rods of the MTS testing machine. *Figure A.II.3* demonstrates the results graphically.

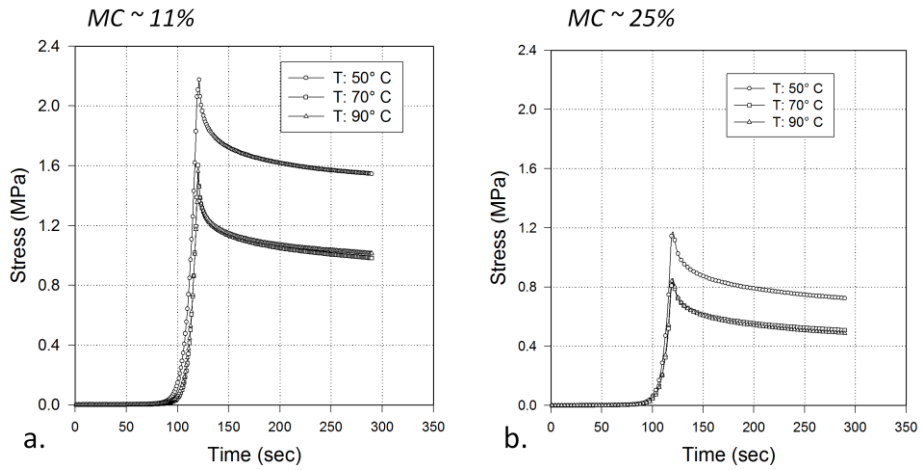

Figure A.II.3. *The effect of temperature on the stress development and relaxation of wood strand mats.* ***a.*** *– 11% at moisture content;* ***b.*** *– 25% at moisture content.*

Follow up improvements of the mat characterization model

Zombori (2001) in his Dissertation enhanced the virtual mat reconstruction introducing the 3-dimensional measures of strands and their densities and orientations. The objective of his research was to model the heat and mass transfer phenomena during hot pressing. Thus, the mat structure, its horizontal and vertical density distributions, as well as void volumes and contact areas were of primary interests. Zombori assumed that all the strands are straight plane elements that deposit parallel to the base of the mat and the voids are created by the lack of strands in a particular layer or layers. *Figure A.II.4* shows a three-layer simulated horizontal density distribution of an OSB mat. This approach resulted in similar features as the finite column model. The calculated non-contacting areas for our model were 6%, while Zombori come up with 7% for the practically the same 600 kg/m^3 target density. Furthermore, the horizontal density distributions are very comparable (*Figures II.13 and A.II.4*).

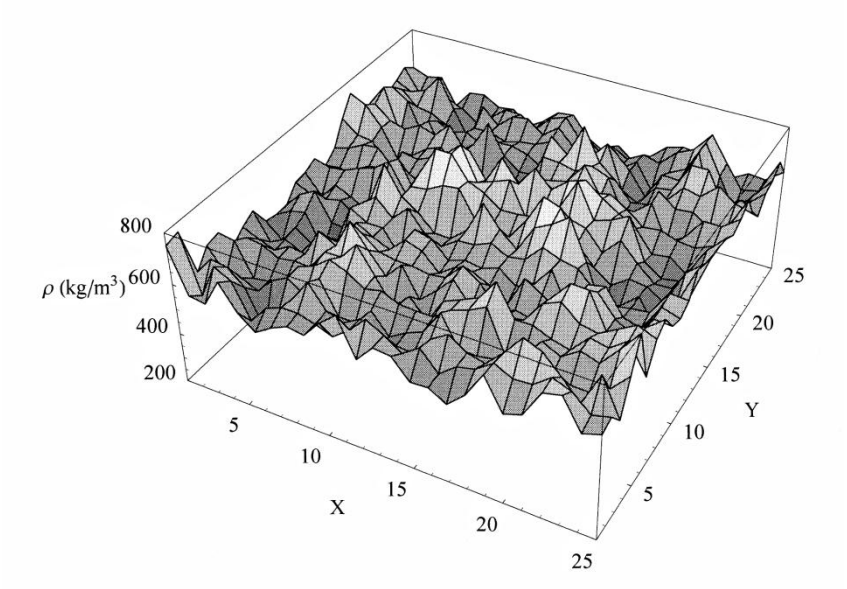

Figure A.II.4. *Predicted horizontal density distribution of the mat compressed to 610 kg/m^3 target density. Average simulated density: 611.7 kg/m^3.The distance between grid points is 18 mm, representing a 450 x 450 mm mat area (Zombori 2001).*

Appendix III

Table A.III.1. *Summary and basic statistics of the experimentally determined shear strength values for North American species.*

ASPEN

Grain angle (φ°)	Rina Orietation (θ°) 0			15			30			45			60			75			90		
	Shear strength (MPa)																				
	N [a]	$\bar{\tau}$ [b]	s [c]	N	$\bar{\tau}$	s	N	$\bar{\tau}$	s	N	$\bar{\tau}$	s	N	$\bar{\tau}$	s	N	$\bar{\tau}$	s	N	$\bar{\tau}$	s
0	15	7.87	0.23	15	7.30	0.50	15	6.77	0.46	15	5.42	0.79	15	6.16	0.64	15	6.17	0.27	15	6.30	0.80
15	9	8.39	0.38	8	8.16	1.05	9	7.98	0.93	8	7.30	1.03	7	6.67	0.84	8	5.78	0.40	9	5.99	0.60
30	10	7.16	0.32	8	6.37	0.90	7	7.21	0.80	8	5.74	0.47	7	5.62	1.03	8	4.99	1.45	7	5.62	0.80
45	6	4.98	0.38	6	4.29	0.34	6	4.75	0.30	6	4.27	0.24	6	4.44	0.24	6	5.02	0.57	6	4.42	0.22
60	6	3.18	0.31	6	3.45	0.45	6	3.43	0.22	5	3.25	0.38	5	2.54	0.50	4	2.61	0.27	5	3.13	0.44
75	6	1.92	0.12	6	2.52	0.36	6	2.81	0.36	6	1.93	0.14	6	1.90	0.09	6	2.73	0.12	6	2.45	0.24
90	10	2.24	0.07	10	1.43	0.13	11	2.24	0.09	11	2.28	0.09	11	3.11	0.09	10	2.98	0.09	10	2.54	0.12

RED OAK

Grain angle (φ°)	Rina Orientation (θ°) 0			15			30			45			60			75			90		
	Shear strength (MPa)																				
	N	$\bar{\tau}$	s	N	$\bar{\tau}$	s	N	$\bar{\tau}$	s	N	$\bar{\tau}$	s	N	$\bar{\tau}$	s	N	$\bar{\tau}$	s	N	$\bar{\tau}$	s
0	15	11.9	1.04	15	12.0	0.95	15	11.6	0.48	15	11.9	1.00	15	12.7	0.64	15	11.3	0.65	15	10.6	0.45
15	8	11.9	0.90	9	11.2	0.67	9	11.5	0.99	9	12.8	0.33	9	13.0	0.89	9	12.1	0.50	9	12.3	0.36
30	8	11.8	0.74	9	11.6	1.76	8	11.4	1.16	8	11.3	0.91	8	11.3	1.12	8	11.1	1.08	8	11.3	0.50
45	5	9.99	0.34	6	9.34	0.75	5	6.64	0.75	6	9.94	0.86	5	8.59	0.37	5	8.38	0.50	5	8.82	0.23
60	7	7.01	0.15	7	8.07	0.39	7	8.14	0.28	6	7.69	0.46	7	7.20	0.21	5	7.80	0.21	7	6.81	0.33
75	7	6.06	0.30	6	5.64	0.26	6	5.65	0.55	7	6.41	0.43	7	6.12	0.13	7	6.84	0.45	6	6.57	0.22
90	11	4.44	1.30	11	5.55	0.86	11	5.72	0.73	10	6.88	0.25	11	7.06	0.51	10	4.62	0.87	10	5.37	0.25

YELLOW-POPLAR

Grain angle (φ°)	Rina Orientation (θ°) 0			15			30			45			60			75			90		
	Shear strength (MPa)																				
	N	$\bar{\tau}$	s	N	$\bar{\tau}$	s	N	$\bar{\tau}$	s	N	$\bar{\tau}$	s	N	$\bar{\tau}$	s	N	$\bar{\tau}$	s	N	$\bar{\tau}$	s
0	15	7.91	0.49	15	7.13	0.60	15	7.13	0.43	15	7.32	0.49	15	7.23	0.75	15	9.06	0.88	15	6.18	0.30
15	9	10.5	0.54	9	8.37	1.26	9	7.31	0.80	9	6.65	0.56	9	6.74	0.35	10	6.77	0.35	10	6.42	0.30
30	6	6.94	0.37	8	6.70	0.74	9	6.57	1.37	7	6.10	1.64	9	5.91	0.85	8	5.61	0.33	8	5.95	1.49
45	5	4.85	0.19	4	4.98	0.33	6	4.85	0.39	6	5.74	0.82	5	5.05	0.55	6	4.35	0.27	5	4.73	0.92
60	6	2.81	0.39	5	3.85	0.42	6	2.81	0.10	6	3.53	0.99	6	3.60	0.63	6	3.13	0.31	6	3.79	0.24
75	6	2.75	0.43	6	2.96	0.42	6	2.28	0.16	6	2.28	0.15	6	1.94	0.06	6	1.94	0.08	6	2.87	0.26
90	3	2.43	0.68	4	2.60	0.52	9	2.86	0.78	11	3.52	0.54	11	3.42	0.20	11	3.35	0.57	11	3.17	0.43

a – sample size.
b – average shear strength (MPa).
c – standard deviation.

Table A.III.1. *Continued.*

TRUE POPLAR

Grain angle	Ring Orietation (θ°) 0			15			30			45			60			75			90	
	Shear strength *(MPa)*																			
(φ°)	N[a]	$\bar{\tau}$	s[c]	N	$\bar{\tau}$	s	N	$\bar{\tau}$	s	N	$\bar{\tau}$	s	N	$\bar{\tau}$	s	N	$\bar{\tau}$	s	N	$\bar{\tau}$	s
0	9	7.0	5.4	6	8.1	0.4	6	7.4	0.4	6	6.0	0.3	6	6.1	0.3	6	6.2	0.3	9	5.8	0.5
15	6	7.0	6.5	6	6.5	0.3	6	7.1	0.4	6	6.0	0.3	6	6.5	0.3	6	6.5	0.3	6	5.9	0.3
30	6	6.2	12.	6	6.5	0.4	6	5.8	0.3	6	6.2	0.3	6	5.2	0.3	6	5.9	0.3	6	5.6	0.3
45	6	5.6	3.5	6	5.7	0.3	6	4.7	0.2	6	4.3	0.2	6	4.8	0.2	6	4.7	0.2	6	4.2	0.2
60	6	3.5	5.4	6	3.8	0.2	6	3.5	0.2	6	3.6	0.2	6	3.7	0.2	6	3.9	0.2	6	3.4	0.2
75	6	2.5	4.5	6	2.9	0.1	6	2.9	0.1	6	3.2	0.2	6	2.7	0.1	6	3.5	0.2	6	2.8	0.1
90	10	2.1	4.6	6	2.5	0.1	6	2.5	0.1	10	2.8	0.2	5	2.7	0.1	6	2.8	0.1	10	2.7	0.2

TURKEY OAK

Grain angle	Ring Orientation (θ°) 0			15			30			45			60			75			90	
	Shear strength *(MPa)*																			
(φ°)	N	$\bar{\tau}$	s	N	$\bar{\tau}$	s	N	$\bar{\tau}$	s	N	$\bar{\tau}$	s	N	$\bar{\tau}$	s	N	$\bar{\tau}$	s	N	$\bar{\tau}$	s
0	10	15.	0.5	6	13.	0.8	6	12.	0.7	6	13.	0.8	6	12.	0.7	6	11.	0.6	10	12.	1.2
15	6	14.	1.2	6	13.	0.8	5	13.	0.8	6	14.	0.7	6	14.	0.8	6	12.	0.6	6	12.	0.7
30	5	10.	0.7	5	11.	0.5	6	12.	0.6	6	12.	0.7	6	13.	0.7	6	11.	0.7	6	9.7	0.5
45	6	9.7	0.4	6	9.7	0.5	6	11.	0.5	6	11.	0.6	6	11.	0.6	6	10.	0.6	6	9.5	0.5
60	6	9.4	0.5	6	9.2	0.5	6	8.7	0.5	6	8.9	0.5	6	8.9	0.5	6	8.9	0.5	6	8.4	0.5
75	6	8.5	0.5	6	7.8	0.4	6	8.2	0.5	6	9.2	0.5	6	8.6	0.5	6	6.5	0.3	6	8.7	0.5
90	10	7.0	0.4	6	7.5	0.4	10	7.9	0.4	6	8.3	0.8	6	9.5	0.5	6	10.	0.6	10	9.3	0.9

a – sample size.
b – average shear strength (MPa).
c – standard deviation.

The r^2 analysis:

Sometimes, the deficiency in complete randomization, does not allow the use conservative statistical fitting procedures. In these certain cases r^2 analysis may be used to evaluate and rank the performance of the fitted models. The coefficient of determination (r^2) is a measure of how well the model describes the data. Larger values, close to 1, indicate that the model describes the relationship between independent and dependent variables well. The value of r^2, by definition, equals one minus the proportion of variability unexplained by the model (Dowdy and Wearden, 1991). For the orthotropy of shear strength, numerically it is given by the following equation:

$$r^2 = 1 - \frac{\sigma^2{}_U}{\sigma^2{}_T} = 1 - \frac{\dfrac{\sum\left(\tau_{\varphi\theta i} - \hat{\tau}_{\varphi\theta}\right)^2}{N-1}}{\dfrac{\sum\left(\tau_{\varphi\theta i} - \bar{\tau}\right)^2}{N-1}} = 1 - \frac{\sum\left(\tau_{\varphi\theta i} - \hat{\tau}_{\varphi\theta}\right)^2}{\sum\left(\tau_{\varphi\theta i} - \bar{\tau}\right)^2} \qquad (A.III.1)$$

where:

σ^2_T – total variance (*or total sum of squares, as provided by the ANOVA*);
σ^2_U – variance unexplained by the model;
N – the *total* number of shear strength measurements on the given species;
$\tau_{\varphi\theta i}$ – the i^{th} measurement at grain angle φ and ring angle θ;
$\bar{\tau}$ – average of the N measurement points (grand average);
$\hat{\tau}_{\varphi\theta}$ – predicted shear strength at grain angle φ and ring angle θ.

Derivation of the tensor models for MOE and Strength of wood:

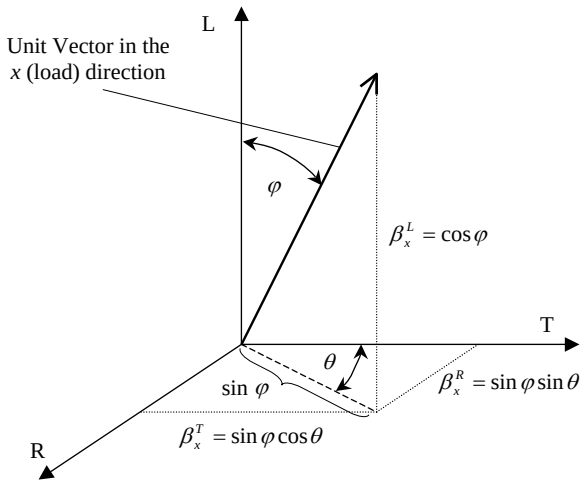

Figure A.III.1. *The unit vector in the load direction(x) and the calculation of its coordinates:* $\beta_x^L \;\; \beta_x^R \;\; \beta_x^T$.

Using the elastic parameters of wood, the compliance matrix of an orthotropic material can be written in the following form:

$$\begin{bmatrix} \frac{1}{E_L} & -\frac{\upsilon_{RL}}{E_R} & -\frac{\upsilon_{TL}}{E_T} & 0 & 0 & 0 \\ -\frac{\upsilon_{LR}}{E_T} & \frac{1}{E_R} & -\frac{\upsilon_{TR}}{E_T} & 0 & 0 & 0 \\ -\frac{\upsilon_{LT}}{E_L} & -\frac{\upsilon_{RT}}{E_R} & \frac{1}{E_T} & 0 & 0 & 0 \\ 0 & 0 & 0 & \frac{1}{G_{RT}} & 0 & 0 \\ 0 & 0 & 0 & 0 & \frac{1}{G_{TL}} & 0 \\ 0 & 0 & 0 & 0 & 0 & \frac{1}{G_{LR}} \end{bmatrix} \qquad (A.III.2)$$

where: E_i – modulus of elasticity of wood in the *i* anatomical direction;

G_{ij} – shear modulus in the main anatomical planes, where *i* is the direction normal to the sheared plane and *j* is the direction of the applied load;

υ_{ij} – Poisson ratio (*i* is the direction of passive strain and *j* is the direction of applied load.

Using the relationships between the elastic parameters of wood, it can be shown that:

$$-\frac{\upsilon_{ij}}{E_j} = \frac{1}{2}\left(\frac{4}{E_{ij}^{45^\circ}} - \frac{1}{E_i} - \frac{1}{E_j} - \frac{1}{G_{ij}}\right) \qquad (A.III.3)$$

where: $E_{ij}^{45^\circ}$ – The modulus of elasticity of wood in the *ij* plane, at a 45° direction between *i* and *j*.

The above relationship provides a way to determine the elements of the compliance matrix without measuring the Poisson's ratios.

$$\begin{bmatrix} \frac{1}{E_L} & \frac{1}{2}\left(\frac{1}{E^{0°}_{45°}}-\frac{1}{E_L}-\frac{1}{E_R}-\frac{1}{G_{RL}}\right) & \frac{1}{2}\left(\frac{1}{E^{90°}_{45°}}-\frac{1}{E_L}-\frac{1}{E_T}-\frac{1}{G_{TL}}\right) & 0 & 0 & 0 \\ \frac{1}{2}\left(\frac{1}{E^{0°}_{45°}}-\frac{1}{E_L}-\frac{1}{E_R}-\frac{1}{G_{RL}}\right) & \frac{1}{E_R} & \frac{1}{2}\left(\frac{1}{E^{45°}_{90°}}-\frac{1}{E_R}-\frac{1}{E_T}-\frac{1}{G_{RT}}\right) & 0 & 0 & 0 \\ \frac{1}{2}\left(\frac{1}{E^{90°}_{45°}}-\frac{1}{E_L}-\frac{1}{E_T}-\frac{1}{G_{TL}}\right) & \frac{1}{2}\left(\frac{1}{E^{45°}_{90°}}-\frac{1}{E_R}-\frac{1}{E_T}-\frac{1}{G_{RT}}\right) & \frac{1}{E_T} & 0 & 0 & 0 \\ 0 & 0 & 0 & \frac{1}{G_{RT}} & 0 & 0 \\ 0 & 0 & 0 & 0 & \frac{1}{G_{TL}} & 0 \\ 0 & 0 & 0 & 0 & 0 & \frac{1}{G_{RL}} \end{bmatrix} \qquad \textit{(A.III.4)}$$

Matrix *A.III.4* is a simplified two-dimensional representation of a four-dimensional tensor. According to the transformation rules of a four-dimensional tensor, when the coordinate system is rotated around its origin, an element of the new tensor can be calculated using the above formula:

$$t_{i'j'k'l'} = \Sigma t_{ijkl}\beta^{i}_{i'}\beta^{j}_{j'}\beta^{k}_{k'}\beta^{l}_{l'} \qquad \textit{(A.III.5)}$$

where: $t_{i'j'k'l'}$ – an element of the new tensor ($i', j', k', l' = x, y, z$)

t_{ijkl} – an element of the original tensor ($i, j, k, l = L, R, T$)

$\beta^{i}_{i'}$ – the length of the orthogonal projection of a unit vector in the direction of the i'^{th} coordinate axis in the new coordinate system, on the i^{th} axis in the old coordinate system (*Figure A.III.1* shows three examples, where $i' = x$ and $i = L, R, T$.)

Let the new coordinate system be chosen so that its x axis is aligned with the compression load, using the definition of ϕ and θ, given on *Figure III.1.* In this case, transforming the first element of the tensor ($t_{LLLL}=1/E_L$), will provide the reciprocal of the MOE in the x direction, i.e. the direction designated by ϕ and θ ($t_{xxxx} = 1/E_x = 1/E^{\theta}_{\varphi}$). The transformation requires the determination of β^{L}_{x}, β^{R}_{x}, and β^{T}_{x} only. *Figure A.III.1* shows the calculation of these coordinates. Applying the transformation rule (*Equation A.III.5*) to the first element of the matrix provides the following formula for the calculation of the MOE in a chosen direction:

$$\begin{aligned}\frac{1}{\hat{E}_{\varphi}^{\theta}} &= \frac{1}{E_L}\cos^4\varphi + \frac{1}{E_R}\sin^4\varphi\sin^4\theta + \frac{1}{E_T}\sin^4\varphi\cos^4\theta \\ &+ \left(\frac{4}{E_{90°}^{45°}} - \frac{1}{E_R} - \frac{1}{E_T}\right)\sin^4\varphi\sin^2\theta\cos^2\theta \\ &+ \left(\frac{4}{E_{45°}^{0°}} - \frac{1}{E_L} - \frac{1}{E_T}\right)\cos^2\varphi\sin^2\varphi\cos^2\theta \\ &+ \left(\frac{4}{E_{45°}^{90°}} - \frac{1}{E_L} - \frac{1}{E_R}\right)\cos^2\varphi\sin^2\varphi\sin^2\theta\end{aligned} \qquad \textit{(A.III.6)}$$

The derivation of the tensorial formula for compression strength is based on a similar transformation of the four-dimensional strength tensor. Ashkenazi (1978) defined the elements of the fourth order strength tensor according to the matrix below:

$$\begin{bmatrix} \frac{1}{\sigma_L} & \frac{1}{2}\left(\frac{1}{\sigma_{45°}^{0°}} - \frac{1}{\sigma_L} - \frac{1}{\sigma_R} - \frac{1}{\tau_{RL}}\right) & \frac{1}{2}\left(\frac{1}{\sigma_{45°}^{90°}} - \frac{1}{\sigma_L} - \frac{1}{\sigma_T} - \frac{1}{\tau_{TL}}\right) & 0 & 0 & 0 \\ \frac{1}{2}\left(\frac{1}{\sigma_{45°}^{0°}} - \frac{1}{\sigma_L} - \frac{1}{\sigma_R} - \frac{1}{\tau_{RL}}\right) & \frac{1}{\sigma_R} & \frac{1}{2}\left(\frac{1}{\sigma_{90°}^{45°}} - \frac{1}{\sigma_R} - \frac{1}{\sigma_T} - \frac{1}{\tau_{RT}}\right) & 0 & 0 & 0 \\ \frac{1}{2}\left(\frac{1}{\sigma_{45°}^{90°}} - \frac{1}{\sigma_L} - \frac{1}{\sigma_T} - \frac{1}{\tau_{TL}}\right) & \frac{1}{2}\left(\frac{1}{\sigma_{90°}^{45°}} - \frac{1}{\sigma_R} - \frac{1}{\sigma_T} - \frac{1}{\tau_{RT}}\right) & \frac{1}{\sigma_T} & 0 & 0 & 0 \\ 0 & 0 & 0 & \frac{1}{\tau_{RT}} & 0 & 0 \\ 0 & 0 & 0 & 0 & \frac{1}{\tau_{TL}} & 0 \\ 0 & 0 & 0 & 0 & 0 & \frac{1}{\tau_{RL}} \end{bmatrix} \qquad \textit{(A.III.10)}$$

Equation III.11 in the text was obtained by transforming the first element of the above matrix - the same way as that of the compliance matrix.

Table A.III.2. *Summary statistics of the experimentally determined compression strength values for the North American species.*

ASPEN

Grain angle (φ°)	Ring Orientation (θ°) 0			15			30			45			60			75			90		
	Compression strength																				
	N [a]	$\bar{\sigma}$ [b]	s [c]	N	$\bar{\sigma}$	s	N	$\bar{\sigma}$	s	N	$\bar{\sigma}$	s	N	$\bar{\sigma}$	s	N	$\bar{\sigma}$	s	N	$\bar{\sigma}$	s
0	--	--	--	--	--	--	--	--	--	10	36.23	1.14	--	--	--	--	--	--	--	--	--
15	--	--	--	--	--	--	--	--	--	10	28.55	2.64	--	--	--	--	--	--	--	--	--
30	6	10.54	1.99	4	11.33	0.33	4	11.05	0.44	6	12.27	1.21	4	13.25	1.17	4	10.54	4.94	6	12.55	0.71
45	6	6.52	0.52	4	8.15	1.12	4	6.09	0.60	6	5.13	0.39	4	6.61	0.78	4	6.16	0.19	6	8.35	0.89
60	6	3.63	0.19	4	4.24	0.19	4	4.05	0.54	6	3.88	0.37	4	3.77	0.02	4	5.81	0.08	6	5.08	1.24
75	6	3.18	0.30	4	2.88	0.12	4	3.01	0.13	6	2.62	0.10	4	3.31	0.60	4	4.97	0.14	6	3.12	0.10
90	6	3.07	0.13	4	3.07	0.18	4	3.38	0.13	6	3.44	0.09	4	3.70	0.24	4	4.14	0.10	5	4.28	0.13

RED OAK

Grain angle (φ°)	Ring Orientation (θ°) 0			15			30			45			60			75			90		
	Compression strength																				
	N	$\bar{\sigma}$	s	N	$\bar{\sigma}$	s	N	$\bar{\sigma}$	s	N	$\bar{\sigma}$	s	N	$\bar{\sigma}$	s	N	$\bar{\sigma}$	s	N	$\bar{\sigma}$	s
0	--	--	--	--	--	--	--	--	--	9	49.72	2.75	--	--	--	--	--	--	--	--	--
15	--	--	--	--	--	--	--	--	--	10	41.76	2.67	--	--	--	--	--	--	--	--	--
30	6	28.31	1.58	4	33.23	1.95	4	26.81	1.74	6	18.17	5.08	4	27.74	2.00	4	25.72	1.62	6	24.25	1.11
45	6	22.13	0.34	4	23.24	1.94	4	17.18	0.69	6	13.14	0.14	4	16.96	2.77	4	14.42	0.31	6	17.01	0.58
60	6	13.91	0.54	4	16.06	0.75	4	12.99	0.99	6	13.62	1.70	4	10.85	0.64	4	10.23	0.05	6	13.07	0.60
75	6	11.25	0.21	4	13.30	0.41	4	9.81	0.30	6	11.03	0.20	4	9.19	0.52	4	8.22	0.13	6	11.29	0.35
90	6	10.17	0.21	3	11.63	0.42	4	9.35	0.24	6	9.77	0.49	4	9.36	0.17	4	7.65	0.29	6	11.32	0.43

YELLOW-POPLAR

Grain angle (φ°)	Ring Orientation (θ°) 0			15			30			45			60			75			90		
	Compression strength																				
	N	$\bar{\sigma}$	s	N	$\bar{\sigma}$	s	N	$\bar{\sigma}$	s	N	$\bar{\sigma}$	s	N	$\bar{\sigma}$	s	N	$\bar{\sigma}$	s	N	$\bar{\sigma}$	s
0	--	--	--	--	--	--	--	--	--	10	35.47	2.52	--	--	--	--	--	--	--	--	--
15	--	--	--	--	--	--	--	--	--	10	33.35	3.74	--	--	--	--	--	--	--	--	--
30	6	20.84	1.44	4	19.03	0.40	4	21.37	0.87	6	19.55	0.97	4	16.70	1.20	4	15.56	1.07	6	17.33	0.41
45	6	13.08	0.68	4	12.89	4.32	4	12.80	0.42	6	13.77	0.88	4	11.46	0.20	4	9.07	0.18	6	9.22	1.76
60	6	8.19	0.09	4	7.97	0.11	4	8.40	0.29	6	7.81	0.29	4	8.07	0.18	4	6.66	0.24	6	8.12	0.22
75	6	6.71	0.19	4	6.50	0.06	4	6.80	0.14	6	5.46	0.37	4	6.35	0.21	4	5.60	0.14	6	5.35	0.28
90	6	4.38	0.15	4	5.99	0.14	4	6.31	0.08	6	4.42	0.08	4	6.40	0.23	4	5.16	0.10	6	7.13	0.16

a – sample size
b – mean compression strength value (MPa)
c – standard deviation (MPa)

Table A.III.3. *Summary statistics of the experimentally determined compression MOE values for the North American species.*

ASPEN

Grain angle (φ°)	Ring Orientation (θ°) 0			15			30			45			60			75			90		
	Compression MOE																				
	N [a]	$\bar{E}$ [b]	s [c]	N	$\bar{E}$	s	N	$\bar{E}$	s	N	$\bar{E}$	s	N	$\bar{E}$	s	N	$\bar{E}$	s	N	$\bar{E}$	s
0	--	--	--	--	--	--	--	--	--	10	10.74	1.71	--	--	--	--	--	--	--	--	--
15	--	--	--	--	--	--	--	--	--	10	6.10	0.83	--	--	--	--	--	--	--	--	--
30	5	1.60	0.25	4	1.70	0.29	4	1.91	0.12	6	1.96	0.59	4	2.31	0.26	4	3.37	1.18	6	2.45	0.44
45	6	0.72	0.10	4	0.99	0.15	4	0.63	0.06	6	0.53	0.11	4	1.45	0.89	4	0.90	0.11	6	2.10	0.46
60	6	0.46	0.27	3	0.42	0.05	4	0.34	0.18	6	0.44	0.09	4	0.43	0.03	4	0.90	0.26	6	0.98	0.19
75	6	0.24	0.05	4	0.18	0.02	4	0.21	0.02	6	0.24	0.03	4	0.42	0.14	4	0.78	0.14	6	0.37	0.05
90	6	0.26	0.03	4	0.24	0.07	3	0.33	0.03	5	0.36	0.03	4	0.36	0.04	4	0.54	0.05	5	0.82	0.26

RED OAK

Grain angle (φ°)	Ring Orientation (θ°) 0			15			30			45			60			75			90		
	Compression MOE																				
	N	$\bar{E}$	s	N	$\bar{E}$	s	N	$\bar{E}$	s	N	$\bar{E}$	s	N	$\bar{E}$	s	N	$\bar{E}$	s	N	$\bar{E}$	s
0	--	--	--	--	--	--	--	--	--	11	14.40	2.16	--	--	--	--	--	--	--	--	--
15	--	--	--	--	--	--	--	--	--	10	8.43	2.20	--	--	--	--	--	--	--	--	--
30	6	3.03	0.33	4	3.44	0.29	4	2.58	0.29	6	2.10	0.86	4	4.46	0.94	4	3.78	0.29	6	3.85	0.21
45	6	2.42	0.20	4	2.03	0.27	4	1.59	0.22	6	1.59	0.10	4	2.19	0.34	4	2.08	0.29	6	2.41	0.29
60	6	1.62	0.23	4	1.49	0.18	4	1.24	0.07	6	1.44	0.18	4	1.68	0.13	4	1.31	0.12	6	1.81	0.27
75	6	1.04	0.10	4	1.13	0.07	4	1.00	0.07	6	1.11	0.05	4	1.72	0.33	4	0.97	0.15	6	1.84	0.22
90	6	1.04	0.14	3	0.93	0.19	4	0.97	0.07	6	0.92	0.06	4	1.32	0.15	4	0.97	0.07	6	1.61	0.29

YELLOW-POPLAR

Grain angle (φ°)	Ring Orientation (θ°) 0			15			30			45			60			75			90		
	Compression MOE																				
	N	$\bar{E}$	s	N	$\bar{E}$	s	N	$\bar{E}$	s	N	$\bar{E}$	s	N	$\bar{E}$	s	N	$\bar{E}$	s	N	$\bar{E}$	s
0	--	--	--	--	--	--	--	--	--	10	10.26	1.47	--	--	--	--	--	--	--	--	--
15	--	--	--	--	--	--	--	--	--	10	7.15	1.33	--	--	--	--	--	--	--	--	--
30	6	3.25	0.84	4	2.72	0.20	4	3.26	0.35	6	2.55	0.15	4	3.20	0.33	4	3.21	0.11	6	2.39	0.22
45	6	1.46	0.11	4	1.64	0.67	4	1.49	0.13	6	1.45	0.16	4	1.64	0.07	4	1.01	0.06	6	1.18	0.35
60	6	0.82	0.09	4	0.80	0.08	4	0.98	0.07	6	0.79	0.08	4	1.13	0.07	4	0.66	0.07	6	0.97	0.13
75	6	0.55	0.24	4	0.65	0.07	4	0.73	0.04	6	0.51	0.05	4	0.60	0.06	4	0.49	0.03	6	0.53	0.14
90	6	0.37	0.04	4	0.73	0.07	4	0.66	0.04	6	0.40	0.02	4	0.73	0.04	4	0.43	0.05	6	0.74	0.11

a – sample size

b – mean compression MOE value (GPa)

c – standard deviation (GPa)

Table A.III.4. Summary statistics of the compression strength and E values of European species.

		True Poplar						*Turkey Oak*					
Grain angle (ϕ °)	*Ring angle* (Θ °)	*Compression E (GPa)*			*Compression strength (MPa)*			*Compression E (GPa)*			*Compression strength (MPa)*		
		n^a	$\bar{x}^b$	*Std.*^{c}	n^a	$\bar{x}^b$	*Std.*^{c}	n^a	$\bar{x}^b$	*Std.*^{c}	n^a	$\bar{x}^b$	*Std.*^{c}
0	--	11	10.35	1.13	300	34.45	2.69	15	11.03	1.57	300	51.97	6.82
45	0	15	0.63	0.07	300	6.32	1.00	14	1.69	0.12	216	21.36	3.11
45	90	15	1.36	0.12	300	8.72	1.20	15	2.66	0.27	298	22.92	3.26
90	0	15	0.25	0.01	300	3.04	0.31	15	0.93	0.11	300	10.02	0.95
90	45	15	0.25	0.02	297	3.00	0.38	14	0.98	0.06	300	10.94	1.21
90	90	15	0.71	0.05	300	4.37	0.65	15	1.97	0.23	30	14.67	1.75

a. - sample size.
b. - mean value.
c. - standard deviation

Table A.III.5. Summary statistics of the experimentally determined E_d values of decorative veneers.

Species & Groups	Statistics	n	Grain Angle (ϕ°)											
			Dynamic Modulus of Elasticity, E_d (GPa)											
			0	*15*	*30*	*45*	*60*	*75*	*90*	*105*	*120*	*135*	*150*	*165*	*180*
Oak Veneer	*Gr.1*	*Mean*	12.62	8.28	3.92	1.57	0.78	0.42	0.53	0.51	0.80	1.82	3.70	7.47	12.29
		9													
		Std.	0.67	0.76	0.30	0.51	0.22	0.12	0.25	0.14	0.18	0.23	0.35	0.71	0.68
	Gr.2	*Mean*	13.83	9.30	4.80	1.47	0.74	0.45	0.24	0.35	0.62	1.45	3.85	8.61	14.20
		12													
		Std.	1.24	1.27	0.80	0.62	0.20	0.16	0.13	0.07	0.22	0.58	1.08	0.90	1.20
	Gr.3	*Mean*	17.39	9.86	4.28	2.04	0.99	0.44	0.20	0.40	0.74	1.58	3.69	6.34	10.37
		8													
		Std.	2.94	1.32	0.66	0.38	0.48	0.20	0.14	0.28	0.52	0.34	0.59	0.76	1.67
	Gr.4	*Mean*	12.62	8.28	3.92	1.57	0.78	0.42	0.53	0.51	0.80	1.82	3.70	7.47	12.29
		16													
		Std.	0.67	0.76	0.30	0.51	0.22	0.12	0.25	0.14	0.18	0.23	0.35	0.71	0.68
	Gr.5	*Mean*	10.94	6.84	3.74	2.01	0.83	0.54	0.43	0.64	1.00	2.19	4.34	7.35	10.57
		15													
		Std.	0.80	0.53	0.28	0.10	0.15	0.14	0.12	0.14	0.12	0.08	0.17	0.32	0.47
Cherry Veneer	*Gr.1*	*Mean*	8.89	7.94	4.89	2.97	1.97	1.45	1.19	1.22	1.46	2.29	3.27	5.93	9.07
		13													
		Std.	0.60	0.62	0.53	0.26	0.19	0.12	0.08	0.10	0.10	0.91	0.21	0.97	0.67
	Gr.2	*Mean*	9.16	5.83	3.10	1.91	1.28	0.98	0.96	1.23	1.87	3.03	5.54	8.41	9.01
		15													
		Std.	0.68	1.31	0.84	0.41	0.25	0.15	0.11	0.23	0.19	0.45	1.09	1.30	0.94
	Gr.3	*Mean*	10.55	7.27	4.15	2.39	1.51	1.03	0.99	1.10	1.49	2.27	4.06	7.44	10.69
		22													
		Std.	0.53	0.48	0.43	0.18	0.10	0.13	0.04	0.11	0.14	0.14	0.25	0.74	0.59
	Gr.4	*Mean*	9.42	8.65	6.00	3.68	2.29	1.71	1.44	1.33	1.74	2.39	3.77	6.01	9.48
		17													
		Std.	1.08	0.72	0.60	0.32	0.17	0.20	0.22	0.19	0.15	0.25	0.48	0.59	0.78
	Gr.5	*Mean*	12.57	10.36	5.60	2.68	1.51	1.02	0.99	1.02	1.27	2.08	3.61	7.43	12.93
		15													
		Std.	0.80	0.64	1.07	0.23	0.21	0.16	0.04	0.13	0.19	0.17	0.29	0.62	0.49

n – sample size.
Std. – Standard deviation.

Appendix IV

Table IV.1. *Type and parameters of the probability density functions of the stochastic input variables.*

Input parameter	***Unit***	***Probability density function***	***Function parameters*** [a]		
			μ	**σ**	**α**
		Original veneer thickness			
Quaking aspen	*mm*	*Extreme Value A*	*3.108*	*0.069*	*--*
Red oak	*mm*	*Logistic*	*3.046*	*0.048*	
Yellow-poplar	*mm*	*2-param. Weibull*	*--*	*3.162*	*42.761*
		LVL [b]			
t_o	*mm*	*Normal*	*2.760*	*0.140*	*--*
		PSL			
u	*#/in²*	*Normal*	*11.64*	*0.36*	*--*
t	*mm*	*Normal*	*2.051*	*0.391*	*--*
α	*°*	*Normal*	*0.030*	*4.668*	*--*
β	*°*	*Normal*	*2.991*	*14.709*	*--*

[a] μ – *location* ; σ – *scale;* α – *shape parameter.*

[b] t_o – *thickness of the two outside layers on both sides* ; t_c – *thickness of the remaining (core) layers.*

Table IV.2. *Simulated and experimental geometric and physical properties of LVL and PSL.*

Property	***Unit***	***Source***	***Mean***	***STD***[1]	***Min.***	***Max.***	***Skewness***
				LVL			
Thickness	*mm*	*Sim.*	*43.0*	*0.50*	*42.1*	*43.9*	*0.005*
		Exp.	*43.6*	*0.15*	*43.1*	*44.0*	*0.013*
Density	*kg/m³*	*Sim.*	*511.0*	*10.00*	*492.0*	*530.0*	*-0.100*
		Exp.	*566.0*	*11.00*	*541.0*	*584.0*	*0.078*
		Exp.[2]	*509.6*	*9.90*	*498.6*	*529.7*	*0.097*
				PSL			
ΣA_i	*cm²*	*Sim.*	*103.7*	*1.4*	*101.4*	*106.1*	*0.029*
$A_{composite}$	*cm²*	*Target*	*106.5*	*-----*	*-----*	*-----*	*-----*
ΣI_i	*cm⁴*	*Sim.*	*498.3*	*6.8*	*486.9*	*509.7*	*0.001*
$I_{composite}$	*cm⁴*	*Target*	*515.1*	*-----*	*-----*	*-----*	*-----*
Density	*kg/m³*	*Sim.*	*673.0*	*11.0*	*652.0*	*694.0*	*-0.037*
		Exp.	*673.0*	*16.0*	*640.0*	*708.0*	*-0.122*

Sample size: n = 20,

1 – Standard Deviation,

2 – Density of overlapping veneer-joint free LVL.

Table IV.3. *Comparison of simulated and experimental bending MOE of LVL and PSL.*

Direction of Bending	Source	n[1]	Mean (GPa)	STD[2] (GPa)	Min. (GPa)	Max. (GPa)	Skewness
			LVL				
Flatwise	*Sim.*	*20x20*	*12.91*	*0.79*	*11.40*	*14.64*	*0.100*
	Exp.	*20*	*13.36*	*0.72*	*12.20*	*15.16*	*0.212*
Edgewise	*Sim.*	*20x20*	*12.70*	*0.41*	*11.95*	*13.49*	*0.063*
	Exp.	*20*	*13.22*	*1.21*	*11.85*	*15.90*	*0.022*
			PSL				
Flatwise	*Sim.*	*20x20*	*14.46*	*0.34*	*13.83*	*15.10*	*0.041*
	Exp.	*20*	*12.57*	*0.57*	*11.64*	*13.92*	*-0.087*
Edgewise	*Sim.*	*20x20*	*14.54*	*0.40*	*13.78*	*15.29*	*-0.052*
	Exp.	*20*	*12.82*	*0.75*	*11.18*	*13.81*	*0.115*

[1] *Replications/sample size.*
[2] *Standard deviation.*

Table IV. 4. *Comparison of simulated and experimental compression MOE of LVL and PSL at different load (θ') and strand (φ') orientations.*

θ'	φ'	Source	Mean (GPa)	STD[1] (GPa)	Min. (GPa)	Max. (GPa)	Skewness
			LVL				
0°	**--**	**Sim.**	**11.33**	**0.46**	**10.61**	**12.11**	**0.065**
		Exp.	**11.87**	**1.06**	**9.71**	**13.34**	**0.142**
45°	**0°**	**Sim.**	**0.79**	**0.02**	**0.75**	**0.83**	**0.109**
		Exp.	**0.87**	**0.07**	**0.76**	**1.01**	**0.004**
45°	*90°*	*Sim.*	*1.52*	*0.06*	*1.43*	*1.61*	*0.124*
		Exp.	*0.84*	*0.06*	*0.75*	*0.96*	*0.545*
90°	**0°**	**Sim.**	**0.41**	**0.01**	**0.39**	**0.43**	**0.108**
		Exp.	**0.44**	**0.03**	**0.41**	**0.44**	**-0.022**
90°	*45°*	*Sim.*	*0.49*	*0.02*	*0.47*	*0.51*	*0.170*
		Exp.	*0.29*	*0.05*	*0.23*	*0.35*	*0.112*
90°	*90°*	*Sim.*	*0.82*	*0.03*	*0.77*	*0.87*	*0.146*
		Exp.	*0.37*	*0.03*	*0.31*	*0.42*	*0.135*
			PSL				
0°	**--**	**Sim.**	**13.34**	**0.43**	**12.63**	**13.99**	**-0.139**
		Exp.	**13.20**	**2.09**	**10.71**	**17.28**	**0.128**
45°	**0°**	**Sim.**	**1.06**	**0.04**	**1.00**	**1.11**	**-0.081**
		Exp.	**1.08**	**0.11**	**0.86**	**1.25**	**-0.002**
45°	*90°*	*Sim.*	*1.90*	*0.06*	*1.80*	*1.99*	*-0.035*
		Exp.	*0.64*	*0.05*	*0.55*	*0.73*	*-0.100*
90°	**0°**	**Sim.**	**0.51**	**0.01**	**0.52**	**0.56**	**-0.141**
		Exp.	**0.48**	**0.07**	**0.39**	**0.60**	**-0.221**
90°	*45°*	*Sim.*	*0.64*	*0.02*	*0.61*	*0.67*	*-0.035*
		Exp.	*0.30*	*0.03*	*0.25*	*0.36*	*0.186*
90°	*90°*	*Sim.*	*1.02*	*0.04*	*0.97*	*1.08*	*-0.053*
		Exp.	*0.23*	*0.03*	*0.19*	*0.28*	*-0.254*

Appendix V

Some additional information for validating the Taguchi's method by L_9 type analyses:

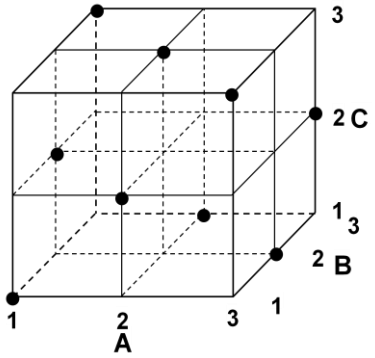

Figure A.V.1. *Three-dimensional representation of the possible combinations for the L_9 type analyses. Nodes indicate the tested combinations.*

Test results of the selected material properties. Note, that both MOE and MOR were adjusted to target density by regression technique.

Table A.V.1. *– Summary statistics of the experimental test results by factor/level combinations.*

Run number	***Factors and Levels***			***n[a]***	***Density***		***Modulus of Elasticity***			***Modulus of Rupture***		
	A	*B*	*C*		$\bar{y}$ *(kg/m³)*	*COV[b] (%)*	$\bar{y}$ *(MPa)*	*COV[b] (%)*	*MOE[c] (MPa)*	$\bar{y}$ *(MPa)*	*COV[b] (%)*	*MOR[c] (MPa)*
1	*1*	*1*	*1*	*8*	*677*	*6.8*	*15351*	*11.3*	*14449*	*110*	*15.8*	*100*
2	*1*	*2*	*2*	*8*	*742*	*6.8*	*15478*	*10.5*	*14176*	*112*	*22.8*	*91*
3	*1*	*3*	*3*	*8*	*756*	*10.2*	*15125*	*16.9*	*14947*	*103*	*31.0*	*101*
4	*2*	*1*	*2*	*8*	*680*	*8.7*	*13516*	*15.9*	*12450*	*81*	*37.5*	*69*
5	*2*	*2*	*3*	*8*	*745*	*3.6*	*14582*	*5.6*	*13373*	*110*	*15.5*	*84*
6	*2*	*3*	*1*	*8*	*762*	*6.6*	*17671*	*7.6*	*17364*	*137*	*10.1*	*134*
7	*3*	*1*	*3*	*8*	*708*	*4.8*	*12879*	*10.4*	*10771*	*85*	*22.3*	*55*
8	*3*	*2*	*1*	*8*	*727*	*8.7*	*15554*	*11.4*	*14833*	*119*	*13.5*	*113*
9	*3*	*3*	*2*	*8*	*778*	*6.8*	*17087*	*7.7*	*16474*	*124*	*12.1*	*117*
Overall average:					*730*	*--*	*15249*	*--*	*14315*	*109*	*--*	*96*

$\bar{y}$ *- sample mean;*

a – sub-sample size;
b – Coefficient of Variation;
c – adjusted mean value.

An example of the Analysis of Variance (ANOVA) results for the pilot study:

Table A.V.2. *- Results of ANOVA. The linear$_{(L)}$ and quadratic$_{(Q)}$ factorial effects on adjusted MOE.*

FACTORS		*SS*	*df*	*MS*	*F*	*p*	*Effect*	*Std. err.*
MEAN VALUE (MPa)							*14315.3*	*225.3*
Solid resin content	A_L	*371368*	*1*	*371368*	*0.813*	*0.4624*	*-497.6*	*551.8*
	A_Q	*28986*	*1*	*28986*	*0.063*	*0.8246*	*120.4*	*477.9*
Final density	B_L	*20591734*	*1*	*20591734*	*45.086*	*0.0215*	*3705.1*	*551.8*
	B_Q	*158700*	*1*	*158700*	*0.347*	*0.6153*	*-281.7*	*477.9*
End-clipping content	C_L	*9514049*	*1*	*9514049*	*20.831*	*0.0448*	*-2518.5*	*551.8*
	C_Q	*12007*	*1*	*12007*	*0.026*	*0.8861*	*77.5*	*477.9*
Error		*913437*	*2*	*456719*				
Total		*31590281*	*8*					
							$R^2 = 0.971$; $R^2_{adj} = 0.884$	
AFTER POOLING:								
Final density	B_L	*20591734*	*1*	*20591734*	*83.227*	*0.0001*	*3705.1*	*406.1*
End-clipping content	C_L	*9514049*	*1*	*9514049*	*38.454*	*0.0008*	*-2518.5*	*406.1*
Error		*1484498*	*6*	*247416*				
							$R^2 = 0.953$; $R^2_{adj} = 0.937$	

The effects of factors on the adjusted MOR:

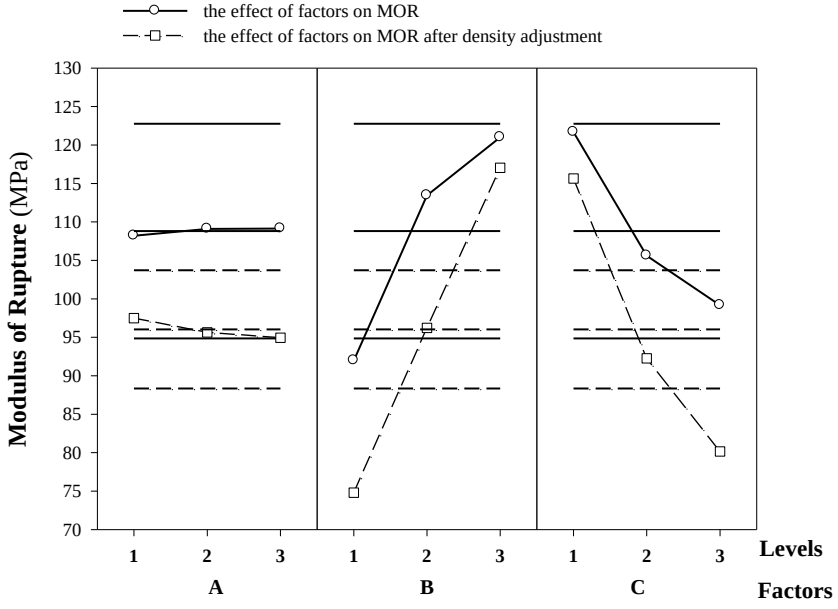

Figure A.V.2. *The effects of factors on the observed and adjusted modulus of rupture (MOR). Horizontal lines represent mean values and ± 2 standard errors.*

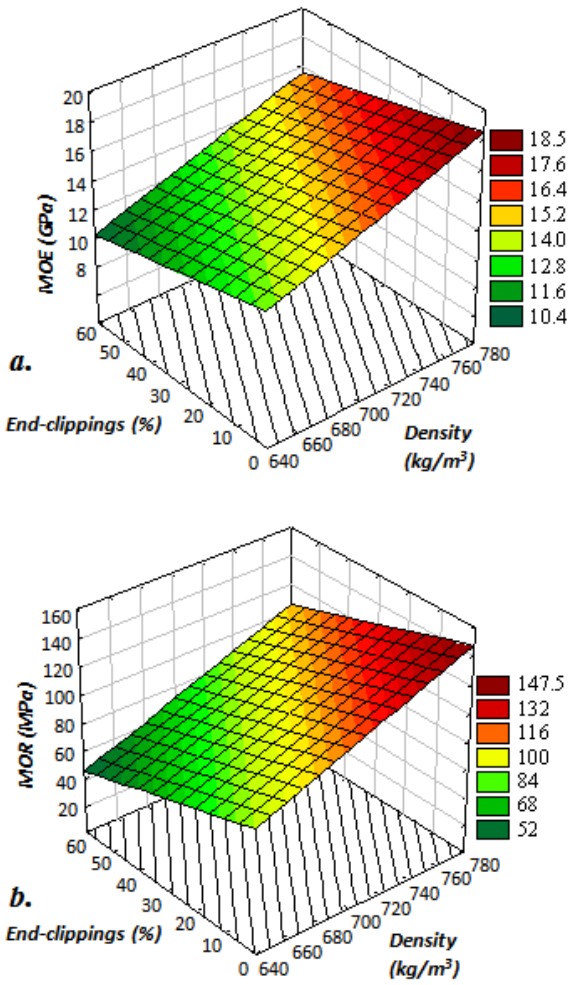

Figure A.V.3. *Response surfaces predicting the expected mechanical properties as a function of factors B and C at fixed 8% resin content level.*
a. *– response surface of MOE;* ***b.*** *– response surface of MOR.*

Vitae

Elemér M. Láng was born in Győr, Hungary in 1947. He graduated from the Révai Miklós High School in 1966. After two years of compulsory military service and two years of work, he enrolled at the University of Forestry and Wood Sciences, College of Wood Sciences in Sopron, Hungary. He graduated as a diplom-engineer of wood science and technology in 1975. He joined the Faculty of the Institute of Product Development and Technology, formerly the Department of Furniture and Joinery Production in 1976.

To complement his education, in 1989 he enrolled as a graduate student at the Department of Wood Science and Forest Products, Virginia Polytechnic Institute and State University, Blacksburg, VA, U.S.A. He received his Ph.D. in Wood Science in 1993.

After two years of Post-doctoral work at the Division of Forestry, West Virginia University, Morgantown, WV, U.S.A. he returned to Sopron and assumed the position of an associate professor at the University of Sopron. In 1996 he was invited by the West Virginia University, Division of Forestry for a faculty position to teach wood mechanics and wood composites and conduct research in the program of Wood Science and Technology. After five years of service, he received his tenure and was promoted to the rank of associate professor.

In 2000, the Doctoral Advisory Committee of the University of West Hungary accredited his Ph.D. and in the same year he acquired his "habilitation" at the same institute. In 2006, by the recommendation of the Hungarian Committee of Accreditation, the President of the Republic of Hungary nominated him as a full professor at the University of West Hungary, Sopron. He retired from his position at the West Virginia University in 2008 and was awarded the Associate Professor Emeritus status at the Division of Forestry and Natural Resources, WVU. Currently, he holds the position of professor at the Institute of Product Development and Technology, University of West Hungary, Sopron.

Sopron/Morgantown, September, 2011.

Elemer M. Lang

Errata

On page 13, Nomenclature I:

Incorrect:	*Correct:*
T *volume*	T *temperature*
V *temperature*	V *volume*

On page 17, § 2:

Incorrect:	*Correct:*
Dai and Steiner (1194a, 1994b)	Dai and Steiner (1994a, 1994b)

On page 21, In headings of Table II.2:

Incorrect:	*Correct:*
Fitted distributio n	***Fitted distribution***

On page 27, Caption of Figure II.8:

Incorrect:

b*. - at mat strain* $\varepsilon \approx 0.3$*;* ***c****. – at mat strain* $\varepsilon \approx 0.3$

Correct:

b*. - at mat strain* $\varepsilon \approx 0.3$*;* ***c****. – at mat strain* $\varepsilon \approx 0.6$